The Hydrogen Economy

Green Hydrogen

Use PV, wind, hydro electricity to make H_2 by hydrolysis

Direct oxidation/reduction reactions to make H_2

Use Algae to produce H_2

Blue Hydrogen

Use methane reforming to produce H_2, sequester CO_2

Brown/Grey Hydrogen (Most current H_2 in the US)

Use methane reforming to produce H_2

Electrolysis of Water (Hydrolysis)

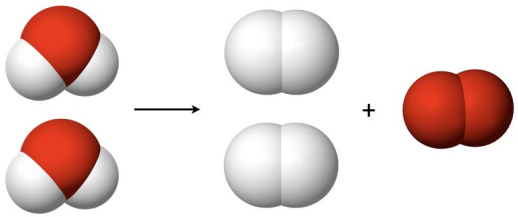

$2H_2O \longrightarrow 2H_2 + O_2$

Anode (oxidation):	$2\ H_2O(l)$	$\rightarrow O_2(g) + 4\ H^+(aq) + 4e^-$	$E^o = +1.23$ V (for the reduction half-equation)[7]
Cathode (reduction):	$2\ H^+(aq) + 2e^-$	$\rightarrow H_2(g)$	$E^o = 0.00$ V

The following cations have lower electrode potential than H^+ and are therefore suitable for use as electrolyte cations: Li^+, Rb^+, K^+, Cs^+, Ba^{2+}, Sr^{2+}, Ca^{2+}, Na^+, and Mg^{2+}. Sodium and lithium are frequently used, as they form inexpensive, soluble salts.

If an acid is used as the electrolyte, the cation is H^+, and there is no competitor for the H^+ created by disassociating water. The most commonly used anion is sulfate (SO_4^{2-}), as it is very difficult to oxidize, with the standard potential for oxidation of this ion to the peroxydisulfate ion being +2.010 volts.[12]

Strong acids such as sulfuric acid (H_2SO_4), and strong bases such as potassium hydroxide (KOH), and sodium hydroxide (NaOH) are frequently used as electrolytes due to their strong conducting abilities.

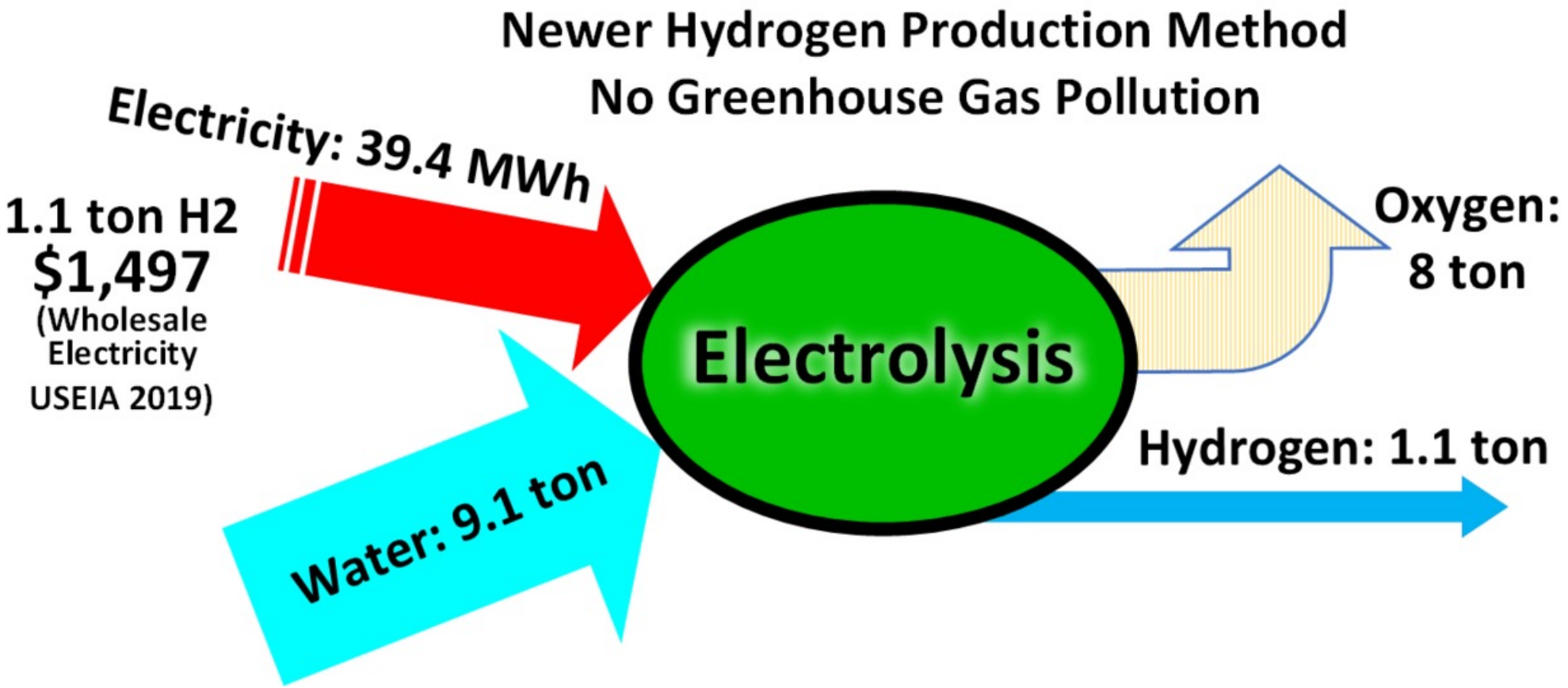
Newer Hydrogen Production Method
No Greenhouse Gas Pollution
Electricity: 39.4 MWh
1.1 ton H2
$1,497
(Wholesale Electricity USEIA 2019)
Water: 9.1 ton
Electrolysis
Oxygen: 8 ton
Hydrogen: 1.1 ton

Electrolysis of Brine

$$2NaCl + 2H_2O \rightarrow Cl_2 + H_2 + 2NaOH$$

5% of H_2 produced currently in US

Steam Reforming of Methane

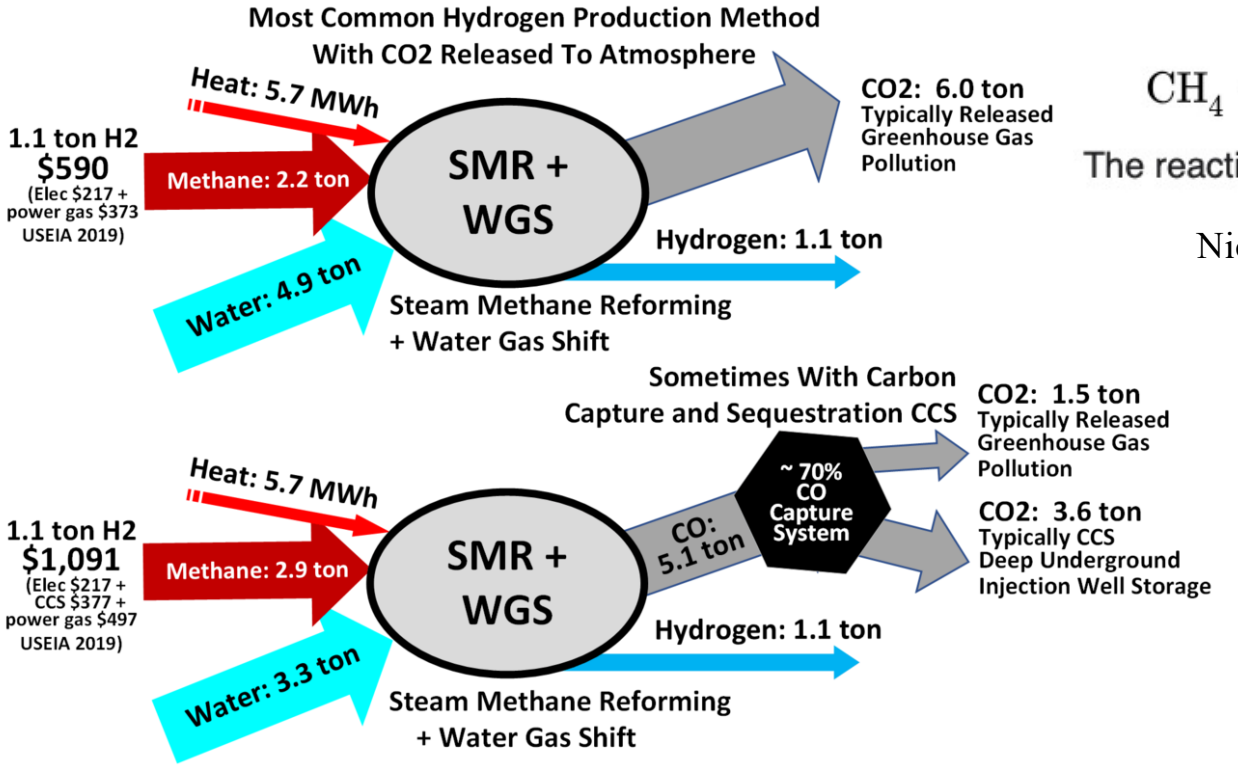

$$CH_4 + H_2O \rightleftharpoons CO + 3\,H_2$$

The reaction is strongly endothermic (ΔH_{SR} = 206 kJ/mol).

Nickel on alumina catalyst

Steam Reforming of Methane

$$\mathrm{CH_4 + H_2O \rightleftharpoons CO + 3\,H_2} \qquad \Delta H_{SR} = 206\ \mathrm{kJ/mol}$$

$$\mathrm{CO + H_2O \rightleftharpoons CO_2 + H_2} \qquad \Delta H_{WGSR} = -41\ \mathrm{kJ/mol}$$

$$\mathrm{CH_4 + 2\,H_2O \rightleftharpoons CO_2 + 4\,H_2} \qquad \Delta H_{DSR} = 165\ \mathrm{kJ/mol}$$

800-900 °C 20-30 bar excess steam S/C ratio of 2.7:1

Separation of Polar CO_2 from H2

Biomass/Syngas

Figure1: Conventional process flow sheet for the production of hydrogen from coal gasification (Bell et al., 2011)

1855

CHEMICAL ENGINEERING TRANSACTIONS
VOL. 32, 2013
A publication of AIDIC
The Italian Association of Chemical Engineering
Online at: www.aidic.it/cet
Chief Editors: Sauro Pierucci, Jiří J. Klemeš
Copyright © 2013, AIDIC Servizi S.r.l.,
ISBN 978-88-95608-23-5; ISSN 1974-9791
DOI: 10.3303/CET1332310

Carbon Dioxide Capture and Hydrogen Purification from Synthesis Gas by Pressure Swing Adsorption

Cheng-tung Chou [a]*, Fei-hong Chen [a], Yu-Jie Huang [a], Hong-sung Yang [b]

[a] Department of Chemical and Materials Engineering, National Central University, Jhong-Li, Taiwan
[b] Center for General Education, Hwa-Hsia Institute of Technology, Chung-Ho District, New Taipei City, Taiwan
t310030@ncu.edu.tw

More Polar Molecules will Adsorb

More Polar Molecules will Adsorb

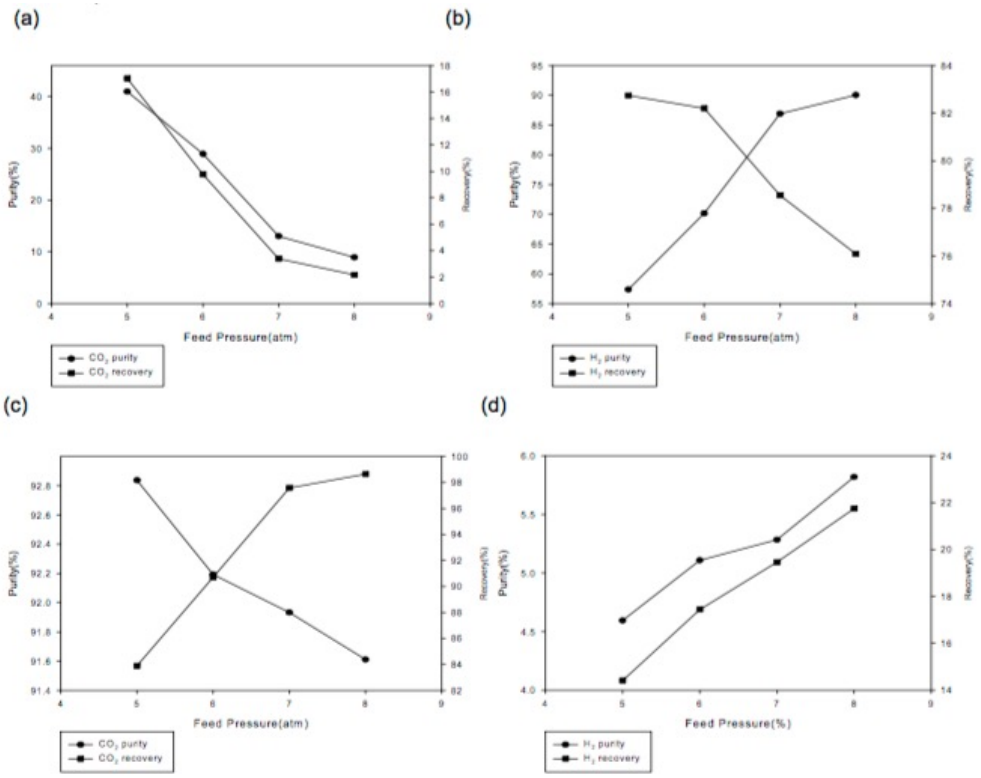

Figure 4: Effect of feed pressure at CO_2-PSA *on (a) CO_2 in top product (b) H_2 in top product (c) CO_2 in bottom product (d) H_2 in bottom product*

Fig *Bell et al., 20*

Fuel / Storage System	P (bar)	Energy Density (GJ/m^3)	Specific Volumetric cost ($US\$/m^3$)	Specific Energy Cost ($US\$/GJ$)
Ammonia gas / pressurized tank	10	13.6	181	13.3
Hydrogen / metal hydride	14	3.6	125	35.2
Gasoline (C_8H_{18}) / liquid tank	1	34.4	1000	29.1
LPG (C_3H_8) / pressurized tank	14	19.0	542	28.5
CNG (CH_4) / integrated storage system	250	10.4	400	38.3
Methanol (CH_3OH) / liquid tank	1	11.4	693	60.9

Haber Reaction to Produce NH_3 from H_2

$$\mathrm{N_2 + 3\,H_2 \longrightarrow 2\,NH_3 \quad \Delta H^\circ = -91.8\,kJ/mol}$$

100 bar 400-500 °C Iron Catalyst

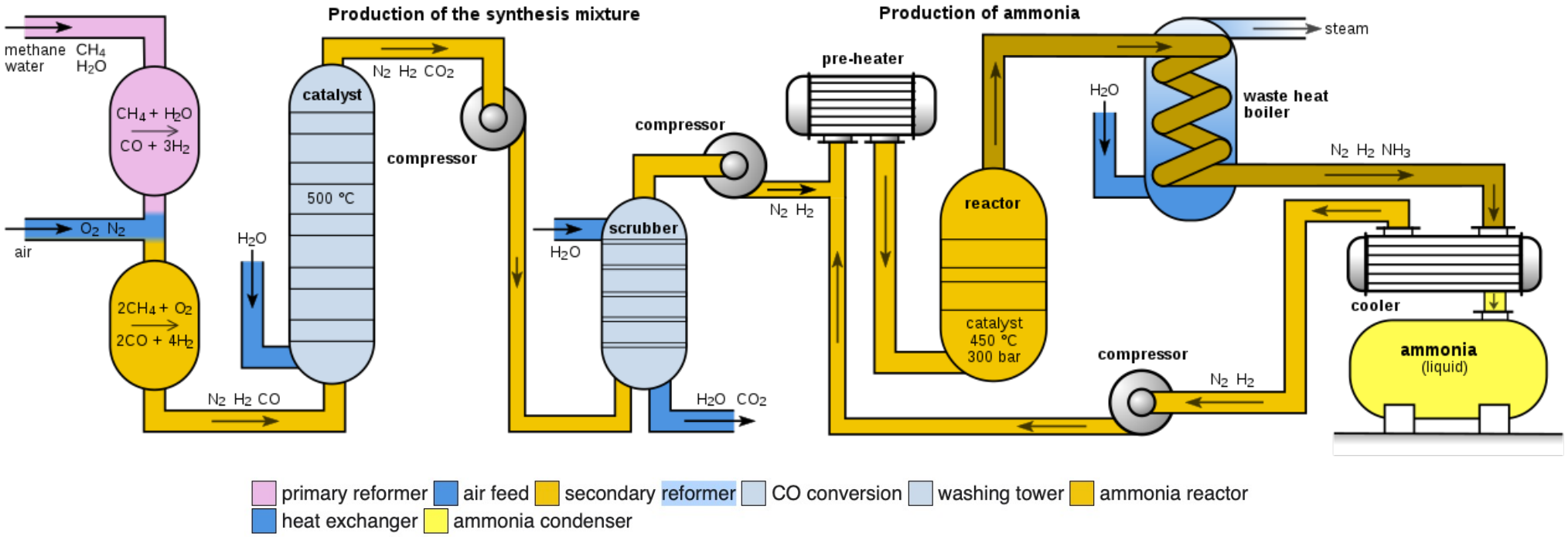

Fischer-Tropsch Reaction to Produce Hydrocarbons from H_2

$$(2n + 1)\,H_2 + n\,CO \rightarrow C_nH_{2n+2} + n\,H_2O$$

(ΔH) of −165 kJ/mol CO combined.

n = 10-20 330-250 °C 10-40 bar

Cobalt, Iron, Ruthenium Catalyst

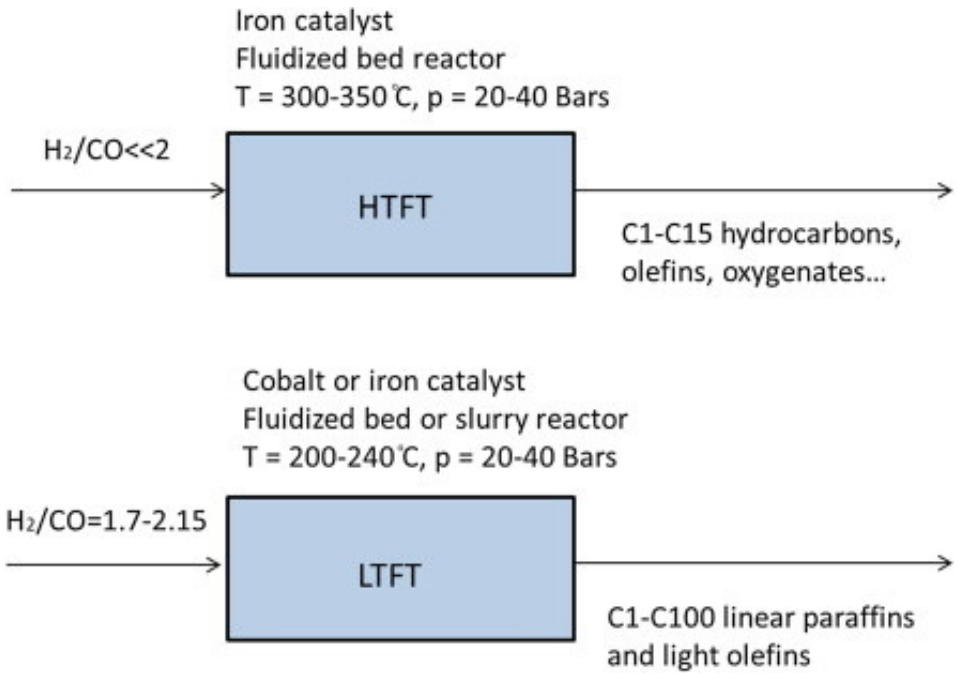

Catalytic Cracking of NH_3 to H_2

$$2NH_3 + 92.4kJ \rightarrow N_2 + 3H_2$$

10 MPa 425 °C Catalyst Fe, Ni, Pt, Ru, Ir, Pd, Rh etc.

Methane from Renewable Source

India Biogas Reactor (https://www.youtube.com/watch?v=9kKRdlAFuZw)

Biogas Reactor for the Developing World (https://www.youtube.com/watch?v=Cwm5Rm8uIsk)

Biomass/Syngas

Single House Biogas (http://www.youtube.com/watch?v=3th2bcqHbsk)

Biomass/Syngas

Biogas in Kenya (http://www.youtube.com/watch?v=qh3mmgiybTw)

Hydrogen from Algae
(Can also produce biofuel and food)

Algae Tower

Algae Building in Germany

NASA Floating Algae Farm Project
(http://www.youtube.com/watch?v=c7Goyg12Reg)

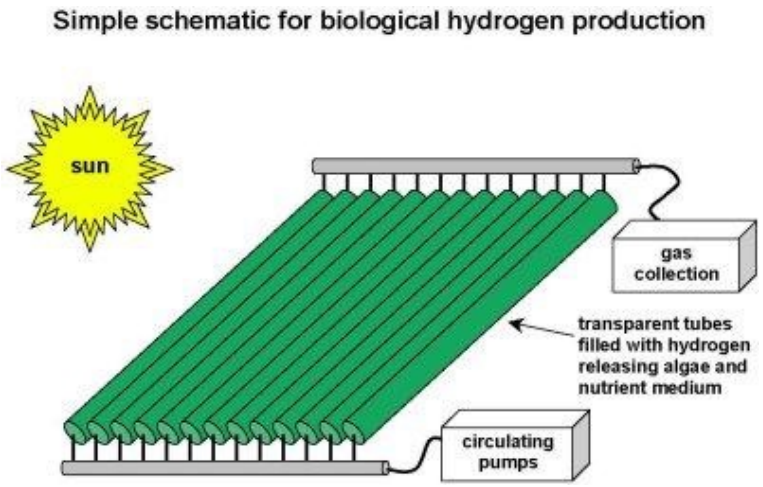

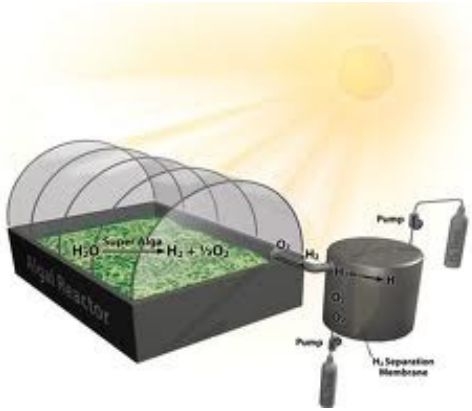

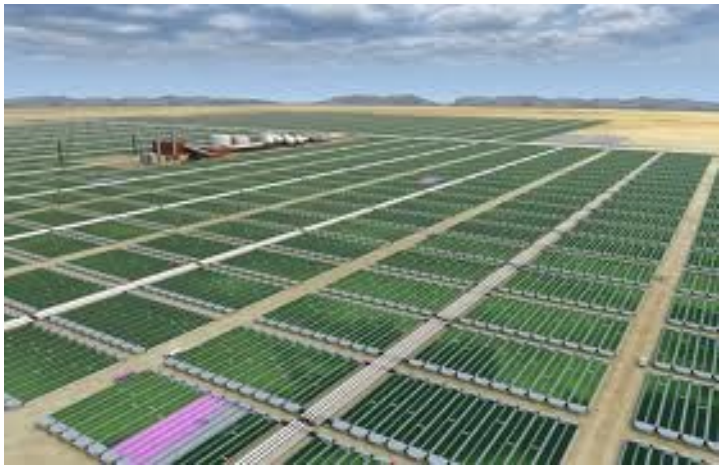

Algae Tower

Simple schematic for biological hydrogen production

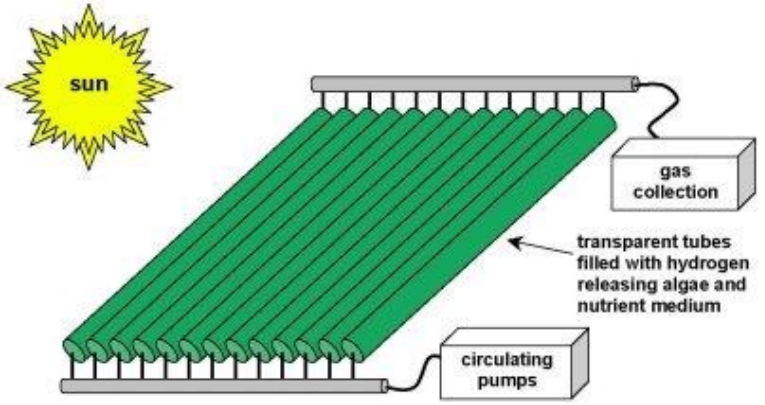

[Hydrogen from Algae](http://www.youtube.com/watch?v=Or_F6qC0sK4) (http://www.youtube.com/watch?v=Or_F6qC0sK4) Comic look at H_2 from Algae

[Hydrogen from Algae Imperial College](https://www.youtube.com/watch?v=OFByDMRbucs)
(https://www.youtube.com/watch?v=OFByDMRbucs)

Solar Redox Reactions for H_2

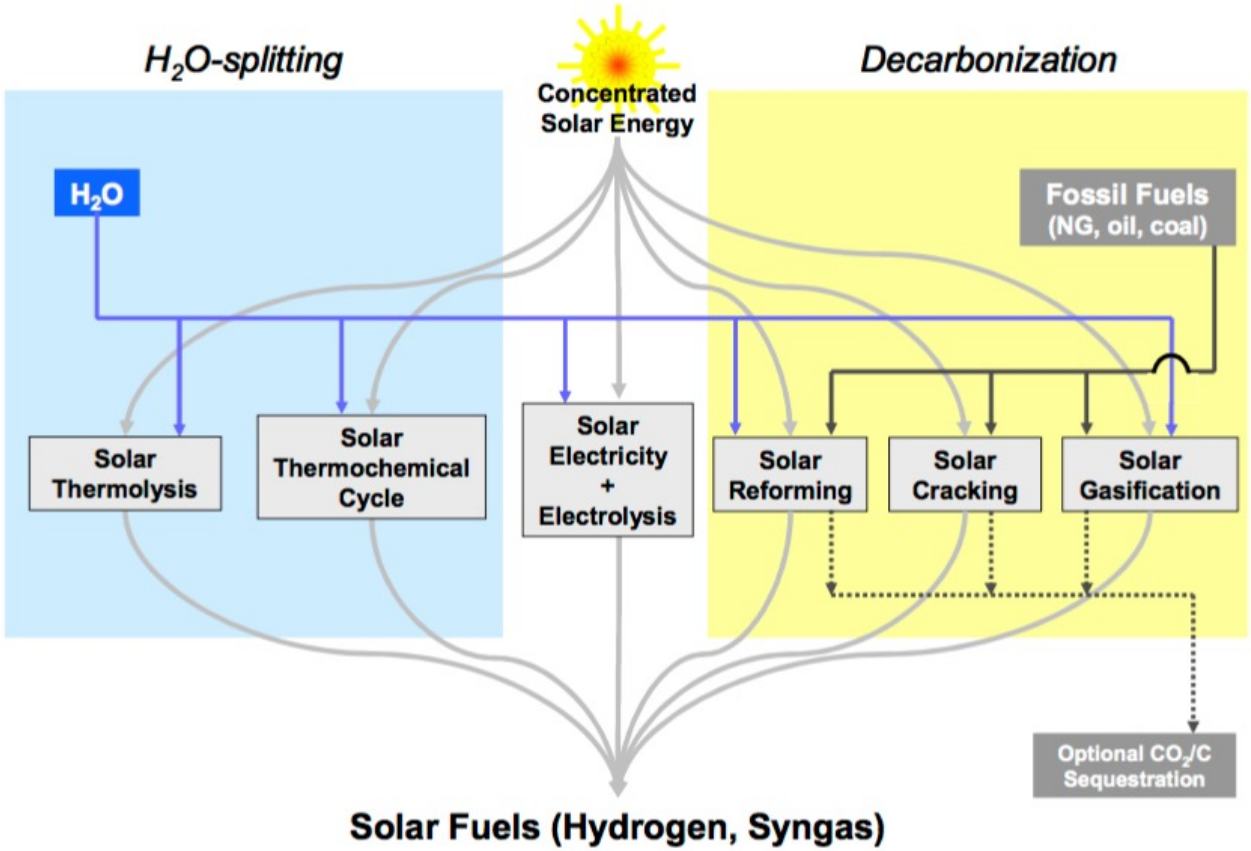

Fig. 2: Thermochemical routes for solar hydrogen production – Indicated is the chemical source of H_2: H_2O for the solar thermolysis and the solar thermochemical cycles; fossil fuels for the solar cracking, and a combination of fossil fuels and H_2O for the solar reforming and gasification. For the solar decarbonization processes, optional CO_2/C sequestration is considered. All of those routes involve energy consuming (endothermic) reactions that make use of concentrated solar radiation as the energy source of high-temperature process heat. Adapted from [1,2].

Photocatalysis

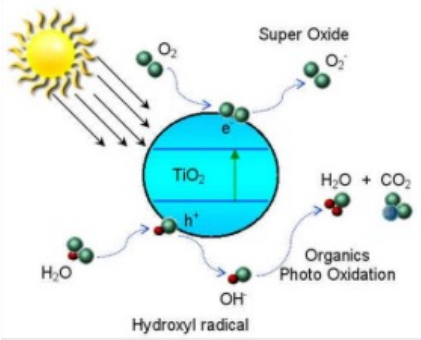

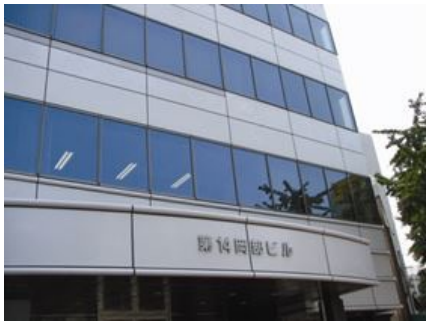

Titania as a photocatalyst

- *Irradiation of semiconductors having a band gap (2 - 4 eV) with UV light energy ≥ energy of the band gap E_g*
- *Generation of charge carriers*

$$TiO_2 \xrightarrow{h\nu} TiO_2\,(e^- + h^+)$$

- *Formation of active radicals (OH*, O_2*)*

$$OH^- + h^+ \longrightarrow OH^\bullet$$

$$O^{2-} + e^- \longrightarrow {}^\bullet O^{2-}$$

- *Recombination process*

$$e^- + h^+ \longrightarrow Heat$$

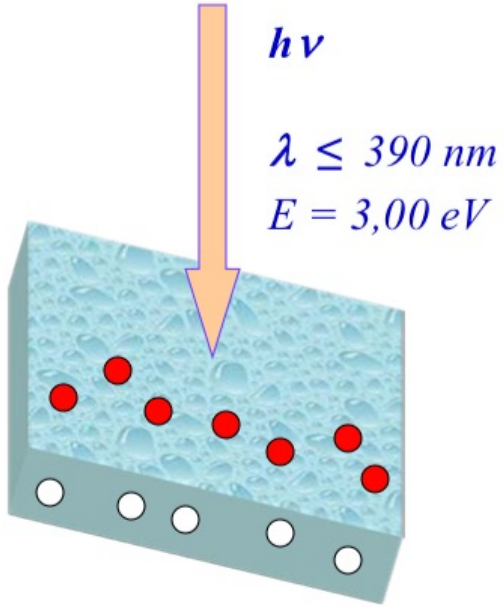

Titania as a photocata

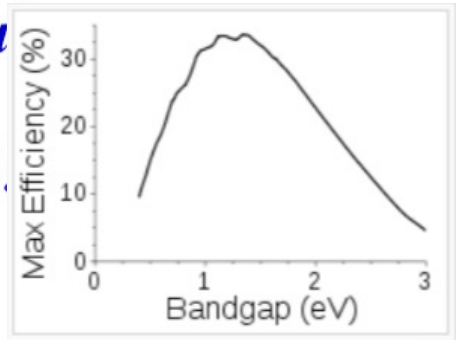

- *Irradiation of semiconductors having a band*
  light energy ≥ energy of the band gap E_g
- *Generation of charge carriers*

$$TiO_2 \xrightarrow{h\nu} TiO_2\,(e^- + h^+)$$

- *Formation of active radicals (OH*, O_2*)*

$$OH^- + h^+ \longrightarrow OH^{\bullet}$$

$$O^{2-} + e^- \longrightarrow {}^{\bullet}O^{2-}$$

- *Recombination process*

$$e^- + h^+ \longrightarrow Heat$$

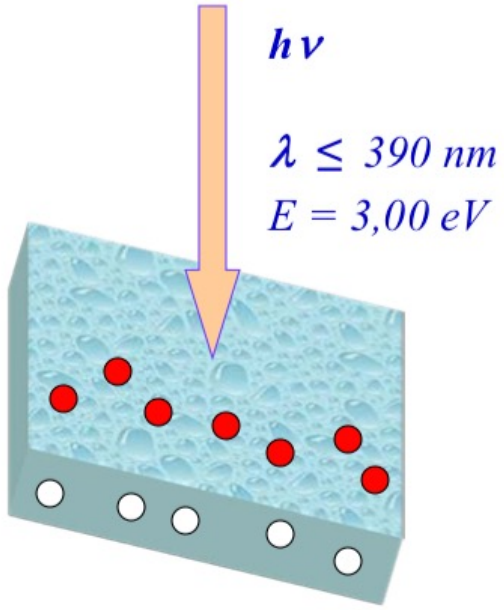

Water is decomposed using only light

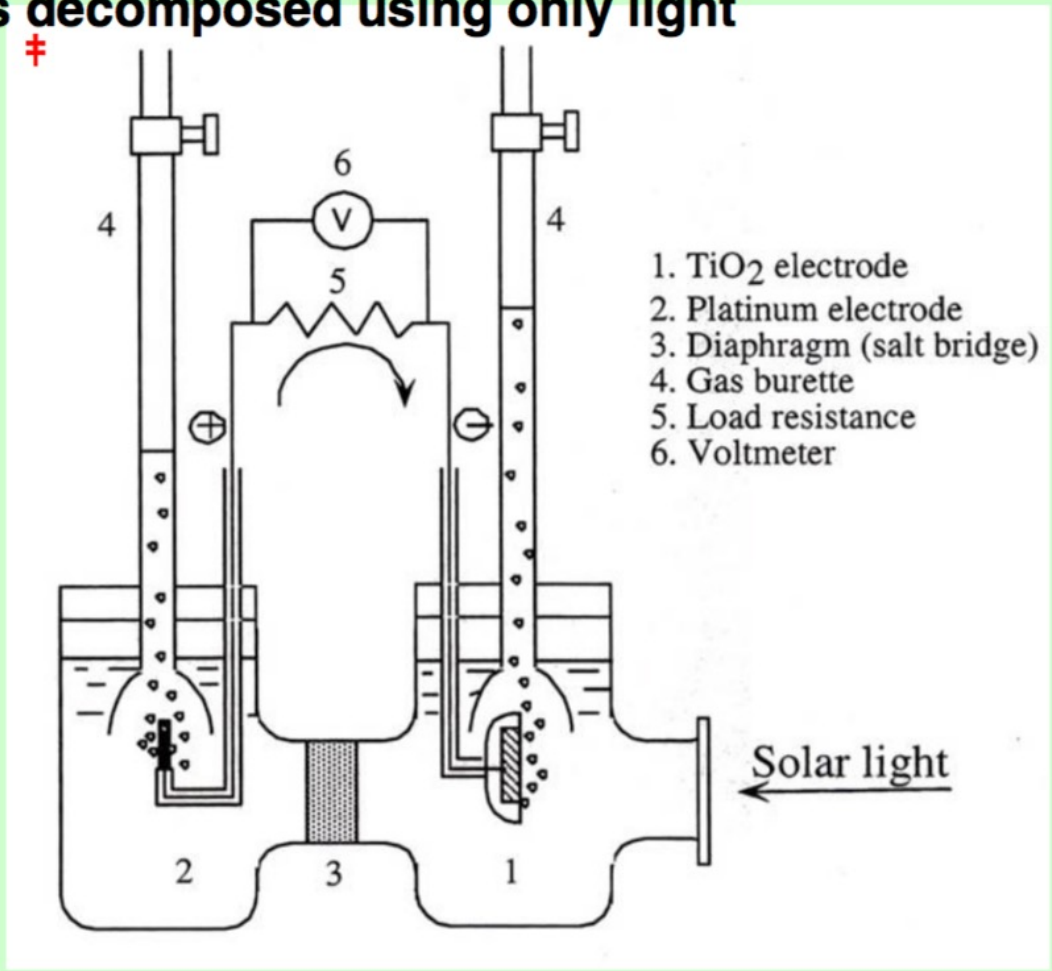

Figure reprinted from;

AKIRA FUJISHIMA, KENICHI HONDA *"Electrochemical Photolysis of Water at a Semiconductor Electrode"* *Nature* 238, 37-38 (1972)

Reaction mechanism of TiO2 photocatalysis

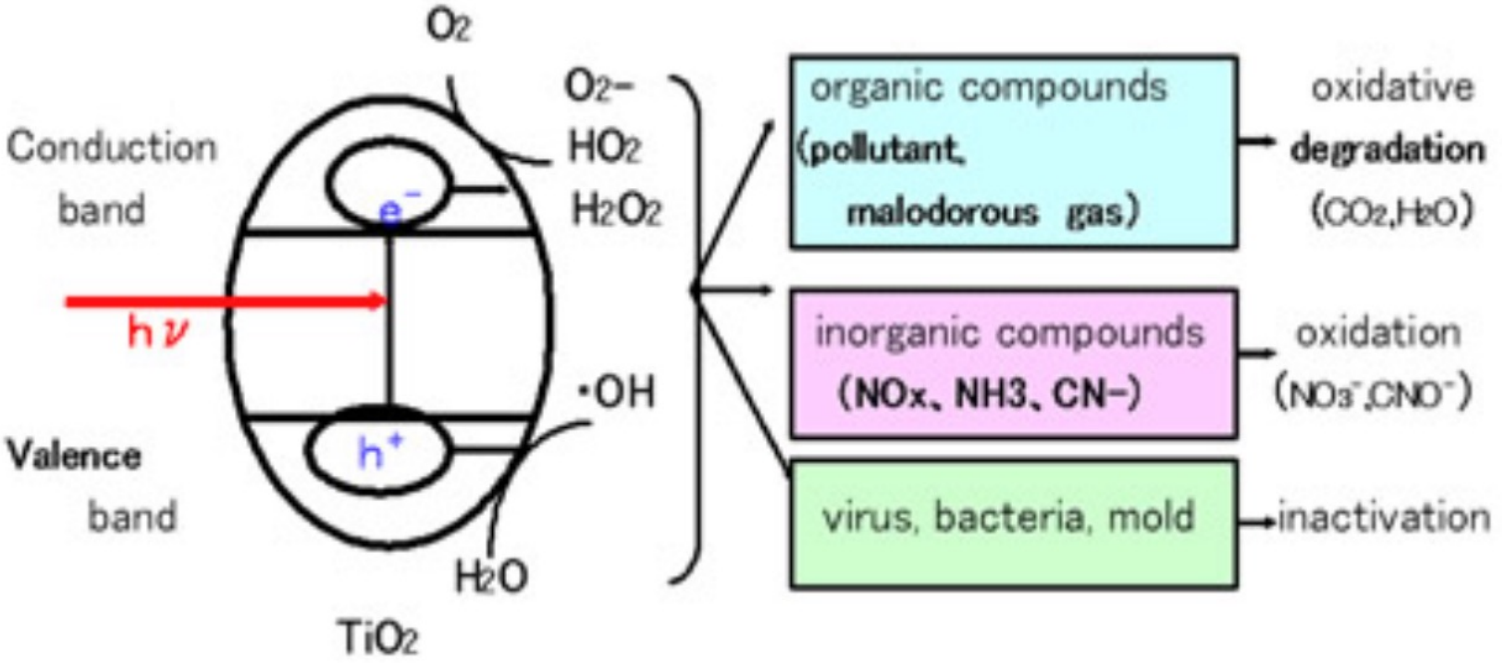

‡

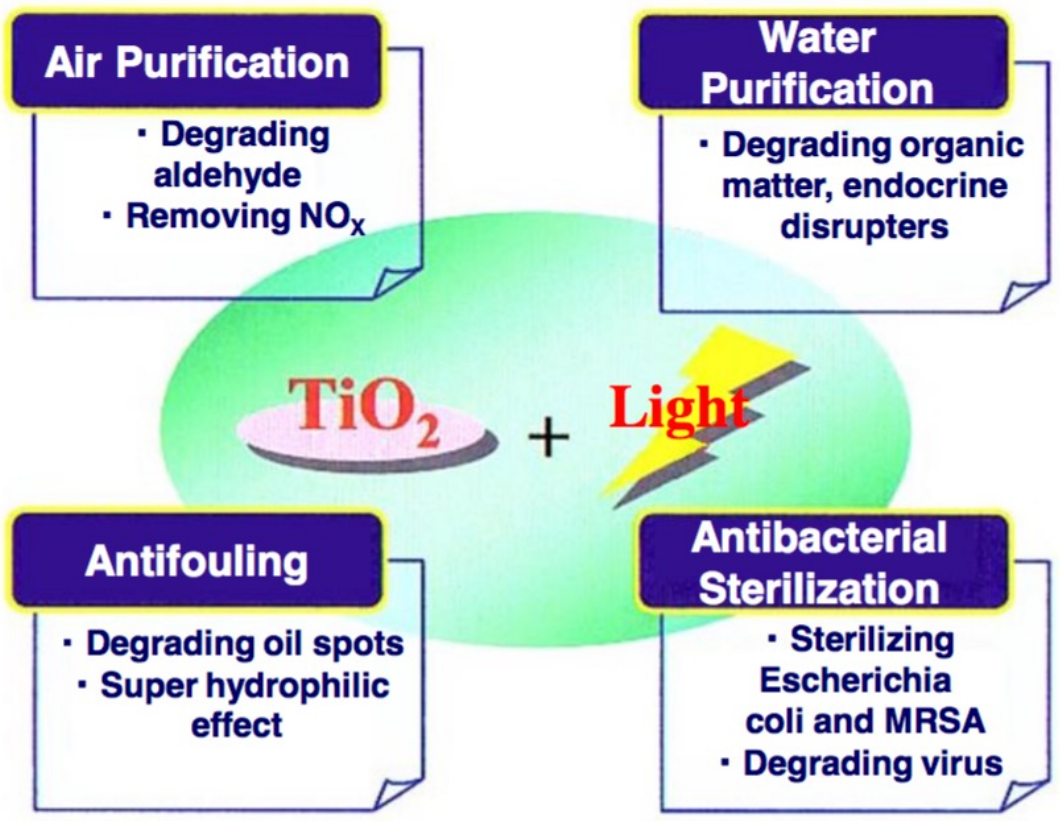

Fig.1 Area of Photocatalyst

Reprinted from "Foster Sensitivity – A Suggestion to Educational Problem from Scientist", Akira Fujishima p19

Degradation of Bacteria

First result

Sterilization

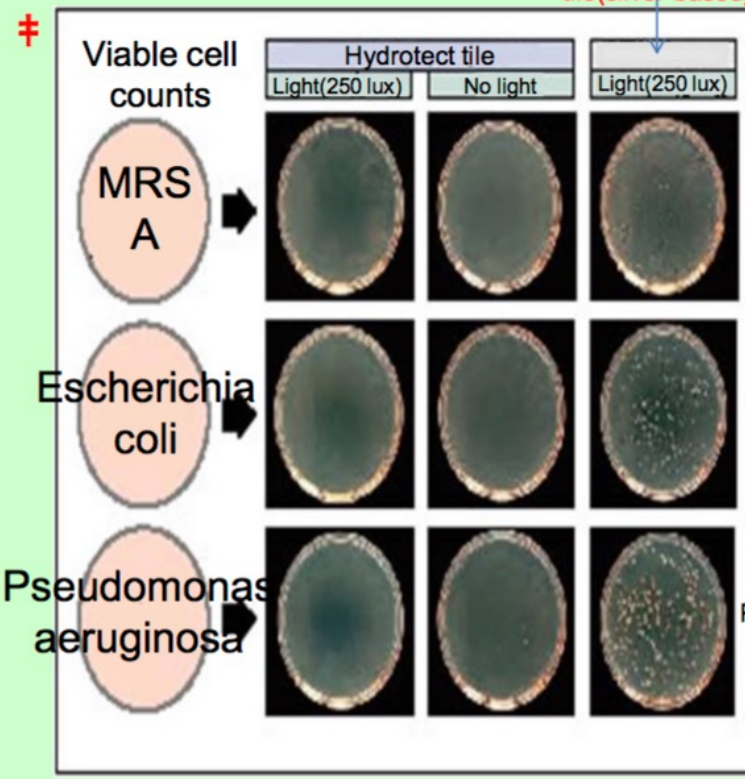

Antimicrobial tile(sliver-based)

Time required to kill bacteria of 99.9% or above(approx)

	Hydrotect tile		
	Light (250 lux)	No light	Light (250 lux)
MRS A	30 min	1 hour	* 24 hours
Escherichia coli	30 min	1 hour	18 hours
Pseudomonas aeruginosa	30 min	1 hour	18 hours

*only 5.5% of bacteria were killed in 24 hours in case of sliver-based antimicrobial tile

Courtesy of TOTO Ltd.

Photocatalyst Filter

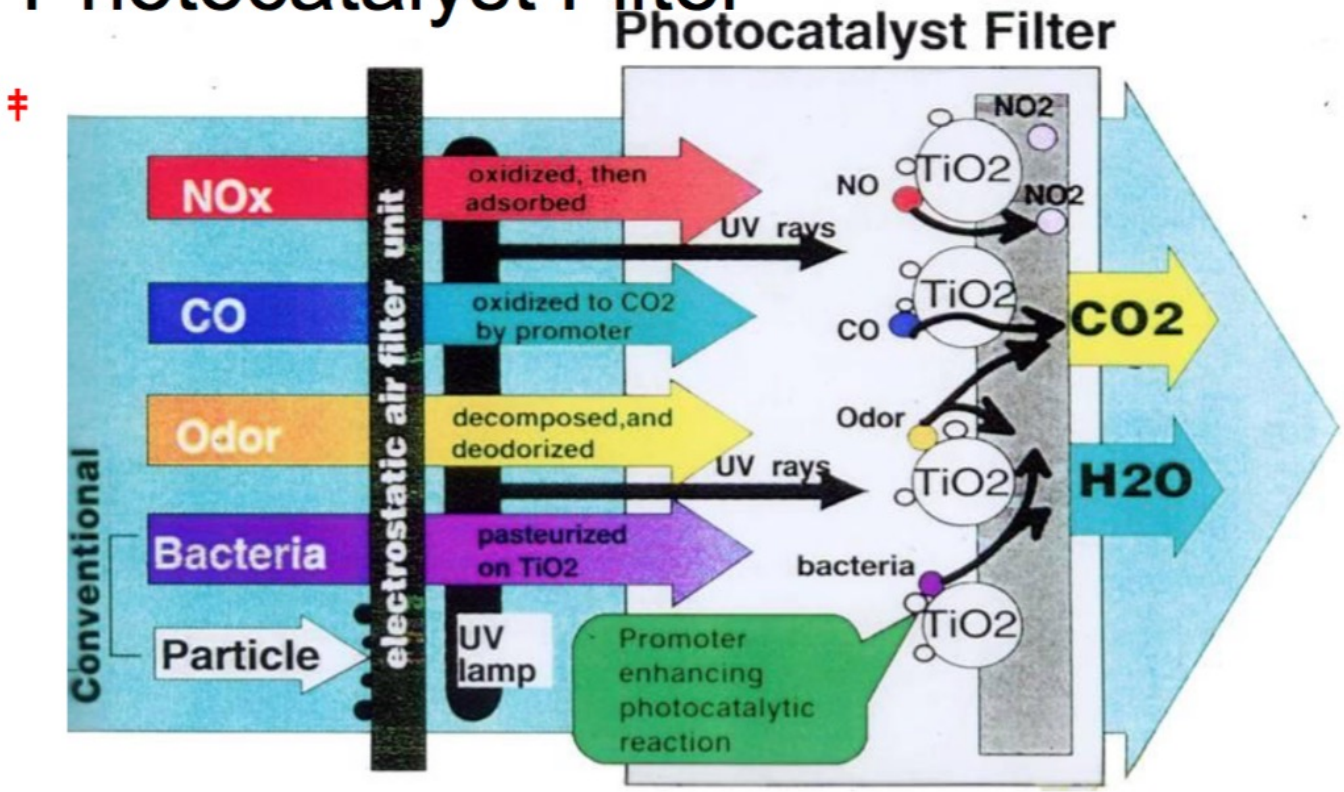

Deodorizing, Sterilization, Degradation

Reprinted from "Foster Sensitivity – A Suggestion to Educational Problem from Scientist", Akira Fujishima p15

Nano-Catalyst Synthesized by Flame Spray Pyrolysis (FSP) for visible light Photocatalysis

A dissertation submitted to the Division of Research and
Advanced Studies of the University of Cincinnati

In partial fulfillment of the
requirement for the degree of

DOCTOR OF PHILOSOPHY

In the Chemical Engineering Program of School of Energy, Environmental, Biological and Medical Engineering

by

Siva Nagi Reddy Inturi

Committee:

Professor Panagiotis (Peter) G. Smirniotis (Chair)

Professor Makram Suidan

Professor Vesselin Shanov

Professor Gregory Beaucage

Assoc. Professor Anastasios Angelopoulos

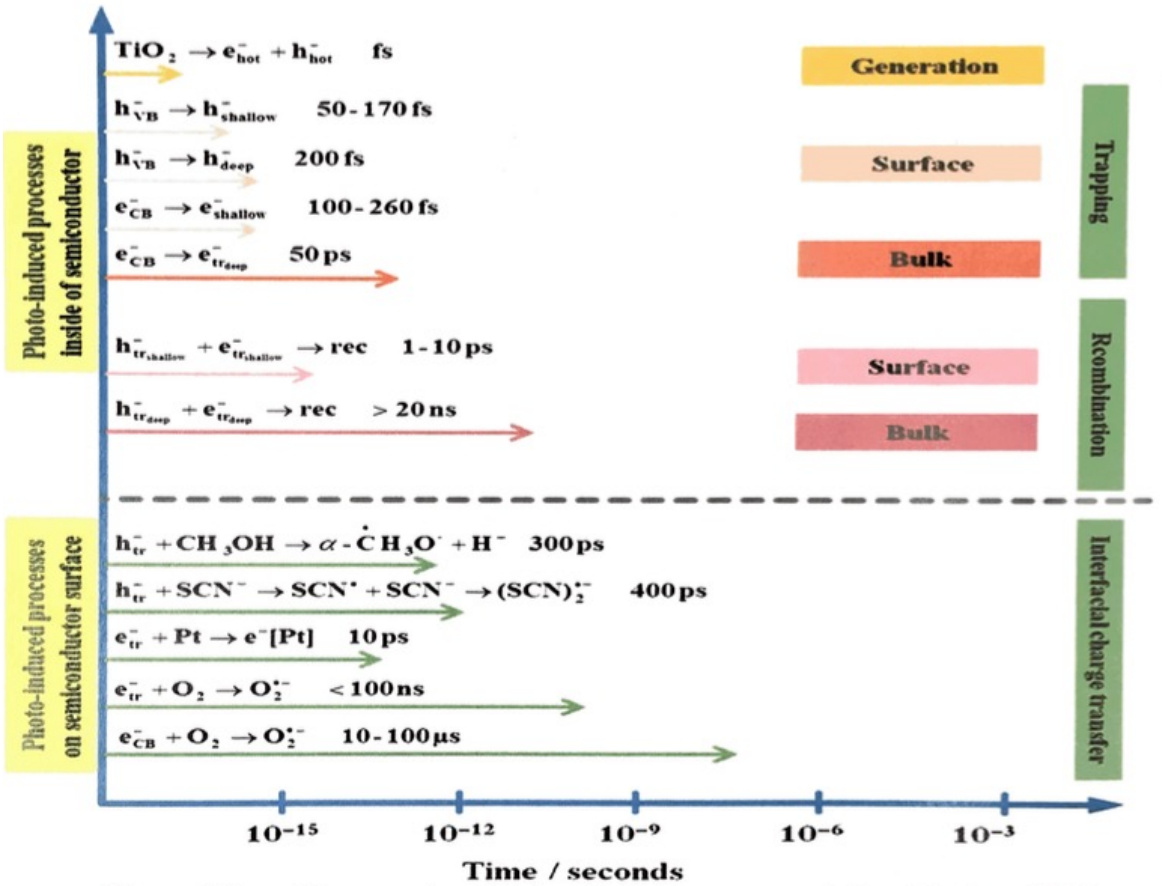

Figure 1.2: The general mechanism for heterogeneous photocatalysis on TiO2.

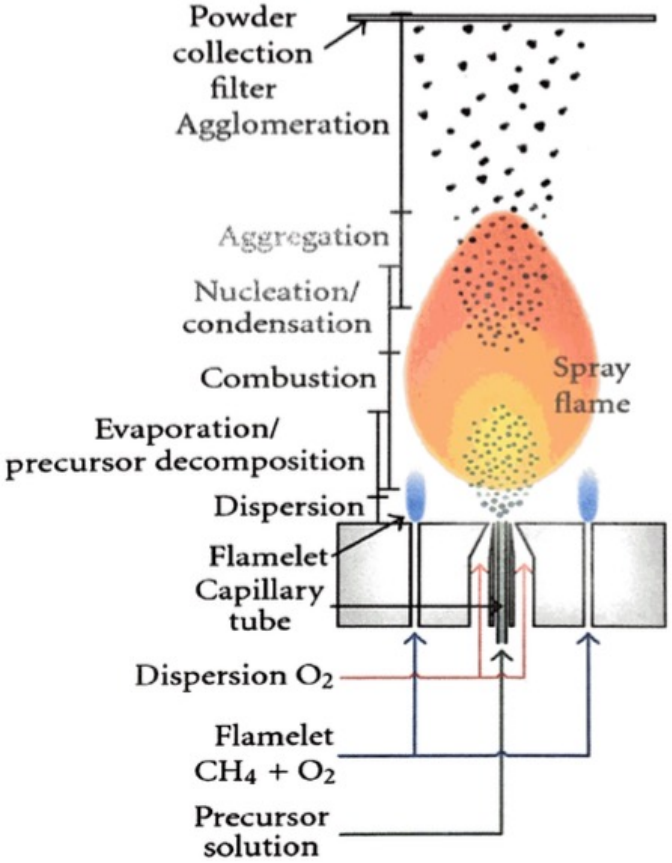

Table 2-5: Photocatalytic activity of the catalyst used in the present study

Catalyst	Absorption region	Band gap (eV)	K_A ($m^3g^{-1}s^{-1}$)
P25	UV	3.11	0.051
FSP TiO_2	UV	3.08	0.098
Ce/TiO_2	UV	3.13	0.014
Co/TiO_2	Visible	2.54	0.021
Cr/TiO_2	Visible	2.82	0.616
Cu/TiO_2	Visible	2.86	0.010
Fe/TiO_2	Visible	2.69	0.152
Mn/TiO_2	Visible	2.86	0.006
Mo/TiO_2	UV	3.19	0.004
Ni/TiO_2	Visible	2.37	0.019
V/TiO_2	Visible	2.63	0.165
Y/ TiO_2	UV	3.20	0.004
Zr/TiO_2	UV	3.21	0.008

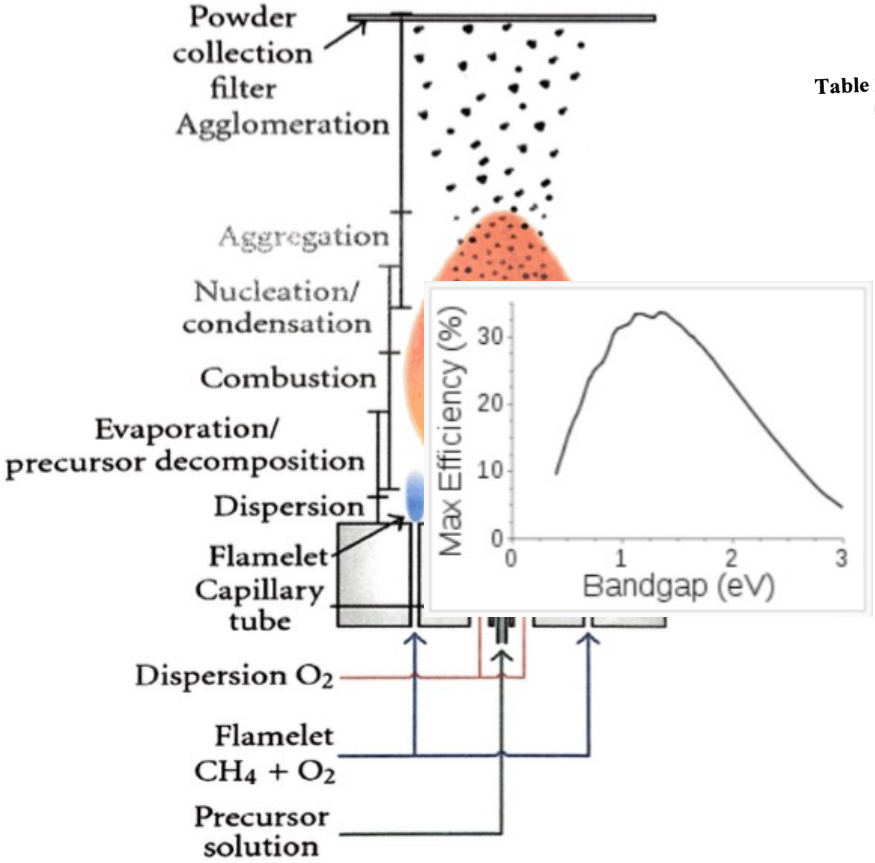

Table 2-5: Photocatalytic activity of the catalyst used in the present study

Catalyst	Absorption region	Band gap (eV)	K_A ($m^3g^{-1}s^{-1}$)
P25	UV	3.11	0.051
FSP TiO_2	UV	3.08	0.098
Ce/TiO_2	UV	3.13	0.014
Co/TiO_2	Visible	2.54	0.021
Cr/TiO_2	Visible	2.82	0.616
Cu/TiO_2	Visible	2.86	0.010
Fe/TiO_2	Visible	2.69	0.152
Mn/TiO_2	Visible	2.86	0.006
Mo/TiO_2	UV	3.19	0.004
Ni/TiO_2	Visible	2.37	0.019
V/TiO_2	Visible	2.63	0.165
Y/ TiO_2	UV	3.20	0.004
Zr/TiO_2	UV	3.21	0.008

Solar Thermolysis

Titania Catalyst (http://www.youtube.com/watch?v=8kJqsDh8cs0)

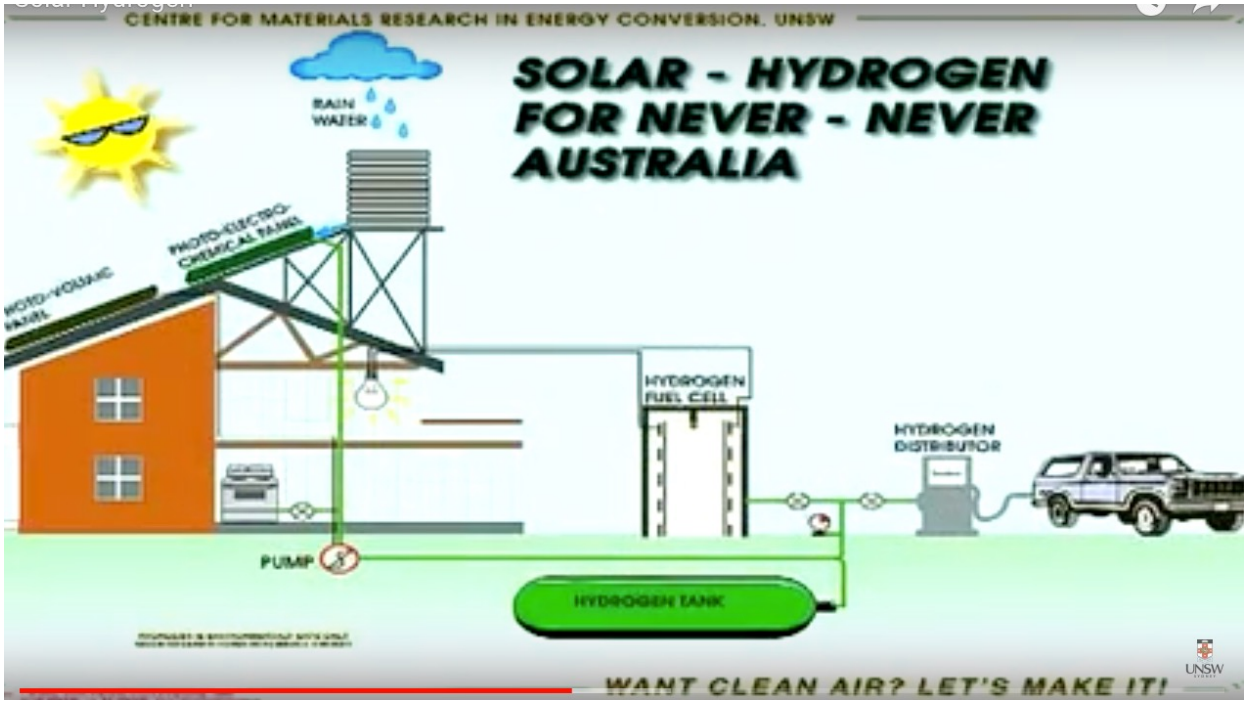

Solar Thermolysis

Titania as a photocatalyst

http://www.mvt.ovgu.de/mvt_media/Vorlesungen/VO_ENAP/Folien_ENAP_10.pdf

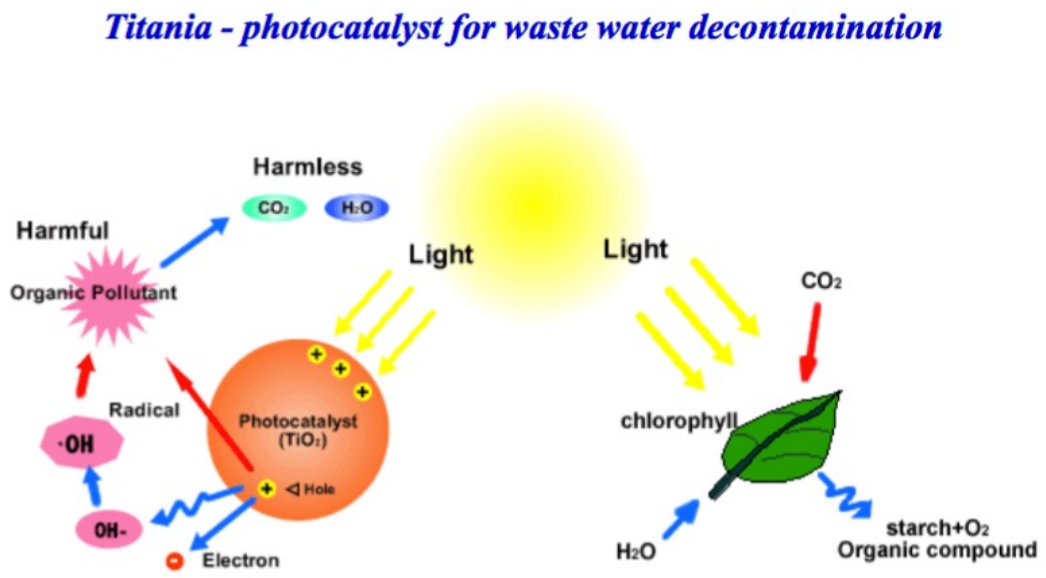

Solar Thermolysis

Titania as a photocatalyst https://cdn.intechopen.com/pdfs-wm/51861.pdf

Chapter 7

Concretes with Photocatalytic Activity

Magdalena Janus and Kamila Zając

Additional information is available at the end of the chapter

http://dx.doi.org/10.5772/64779

Solar Thermolysis

Titania as a photocatalyst

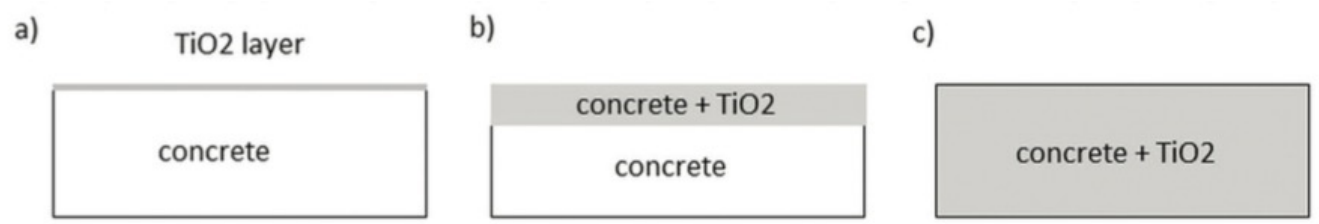

Figure 2. Scheme of possible ways for concrete modification by photocatalysts.

Solar Thermolysis

Titania as a photocatalyst

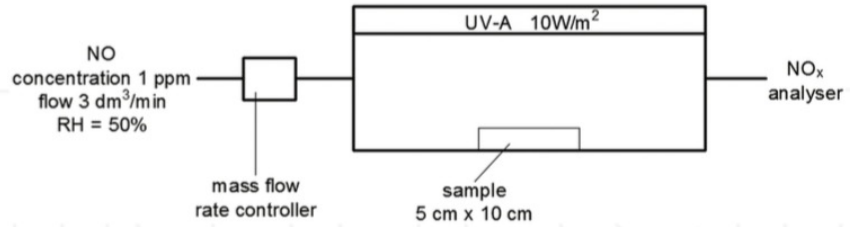

Figure 3. Photoreactor according to ISO 22197-1.

Figure 4. Separate parking lanes at the Leien of Antwerp with photocatalytic pavement blocks [15].

Solar Thermolysis

Titania as a photocatalyst

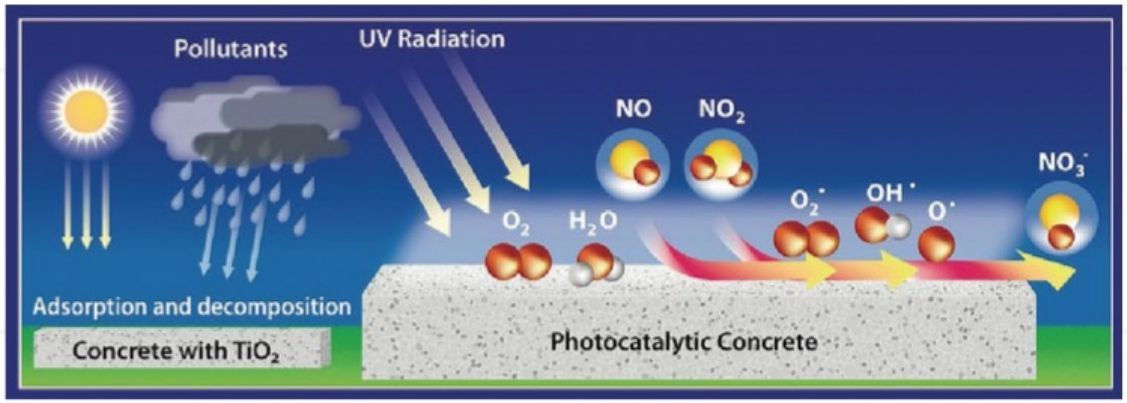

Figure 6. Scheme of photocatalytic air purifying pavement [15].

Solar Thermolysis

Titania as a photocatalyst

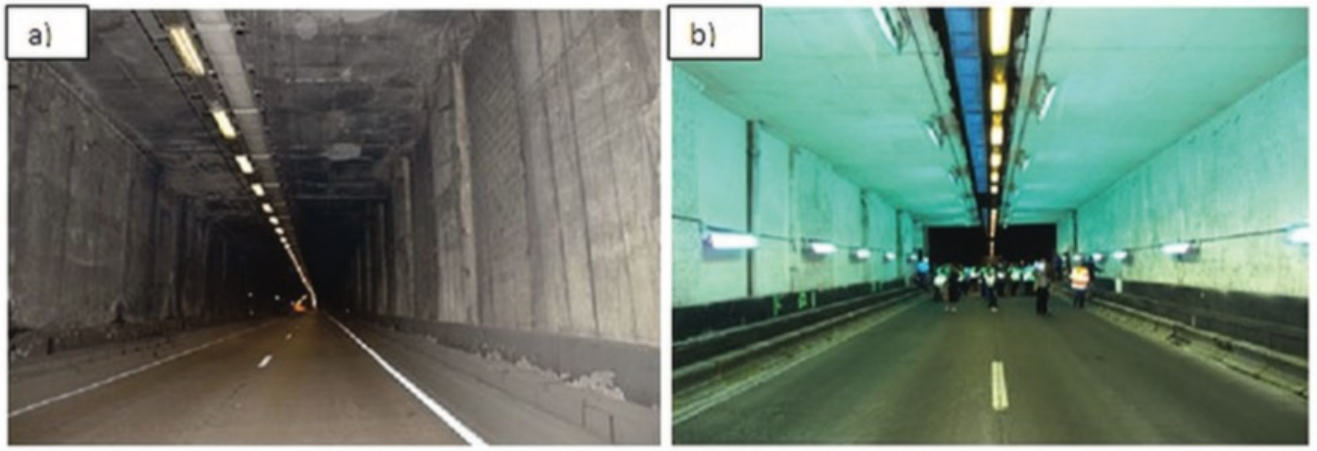

Figure 7. Inside view of test site within Leopold II tunnel in Brussels **(a)** before renovation, **(b)** after renovation with using photocatalytic walls [15].

Solar Thermolysis

Titania as a photocatalyst

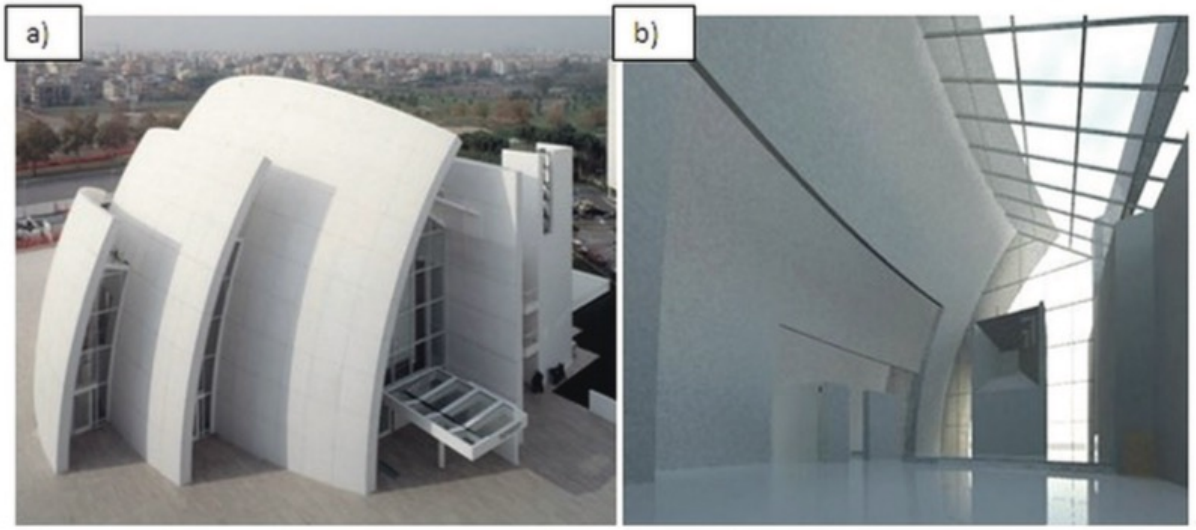

Figure 8. Dives in Misericordia Church in Rome **(a)**, zoom insight **(b)** [41].

Titania as a photocatalyst

[42, 43]. It is impressive that according to Fujishima and Zhang [44] by 2003, self-cleaning TiO_2-based tiles had been used in over 5000 buildings in Japan. Among them the most famous is the Maru Building, located in Tokyo's main business district.

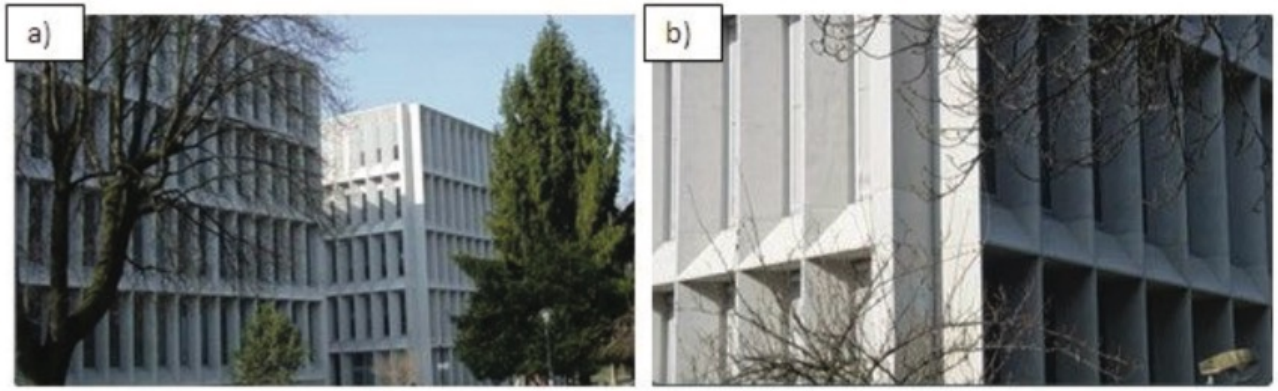

Figure 9. Cité de la Musique et des Beaux- Arts in Chambéry [45].

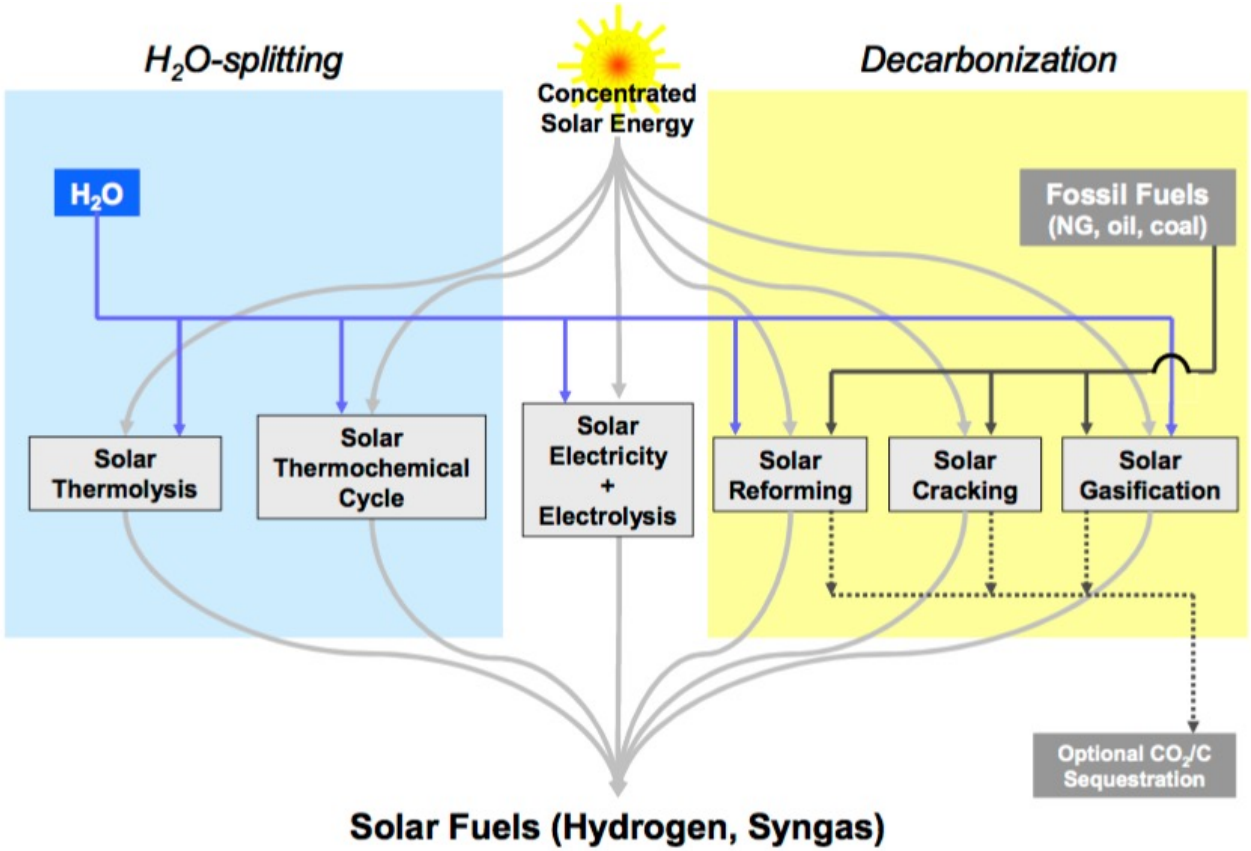

Fig. 2: Thermochemical routes for solar hydrogen production – Indicated is the chemical source of H_2: H_2O for the solar thermolysis and the solar thermochemical cycles; fossil fuels for the solar cracking, and a combination of fossil fuels and H_2O for the solar reforming and gasification. For the solar de-carbonization processes, optional CO_2/C sequestration is considered. All of those routes involve energy consuming (endothermic) reactions that make use of concentrated solar radiation as the energy source of high-temperature process heat. Adapted from [1,2].

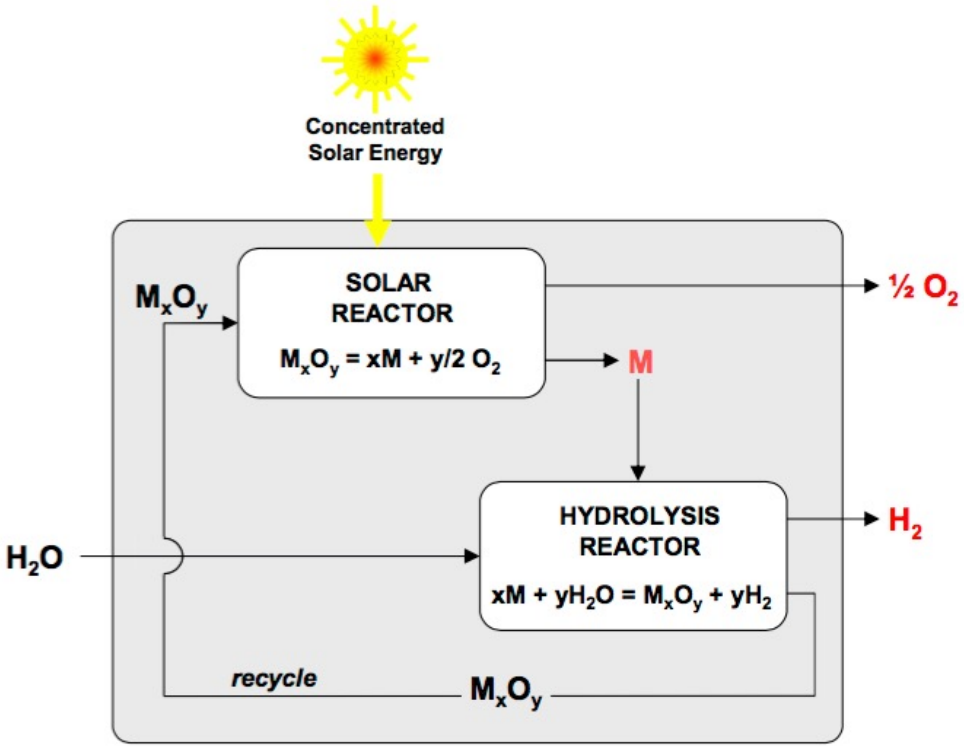

Fig. 3: Thermochemical route based on metal oxide redox reactions – The first step of the cycle is the solar thermal release of O_2 from the metal oxide (M_xO_y). This step requires very high temperatures. The second step is the reaction of the metal (M) with H_2O to form H_2 and the corresponding M_xO_y. This step proceeds at lower temperatures and does not require additional heating in some cases. Since H_2 and O_2 are formed in different steps, the need for high-temperature gas separation is thereby eliminated. This cycle was originally proposed for an iron oxide FeO/Fe_3O_4 redox system. Adapted from [1].

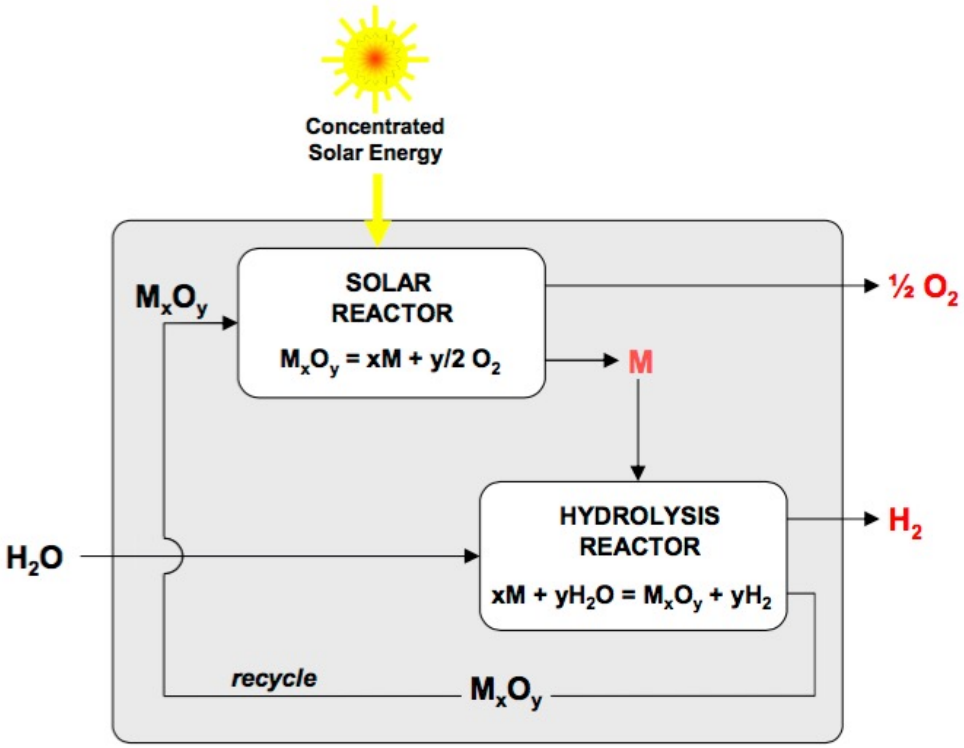

-FeO and Fe_3O_4 are solids
-The reactions proceed from the surface

-This is optimum for nanoparticle aerosols

-At high temperatures nanoparticles will coalesce into larger particles so the iron oxide is eventually consumed in the reaction

-How to make an aerosol of the particles in low enough concentration that they don't coalesce and high enough to get a reasonable yield

-How to make a continuous aerosol process of this type

International Journal of Energy and Power Engineering
2015; 4(1): 15-22
Published online January 27, 2015 (http://www.sciencepublishinggroup.com/j/ijepe)
doi: 10.11648/j.ijepe.20150401.13
ISSN: 2326-957X (Print); ISSN: 2326-960X (Online)

Hydrogen generation through cuprous chloride-hydrochloric acid electrolysis

Natarajan Sathaiyan[1, *], Venkataraman Nandakumar[1], Ganapathy Sozhan[2], Jegan Gandhibha Packiaraj[1], Elumalai Thambuswamy Devakumar[1], Damaraju Parvatalu[3], Anil Bhardwaj[3], Bantwal Narayana Prabhu[3]

[1]Electro Hydro Metallurgy Division, CSIR-Central Electro-Chemical Research Institute, Karaikudi, India
[2]Electro Inorganic Chemicals Division, CSIR-Central Electro-Chemical Research Institute, Karaikudi, India
[3]ONGC Energy Centre, IEOT, Panvel, Navi Mumbai, India

Email address:
enes@rediffmail.com (N. Sathaiyan)

To cite this article:
Natarajan Sathaiyan, Venkataraman Nandakumar, Ganapathy Sozhan, Jegan Gandhibha Packiaraj, Elumalai Thambuswamy Devakumar, Damaraju Parvatalu, Anil Bhardwaj, Bantwal Narayana Prabhu. Hydrogen Generation through Cuprous Chloride-Hydrochloric Acid Electrolysis. *International Journal of Energy and Power Engineering.* Vol. 4, No. 1, 2015, pp. 15-22. doi: 10.11648/j.ijepe.20150401.13

-Low temperatures and nontoxic
-Involves solid/liquid transitions
-Requires electrolysis
-Requires pressure and vacuum

$$2CuCl{\cdot}nH_2O(aq) + 2HCl{\cdot}mH_2O(aq) \rightarrow 2CuCl_2{\cdot}(n+m)H_2O(aq) + H_2(g), \quad \text{electrolysis}(25\text{–}80^\circ C) \qquad [1]$$

$$2CuCl_2(s) + H_2O(g) \rightarrow CuCl_2{\cdot}CuO(s) + 2HCl(g), \quad \text{hydrolysis}(310\text{–}375^\circ C) \qquad [2]$$

$$CuCl_2{\cdot}CuO(s) \rightarrow 2CuCl(s) + (1/2)O_2(g), \quad \text{decomposition}(450\text{–}530^\circ C) \qquad [3]$$

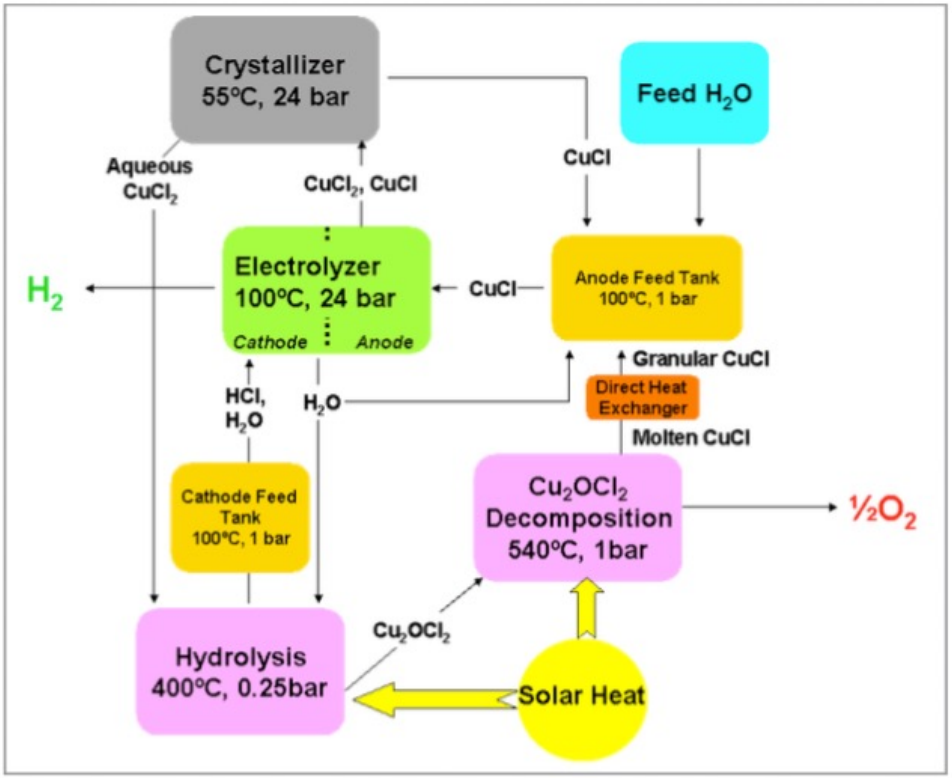

Figure 4.9.2. Hy-CuCl conceptual block flow chart.

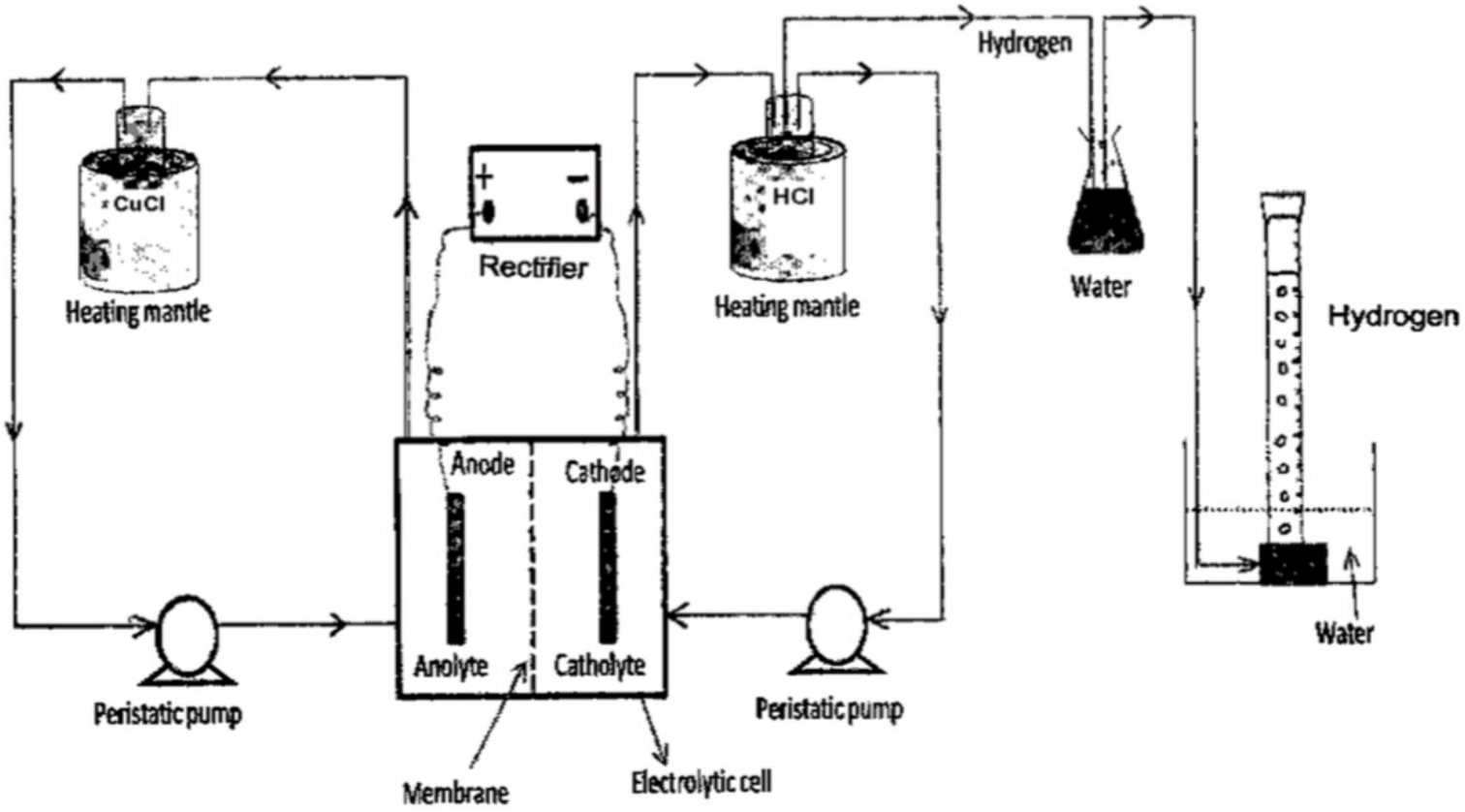

Fig 1. *Cell Set-Up for the hydrogen generation through CuCl-HCl electrolysis*

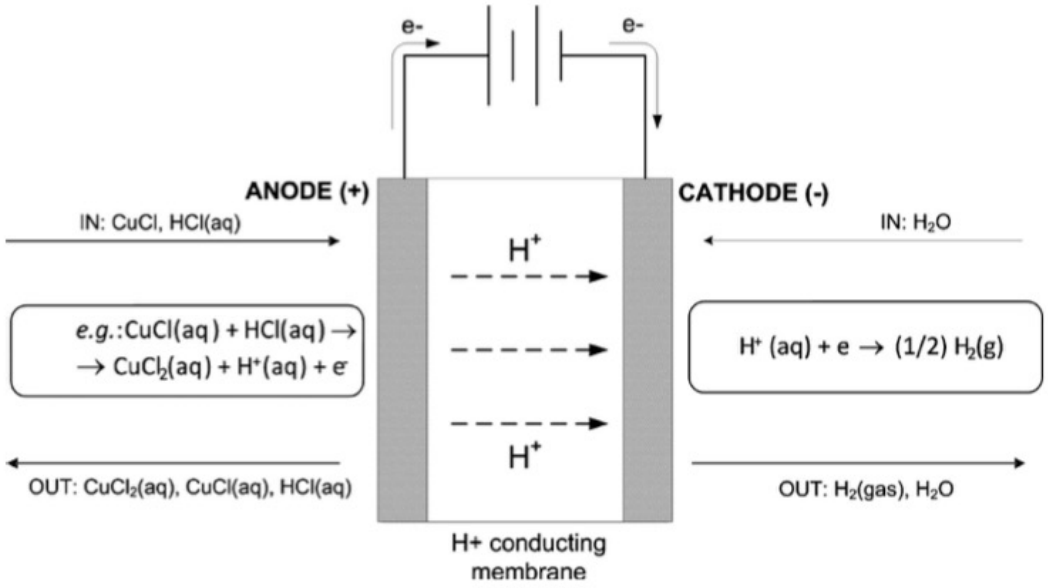

Figure 1. Conceptual scheme of the CuCl electrolysis in a cell with a proton-conducting membrane.

$NiFe_2O_4$

-Aerosol process

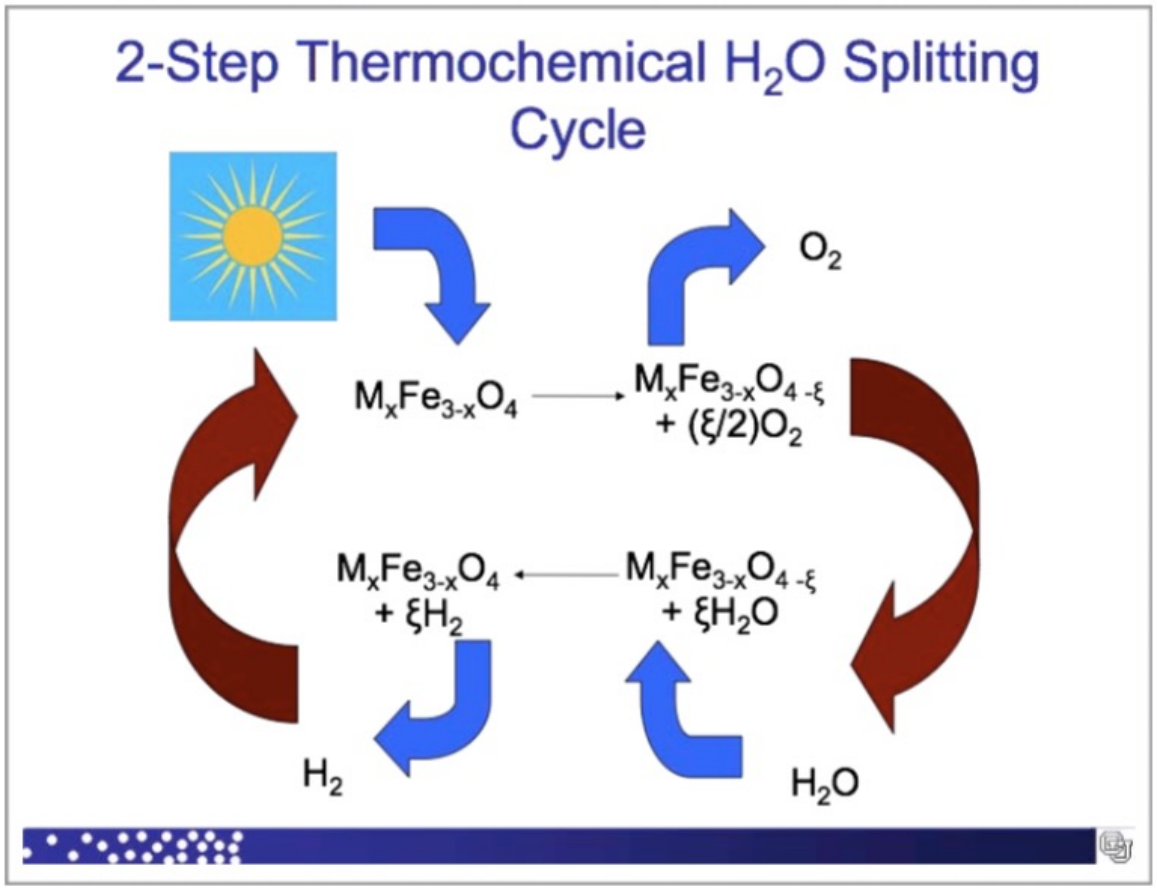

Figure 4.8.1. Schematic chemistry of a water-splitting ferrite cycle.

Mixed Iron Oxide Cycle. Other metal oxides such as manganese oxide or cobalt oxide, as well as mixed oxides redox pairs – mainly based on iron – have also been considered [17-20]. For example, a mixed iron oxide cycle was demonstrated within the European P&D project *HYDROSOL-2* [21]. Figure 5 depicts the monolithic dual chamber solar reactor. A quasi-continuous H_2 flow is produced by cyclic operation of the two reaction chambers through sequential oxidation and reduction steps at 800°C and 1200°C, respectively.

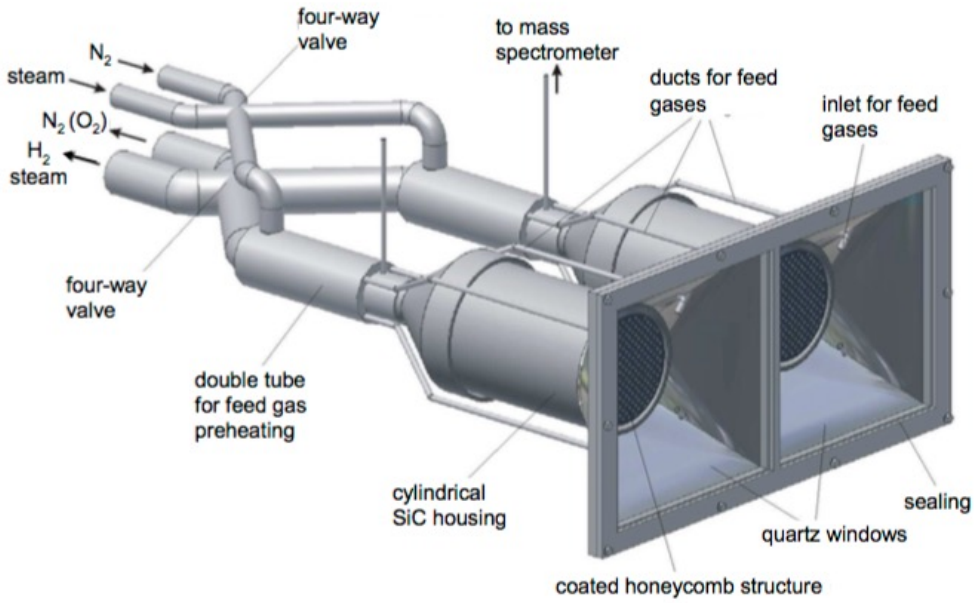

Fig. 5: Monolithic dual chamber solar receiver-reactor for continuous H_2 production – The concept features a closed receiver-reactor constructed from ceramic multi-channeled monoliths. Cyclic operation of the water-splitting and regeneration steps is established in two reaction chambers. Their individual temperature levels are controlled by focusing and defocusing heliostats. Adapted from [21].

Semi-continuous production of H_2 with dual reactors.

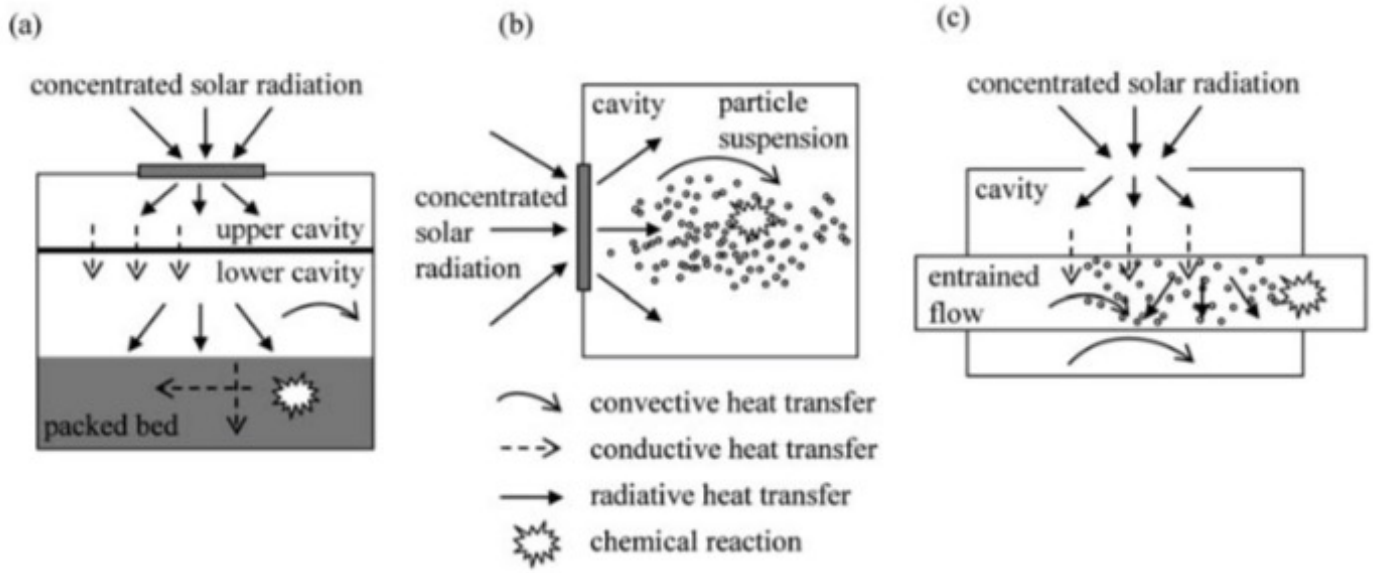

Fig. 10 Modeling schematics for the three solar reactor concepts: (a) indirectly irradiated packed-bed; (b) directly irradiated vortex-flow, and (c) indirectly irradiated entrained flow.

Directly irradiated vortex-flow reactor

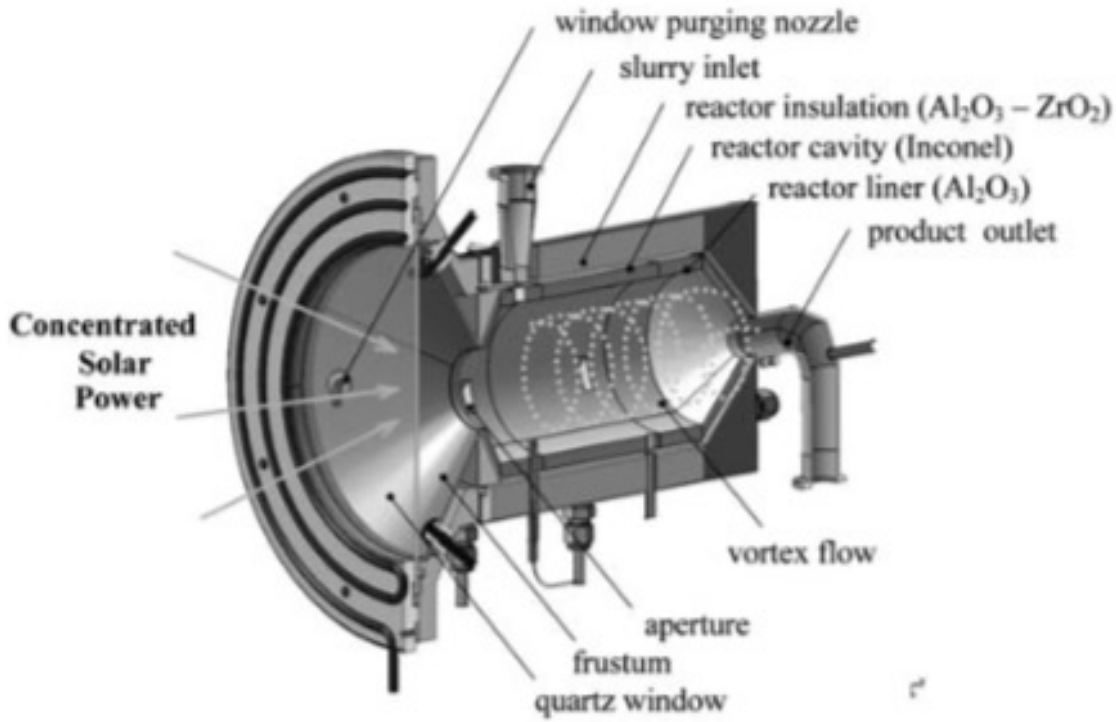

Fig. 6 Scheme of the directly irradiated vortex-flow solar reactor configuration, featuring a helical flow of carbonaceous particles and steam confined to a cavity-receiver and directly exposed to concentrated solar radiation.

Indirectly irradiated packed-bed reactor

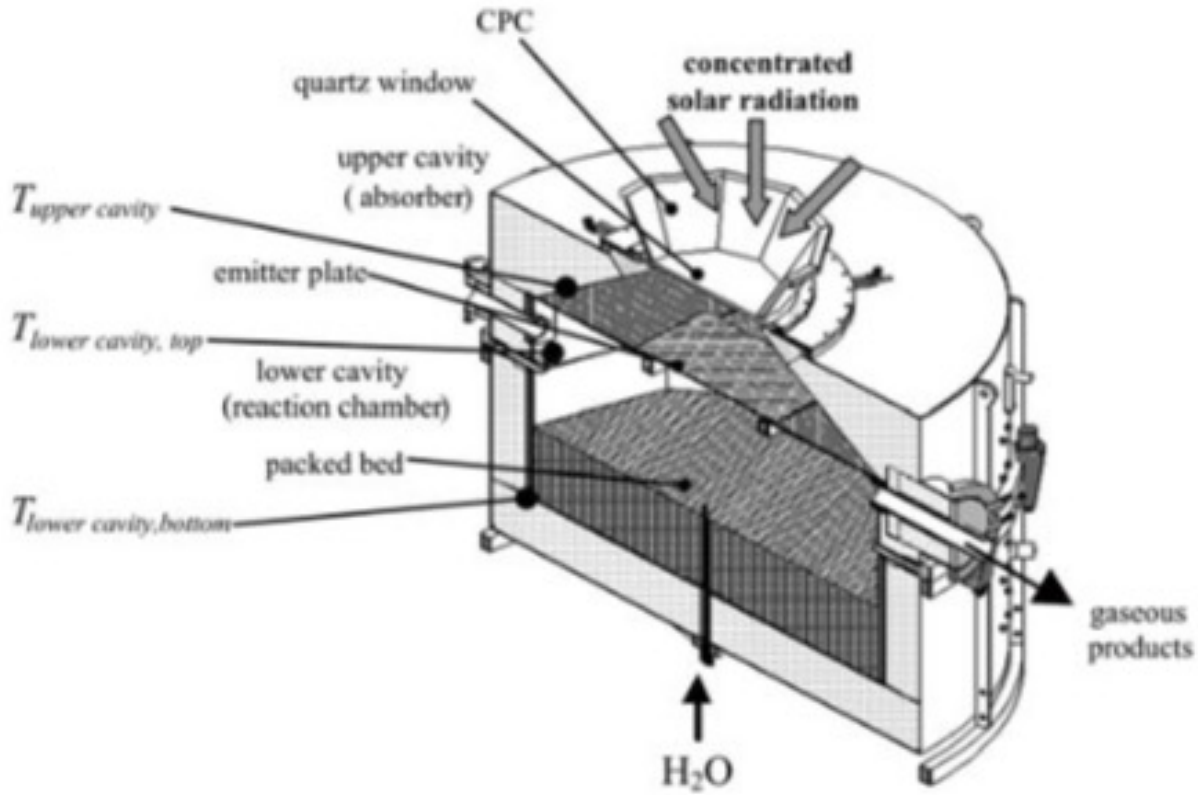

Fig. 4 Scheme of the indirectly irradiated packed-bed solar reactor configuration, featuring two cavities separated by an emitter plate, with the upper one serving as the radiative absorber and the lower one containing the reacting packed bed that shrinks as the reaction progresses.

Indirectly irradiated entrained-flow reactor

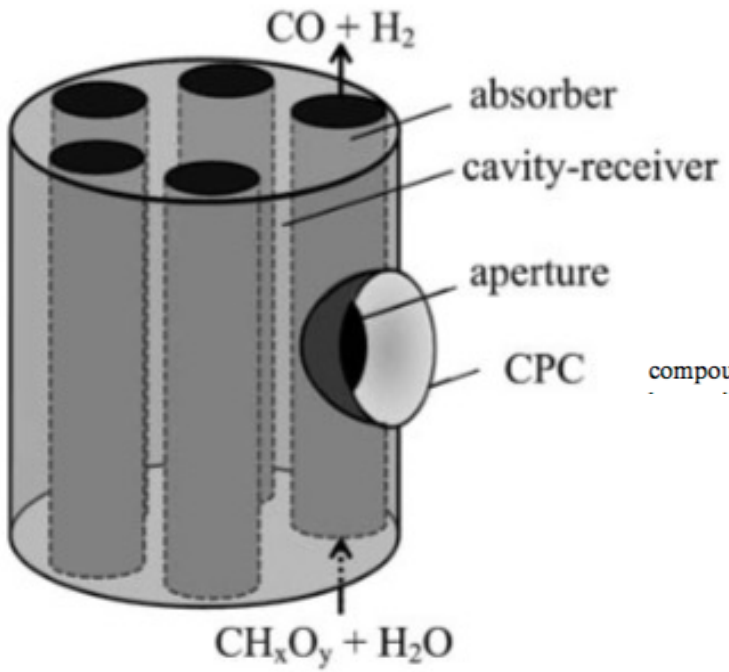

compound parabolic concentrators (CPCs[31])

Fig. 8 Scheme of the indirectly irradiated entrained-flow solar reactor configuration, featuring a cylindrical cavity-receiver containing an array of tubular absorbers through which a continuous flow of water vapor laden with carbonaceous particles reacts to form syngas.

Solar Reduction/Oxidation Reactions

-Ceria Oxide system
-Use a nano/micro felt rather than an aerosol
-Use a batch operation
-Couple reduction of water and reduction of CO_2

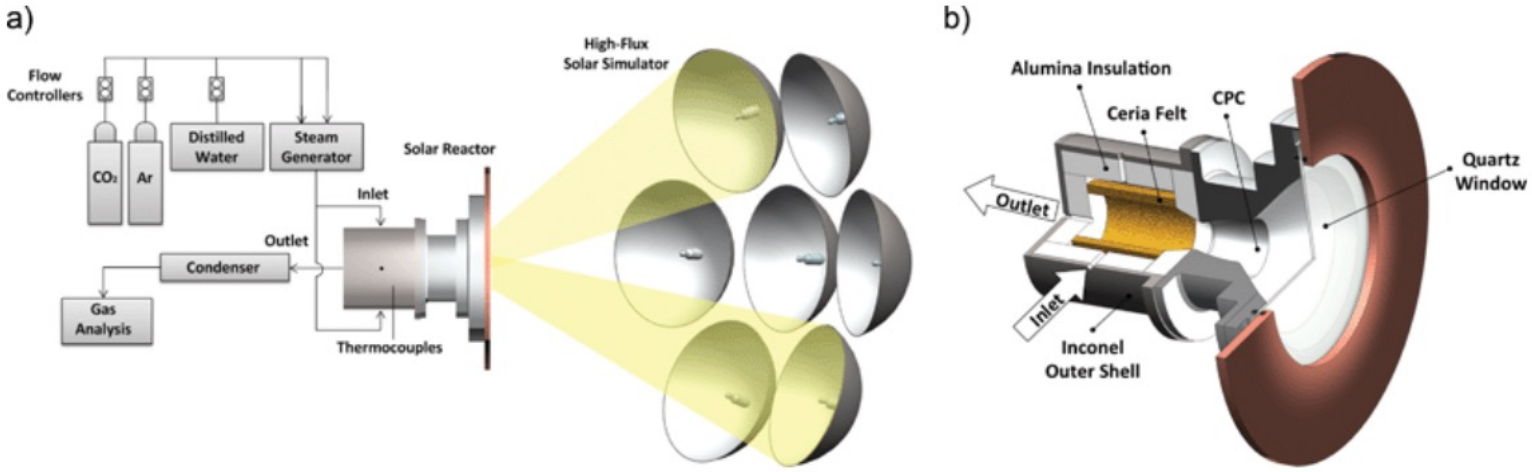

Fig. 1 (a) Experimental setup of ETH's High-Flux Solar Simulator and (b) schematic of the solar reactor configuration.

Paper on ETHZ's program in solar redox

Solar Reduction/Oxidation Reactions

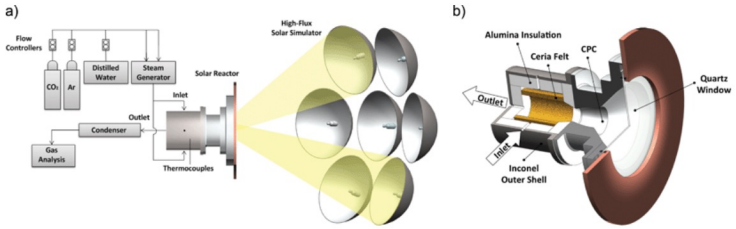

Fig. 1 (a) Experimental setup of ETH's High-Flux Solar Simulator and (b) schematic of the solar reactor configuration.

2000K

$$\text{High-T reduction: } CeO_2 \xrightarrow{\Delta H} CeO_{2-\delta} + \frac{\delta}{2} O_2 \quad (1)$$

$$\text{Low-T oxidation with } H_2O\text{: } CeO_{2-\delta} + \delta H_2O \rightarrow CeO_2 + \delta H_2 \quad (2)$$

1000K

$$\text{Low-T oxidation with } CO_2\text{: } CeO_{2-\delta} + \delta CO_2 \rightarrow CeO_2 + \delta CO \quad (3)$$

Solar Reduction/Oxidation Reactions

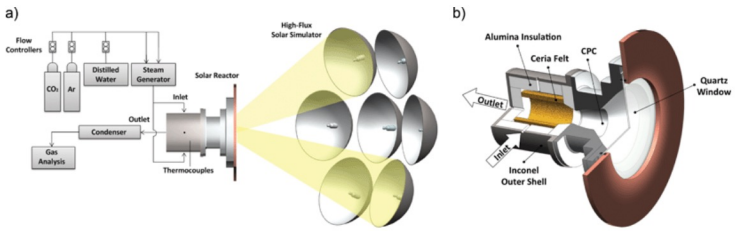

Fig. 1 (a) Experimental setup of ETH's High-Flux Solar Simulator and (b) schematic of the solar reactor configuration.

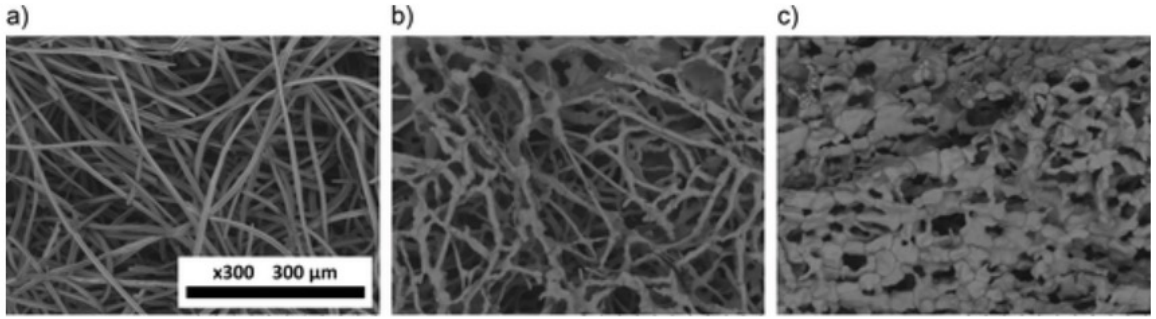

Fig. 6 (a) SEM micrographs of unreacted ceria felt, (b) the outermost surface of the ceria felt, and (c) the innermost ceria felt after the experimental campaign.

Solar Reduction/Oxidation Reactions

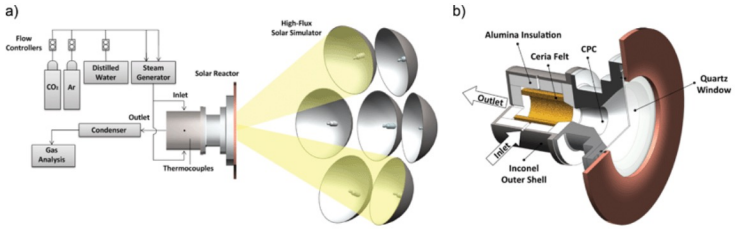

Fig. 1 (a) Experimental setup of ETH's High-Flux Solar Simulator and (b) schematic of the solar reactor configuration.

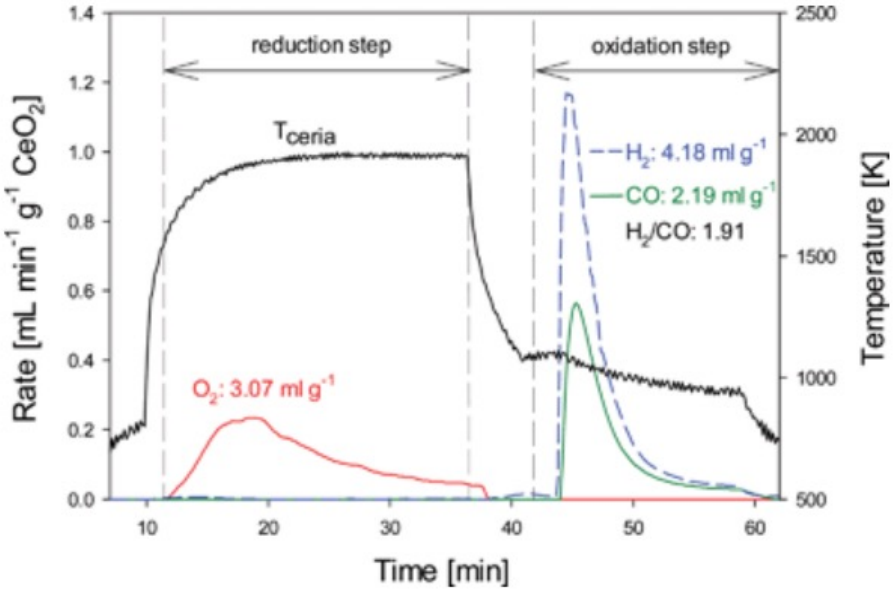

~2,000K and 1,000 K for the two reactions

Solar Reduction/Oxidation Reactions

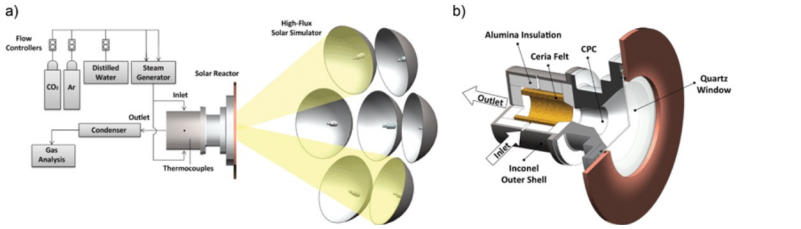

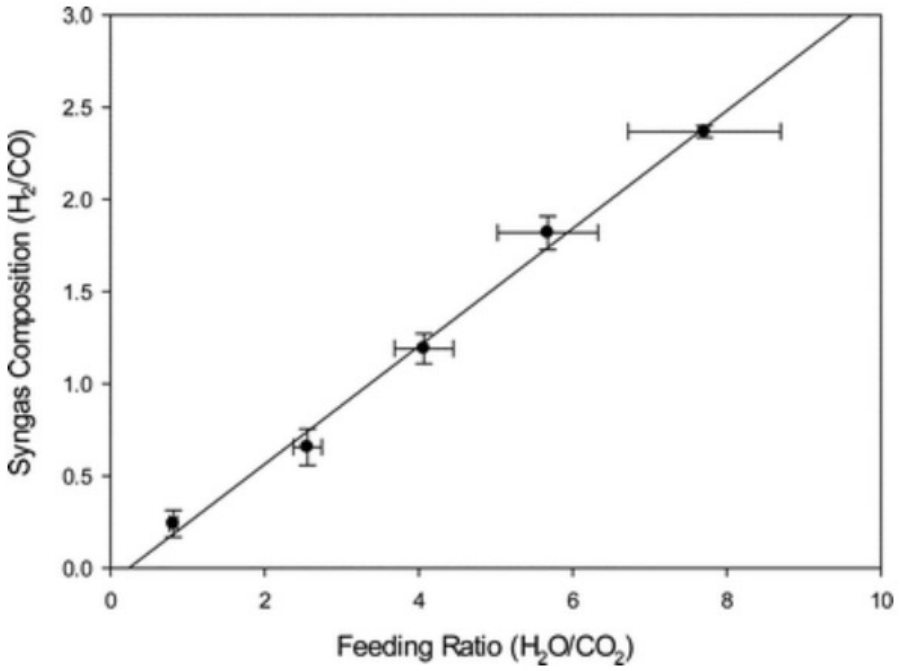

Solar Reduction/Oxidation Reactions

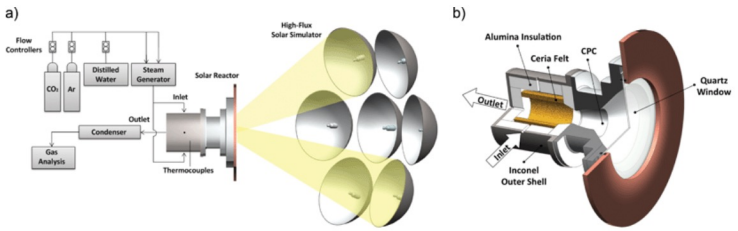

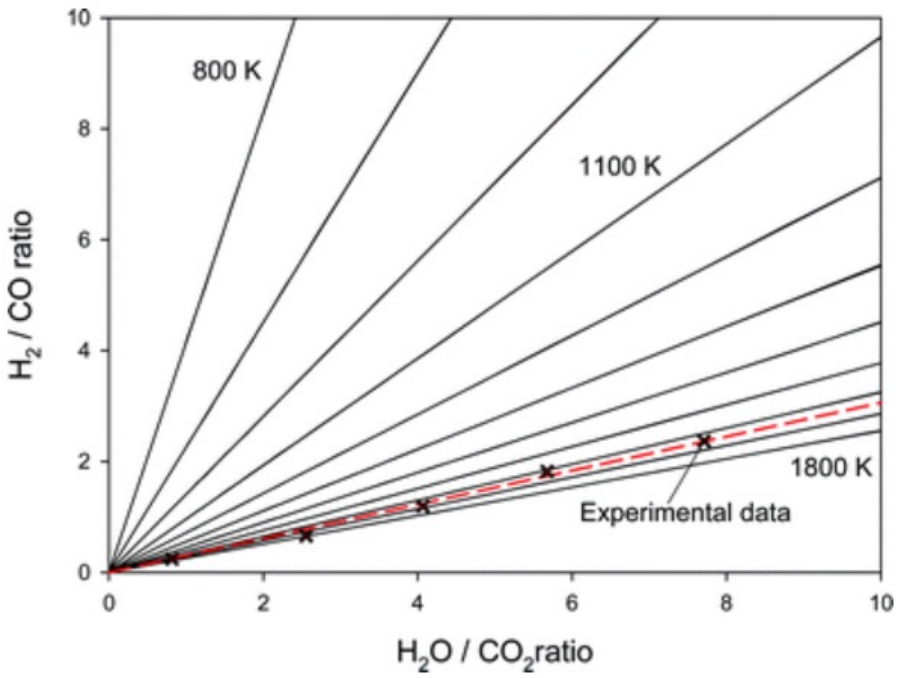

Lower Temperatures works for H_2 but not for CO

Solar Reduction/Oxidation Reactions

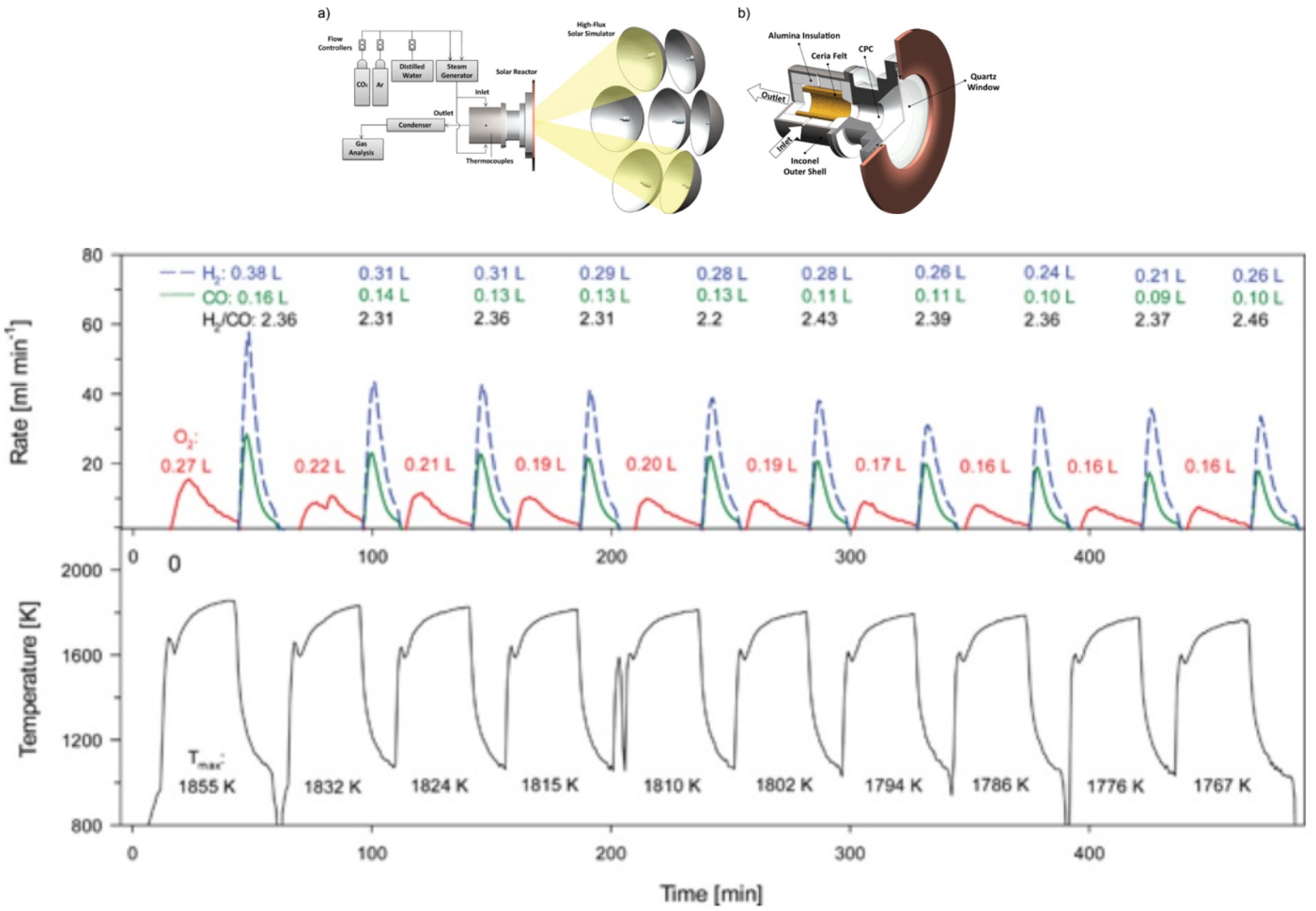

Solar Reduction/Oxidation Reactions

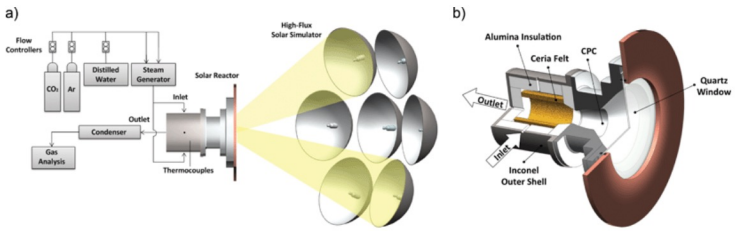

Fig. 1 (a) Experimental setup of ETH's High-Flux Solar Simulator and (b) schematic of the solar reactor configuration.

Calculation of Efficiency

$$\eta_{average} = \frac{\Delta H_{fuel} \int r_{fuel} dt}{\int P_{solar} dt + E_{inert} \int r_{inert} dt}$$

$$\eta_{peak} = \frac{2 r_{oxygen} \Delta H_{fuel}}{P_{solar} + r_{inert} E_{inert}}$$

One and Ten Cycles

	$n_{average}$	n_{peak}
One Cycle	15%	31%
Ten Cycles	9%	16%

20% is the target for commercial use (PV panel 15-20%)

But there are some advantages to H_2

-Similar temperatures to ceria oxide system

-Continuous aerosol process

Zn => ZnO Cycle (http://en.wikipedia.org/wiki/Zinc%E2%80%93zinc_oxide_cycle)

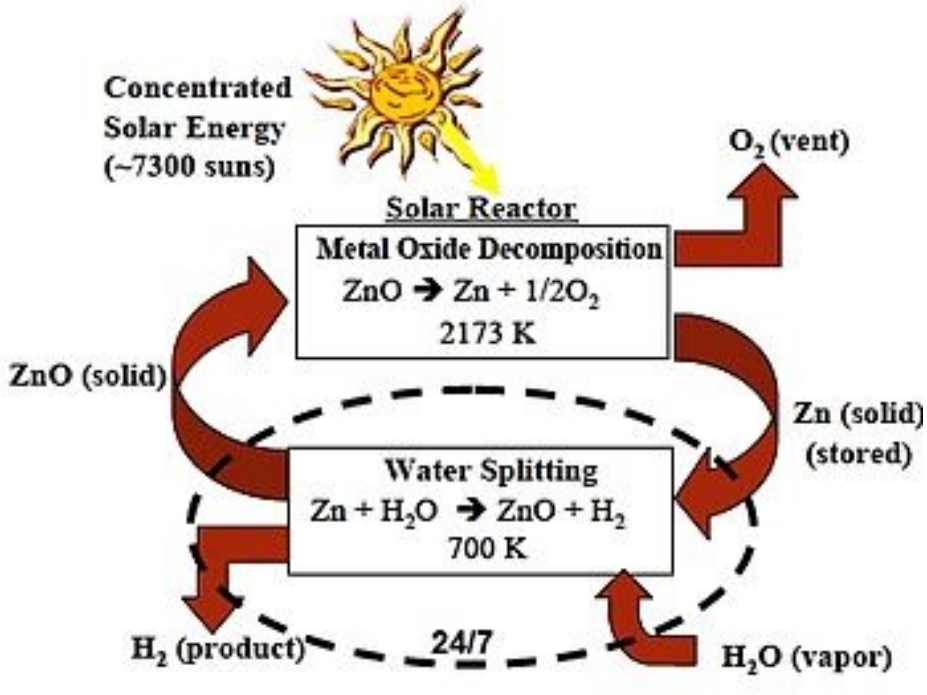

Overview of different redox reactions

UNLV (http://www.hydrogen.energy.gov/pdfs/review06/pd_10_weimer.pdf)

PSI/ETHZ (https://www.psi.ch/media/producing-pure-recycling-zinc-with-concentrated-solar-energy)

France Solar Furnace Talk (http://sfera.sollab.eu/downloads/Conferences/SolarPACES_2012_SFERA_Meier.pdf)

Zn => ZnO Cycle (http://en.wikipedia.org/wiki/Zinc%E2%80%93zinc_oxide_cycle)

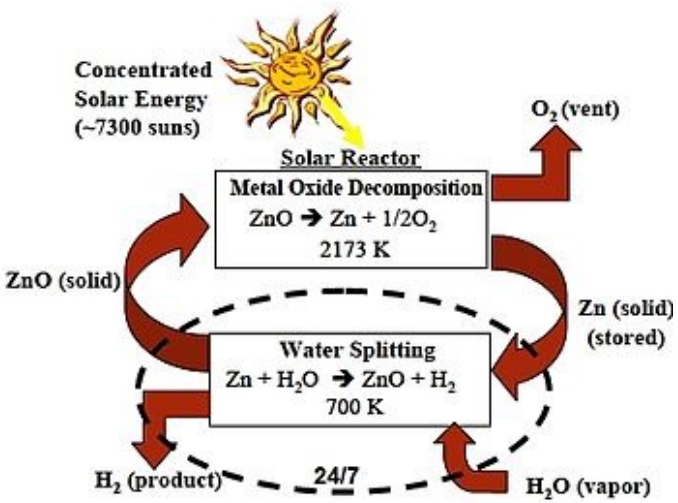

Aerosol Reactor

Zn => ZnO Cycle (http://en.wikipedia.org/wiki/Zinc%E2%80%93zinc_oxide_cycle)

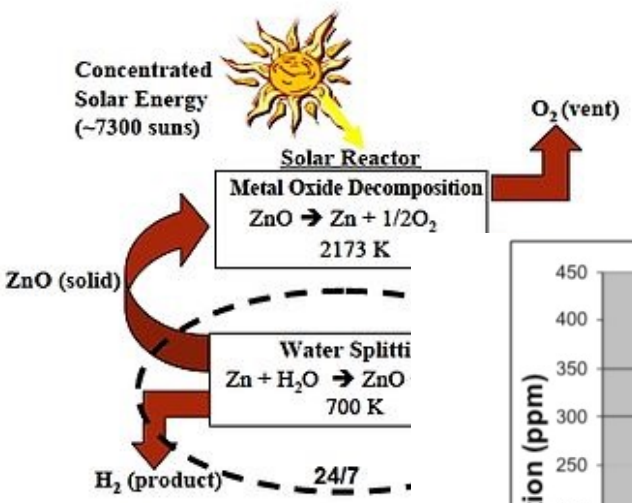

Reduction

$ZnO \rightarrow Zn + 1/2O_2$; 1600 °C; Al_2O_3 tube

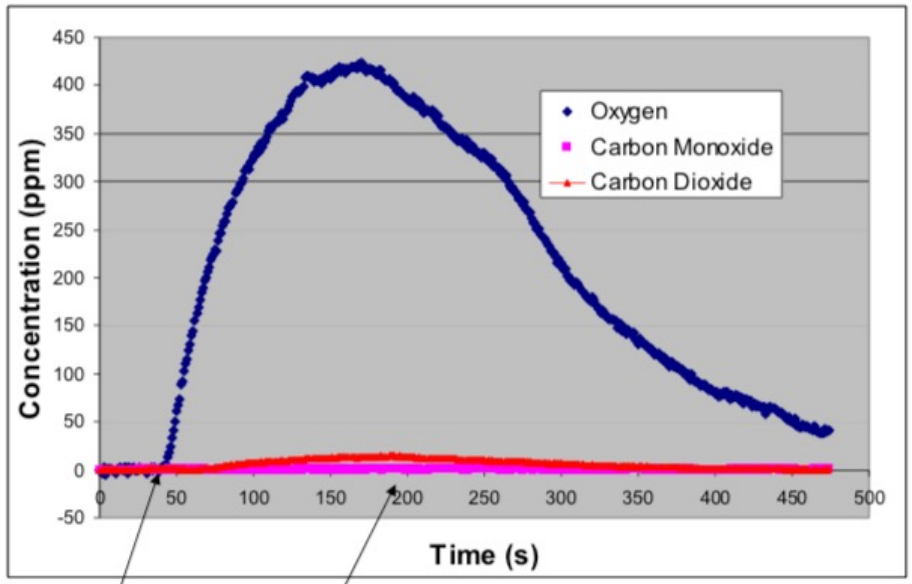

Feeding initiated Feeding stopped

- Demonstration of rapid (< 1s) ZnO dissociation for Zn/ZnO cycle
- Highest conversion ever (>40%) for thermal dissociation of ZnO
- Conversion consistent with kinetic model

Zn => ZnO Cycle (http://en.wikipedia.org/wiki/Zinc%E2%80%93zinc_oxide_cycle)

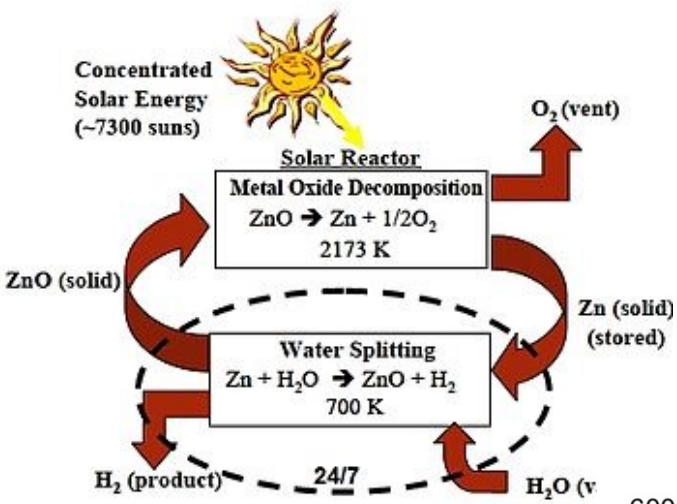

57 to 68 % Efficiency

Oxidation

$$Zn + H_2O \rightarrow ZnO + H_2$$

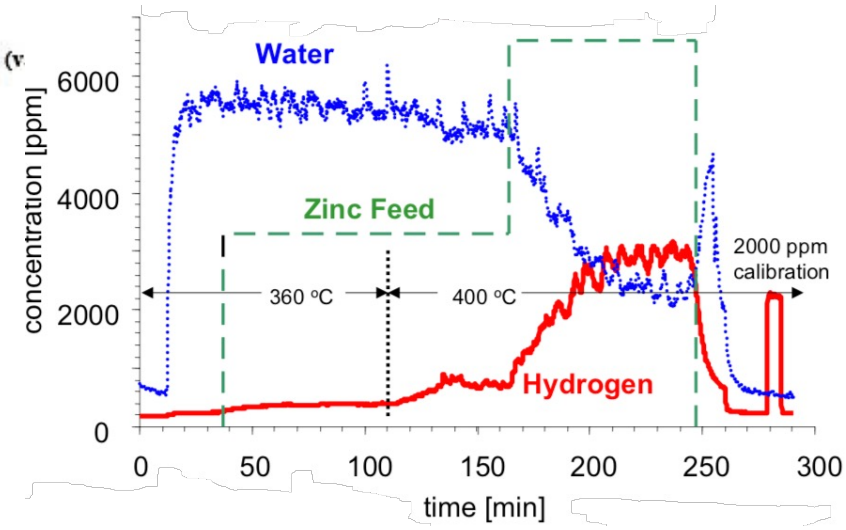

Swiss Aerosol Reactor ETHZ/PSI

Zn => ZnO Cycle
(Solar Driven Redox Reactions)

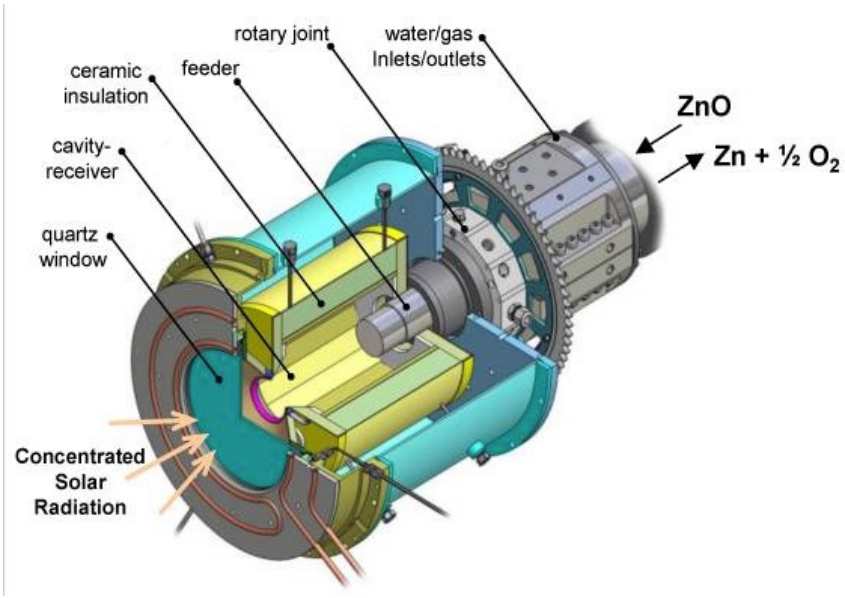

Need to rapidly quench and dilute Zn + O_2 mixture

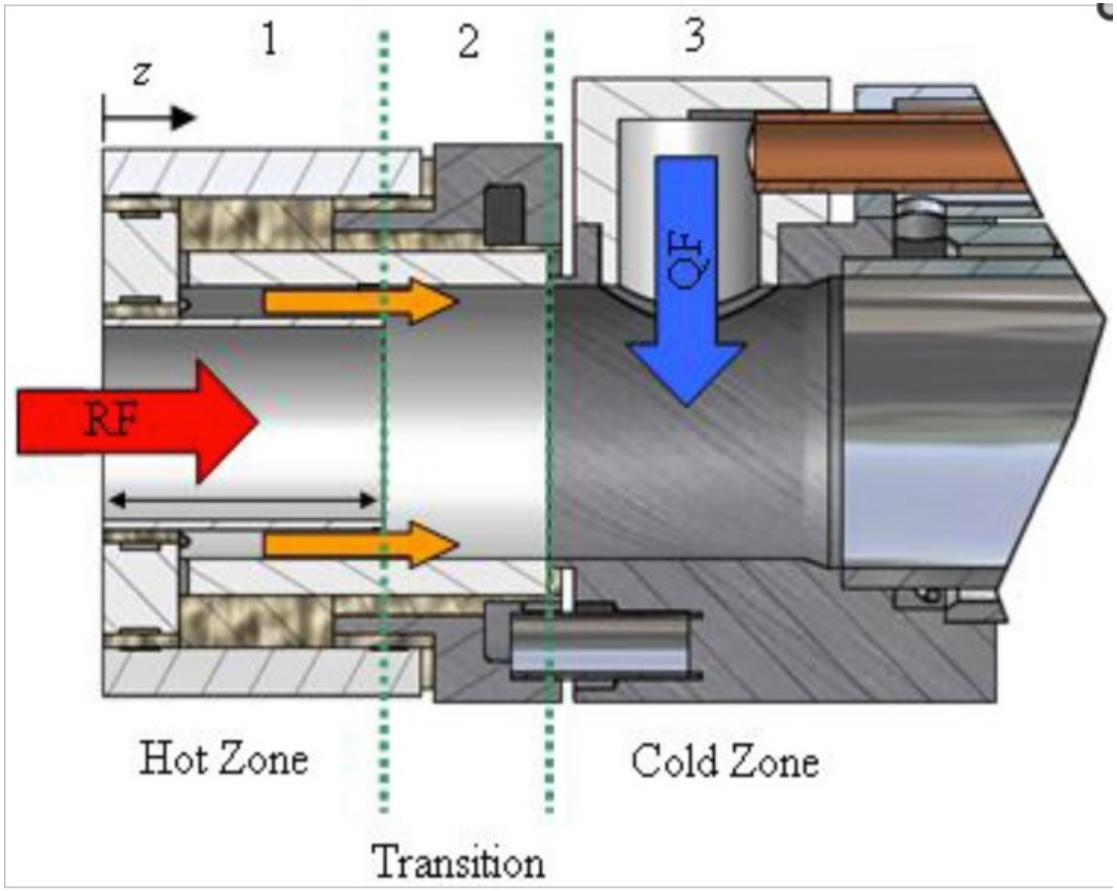

http://sfera.sollab.eu/downloads/Conferences/SolarPACES_2012_SFERA_Meier.pdf

Outline

100 kW Pilot Plant at MWSF

- Installation
- Commissioning

Scientific Background

- Solar ZnO dissociation at 2000 K
- Solar reactor technology

Experimental Results

- Solar reactor experiments
- Flux measurements

Outlook / Acknowledgements

CNRS 1 MW Solar Furnace
Odeillo, France

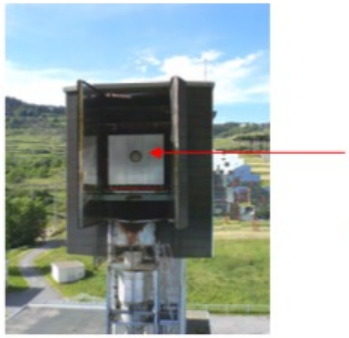

Table 1. Major assumptions and findings for cost and efficiency of the Zn/ZnO cycle from Steinfeld [5] and Charvin et al. [22].

	Steinfeld ($792 kg/hr$)[5]	Charvin et al., ($250 kg/hr$)[22]	Charvin et al., ($50 kg/hr$)[22]
Plant size, energy and mass flows			
Concentration ratio, C	5,000 suns	5,000 suns	5,000 suns
Solar plant size (power input to solar reactor) [MW_{th}]	90	55	11
Beam irradiation [$kWh_{th}/m^2\,yr$)]	2300	2000	2000
Heliostat area [m^2]	155,172	54,800	10,960
Efficiencies			
Optical efficiency of solar concentration system, η_{optics}	58%	68.4%	not included
Cycle efficiency, η_{cycle}	29%	30.4%	not included
Global efficiency, η_{global}	17%	20.8%	not included
Assumptions			
Pump or work input	none	none	none
Solar step temperature [K]	2300	2000	2000
Reactor re-radiation losses	accounted for	accounted for	accounted for
Endothermic reaction losses	accounted for	accounted for	accounted for
Heat recovery from quenching after first step	no heat recovery	heat recovery	heat recovery
Recovery of heat of exothermic reaction	no heat recovery	complete heat recovery	complete heat recovery
Efficiency of separation of Zn & O_2	no recombination	20% recombination	20% recombination
Efficiency of hydrolysis step	complete hydrolysis	complete hydrolysis	complete hydrolysis
Hydrogen energy content [kJ/mol]	241(LHV)	286 (HHV)	286 (HHV)
Costs			
Heliostat field [M\$, assuming \$150/m^2]	23.28	8.22	1.65
Land [M\$, assuming \$1/m^2]	not included	0.28	0.06
Tower [M\$]	3.60	1.50	1.00
Tower reflector and CPCs [M\$]	5.30	not included	not included
Solar receiver-reactor + periphery [M\$]	7.00	2.00	1.00
Quencher [M\$]	3.00	not included	not included
Hydrolyzer [M\$]	4.00	1.00	0.50
Balance of plant, indirects, contingency [M\$]	8.90	2.00	1.00
H_2 storage [M\$]	not included	1.00	0.50
Total capital cost for solar H_2 [M\$]	55.08	16.00	5.70
Annual Cost			
Annual fixed charge rate [M\$]	15%	not included	not included
Capital cost for solar H_2 [M\$]	8.26	not included	not included
O&M cost for solar H_2 [M\$]	1.10	1.01	0.42
Total annual cost for solar H_2 [M\$]	9.36	1.01	0.42
Hydrogen production rate [kg/hr]	792	250	50
Hydrogen cost [$/$kg$]	5.02	7.98	14.75

Proceedings of the ASME 2010 4th International Conference on Energy Sustainability
ES2010
May 17-22, 2010, Phoenix, Arizona, USA

ES2010- 0

RENEWABLE HYDROGEN FROM THE Zn/ZnO SOLAR THERMOCHEMICAL CYCLE: A COST AND POLICY ANALYSIS

Julia F. Haltiwanger*
Mechanical Engineering
University of Minnesota
Minneapolis, Minnesota 55407

Jane H. Davidson
Mechanical Engineering
University of Minnesota
Minneapolis, Minnesota 55407

Elizabeth J. Wilson
Humphrey Institute of Public Affairs
University of Minnesota
Minneapolis, Minnesota 55407

steam methane reforming (SMR).

Prior work projects that hydrogen produced by the zinc/zinc-oxide cycle will cost between \$5.02 and \$14.75/kg, compared to \$2.40 to \$3.60/kg for steam methane reforming. Overcoming this cost difference would require a carbon tax of \$119 to \$987/tCO_2, which is significantly higher than is likely to be implemented in most countries. For the technology to become cost competitive, incentive policies that lead to early implementation of solar hydrogen plants will be necessary to allow the experience effect to draw down the price. Under such policies, a

Cost for zinc oxide reaction $5 to $15 /kg syngas

Commercial from steam reforming $3/kg

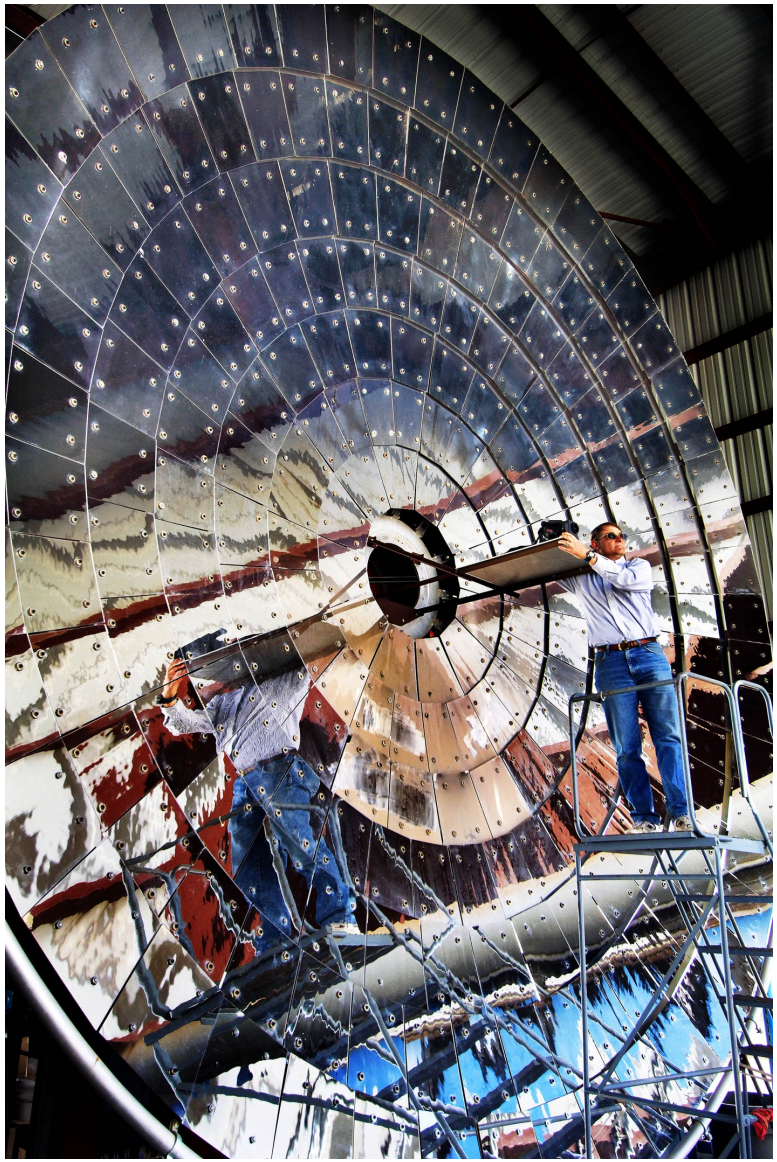

-Make a continuous process without an aerosol

-Rotate the felt from the Ceria device

-Added advantage is heat recovery i.e., efficiency

Sandia Solar Furnace

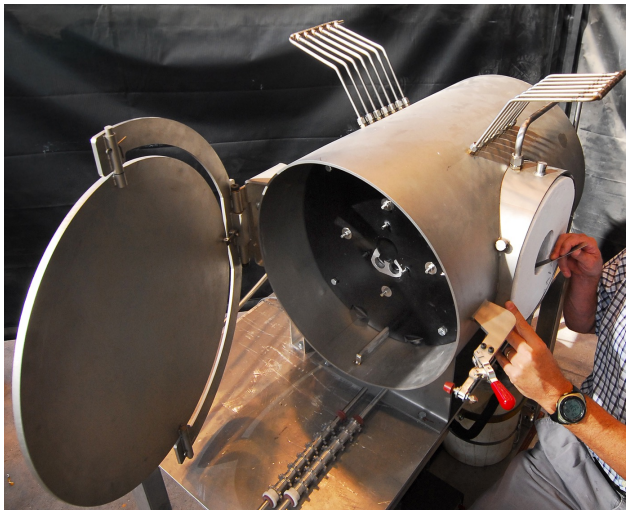

Counter Rotating Ring Reactor (Recovers Heat)

Counter Rotating Ring Reactor (Recovers Heat)

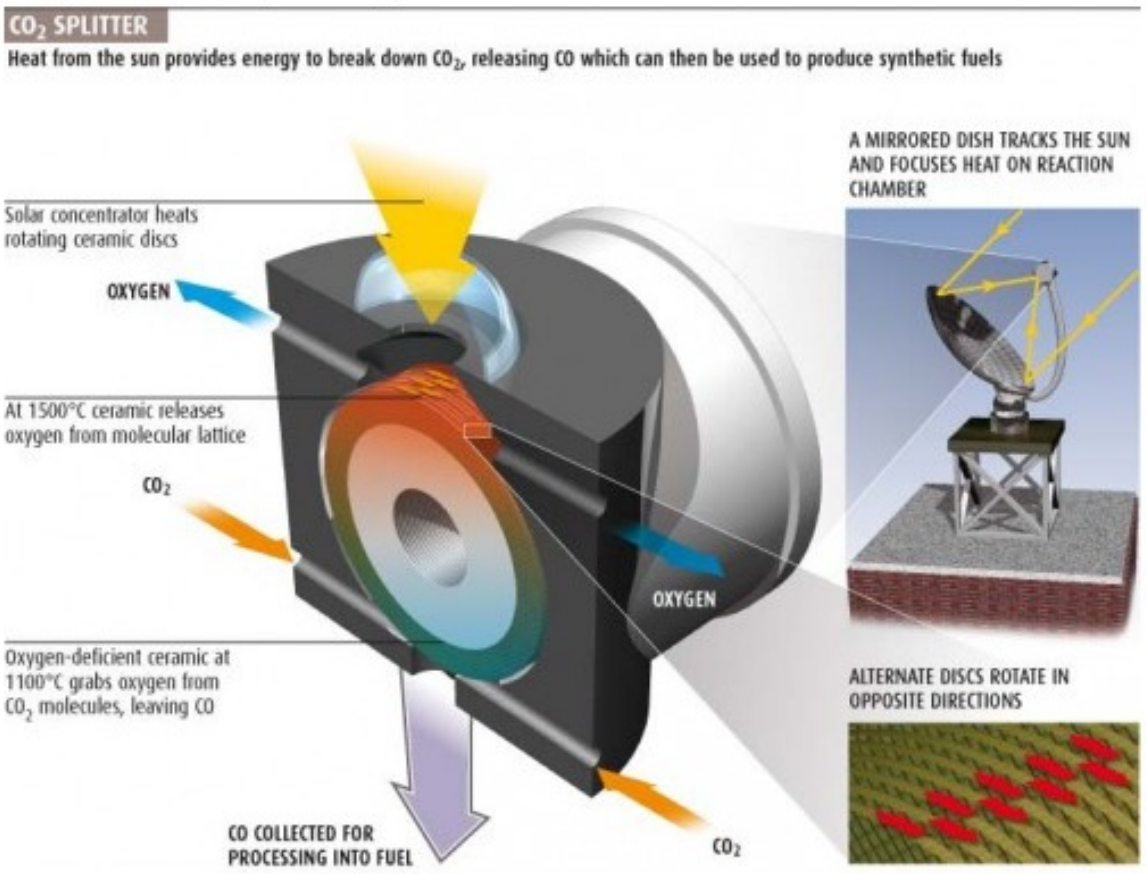

Counter Rotating Ring Reactor (Recovers Heat)

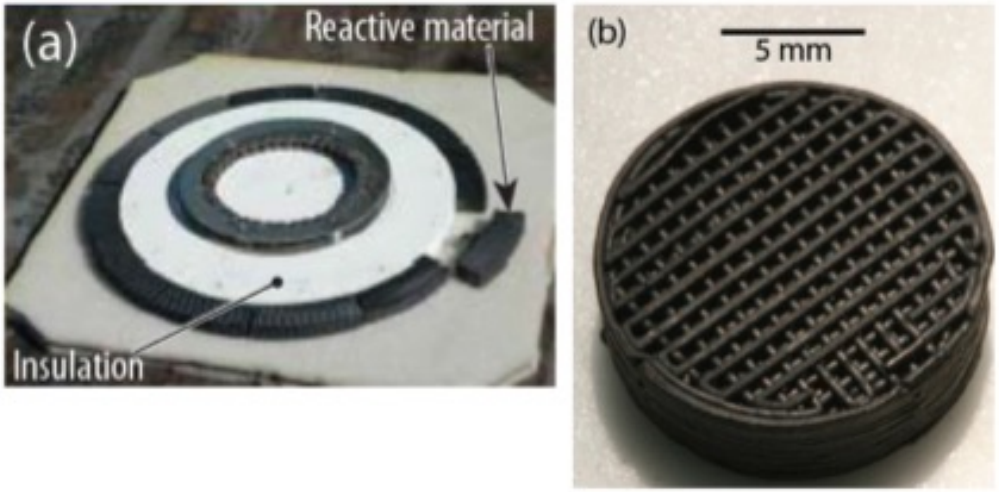

(a) The CR5 device employs a mixed valent metal oxide, arranged around the perimeter of a rotating ring. Shown here are iron oxides supported in a yttria stabilized zirconia (YSZ) matrix that exploit the "ferrite" thermochemical cycle in which Fe^{+3} reduces to Fe^{+2} and reoxidizes back to Fe^{+3}. (b) A monolithic test sample fabricated from a cobalt ferrite/YSZ composite. Its lattice structure provides high geometric surface area.

Counter Rotating Ring Reactor (Recovers Heat)

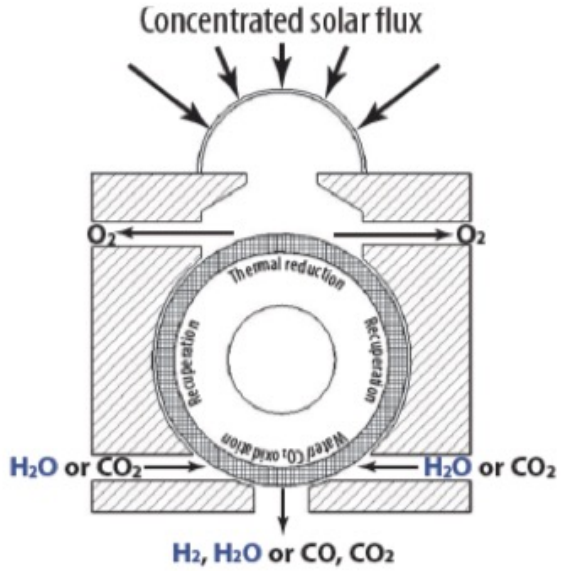

Side view of the CR5 showing a single ring.
In the top chamber, concentrated solar irradiation heats the ferrite to ~1500 °C and thermally reduces the iron, driving off some oxygen. In the opposite chamber, the oxygen-deficient reduced ferrite is exposed to either water vapor or carbon dioxide at a lower temperature to produce either hydrogen or carbon monoxide. Heat is recuperated between the ceramic oxide materials as they leave the two reactant chambers by counter rotating the reactive rings relative to one another.

Zn => ZnO Cycle
(Solar Driven Redox Reactions)

CARBON NEUTRAL SOLAR SYNGAS: COST AND POLICY CONSIDERATIONS

Julia Haltiwanger Nicodemus
Engineering Studies
Lafayette College
Easton, PA
Email: nicodemj@lafayette.edu

Morgan McGuinness
Physics and Math
Lafayette College
Easton, PA

To put these costs in perspective, comparison to the cost of natural gas is appropriate. The industrial cost of natural gas is $\$0.246/kg$, or, on an energy basis, $\$0.0046/MJ$[1]. Because the heating value of natural gas is about twice that of syngas, costs are better compared on an energy basis. Table 2 lists the costs of solar syngas for $100 MW_{th}$ and $500 MW_{th}$ plants, for low cost water ($\$0.01/L$) and high cost water ($\$0.1/L$) for all six carbon pricing scenarios. Assuming low cost water and CO_2 captured from a power plant with no additional costs, the cost of solar syngas is 4 and 5 times the cost of natural gas for the $100 MW_{th}$ and $500 MW_{th}$ plants, respectively.

In this analysis, we will consider six possible scenarios for pricing CO_2: carbon capture from a power plant (CC), carbon capture plus the social cost of carbon (CC+SCC), carbon capture plus a carbon tax (CC+tax), CO_2 supplied by a chemical supplier (Chem), CO_2 from a chemical supplier plus the social cost of carbon (Chem+SCC), and CO_2 from a chemical supplier plus a carbon tax (Chem+tax).

TABLE 2: SYNGAS COST PER MEGAJOULE (MJ)

	$100 MW_{th}$		$500 MW_{th}$	
	low H_2O cost	high H_2O cost	low H_2O cost	high H_2O cost
CC	$0.0246	$0.0282	$0.0190	$0.0226
CC + SCC	$0.0252	$0.0288	$0.0196	$0.0232
CC + tax	$0.0354	$0.0390	$0.0299	$0.0334
Chem	$0.0257	$0.0293	$0.0201	$0.0237
Chem + SCC	$0.0263	$0.0299	$0.0207	$0.0243
Chem + tax	$0.0365	$0.0401	$0.0310	$0.0345

Syngas production depends on the cost of CO_2
Depends on size of plant and considerations like
CC carbon capture at power plant
SCC Society cost of CO_2
tax = Carbon tax
Chem = from chemical synthesis of CO_2

-Consider a liquid/vapor phase process
-Don't need to worry about growth of phases and consumption of metal oxide

First process was a hybrid electrolysis process reminiscent of the titania process

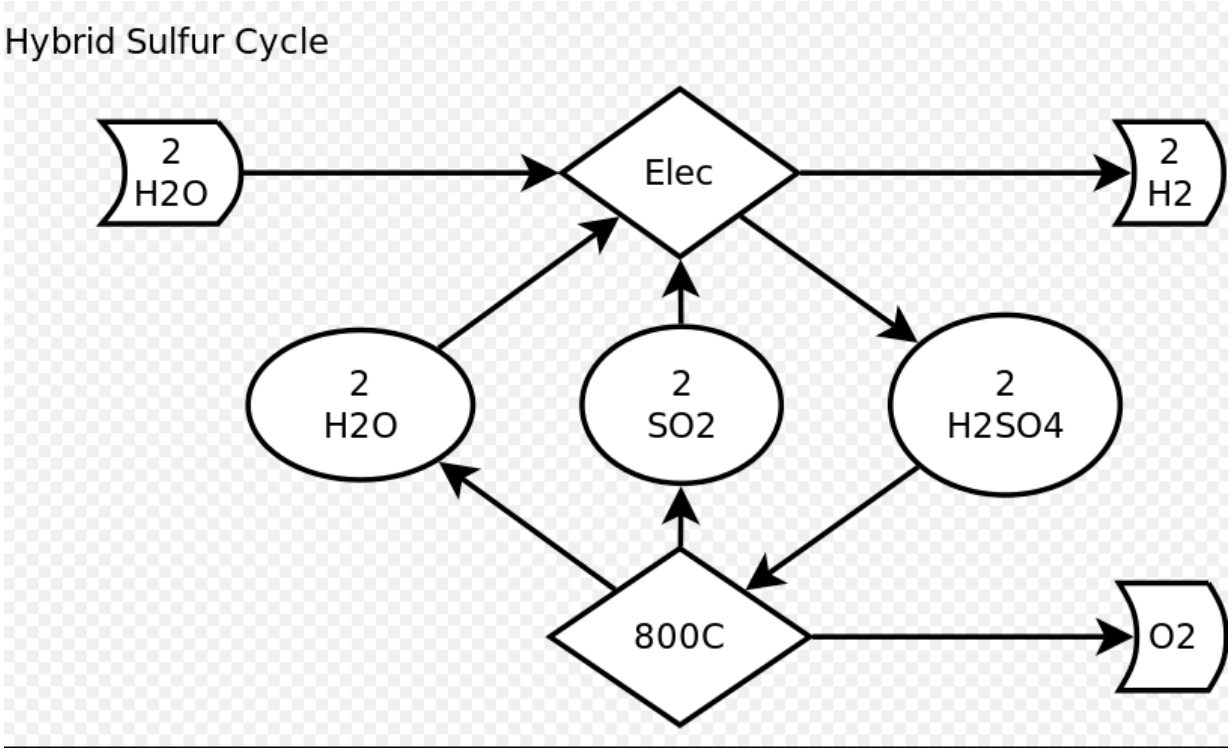

Electricity Needed (about 1/2 of electrolysis)

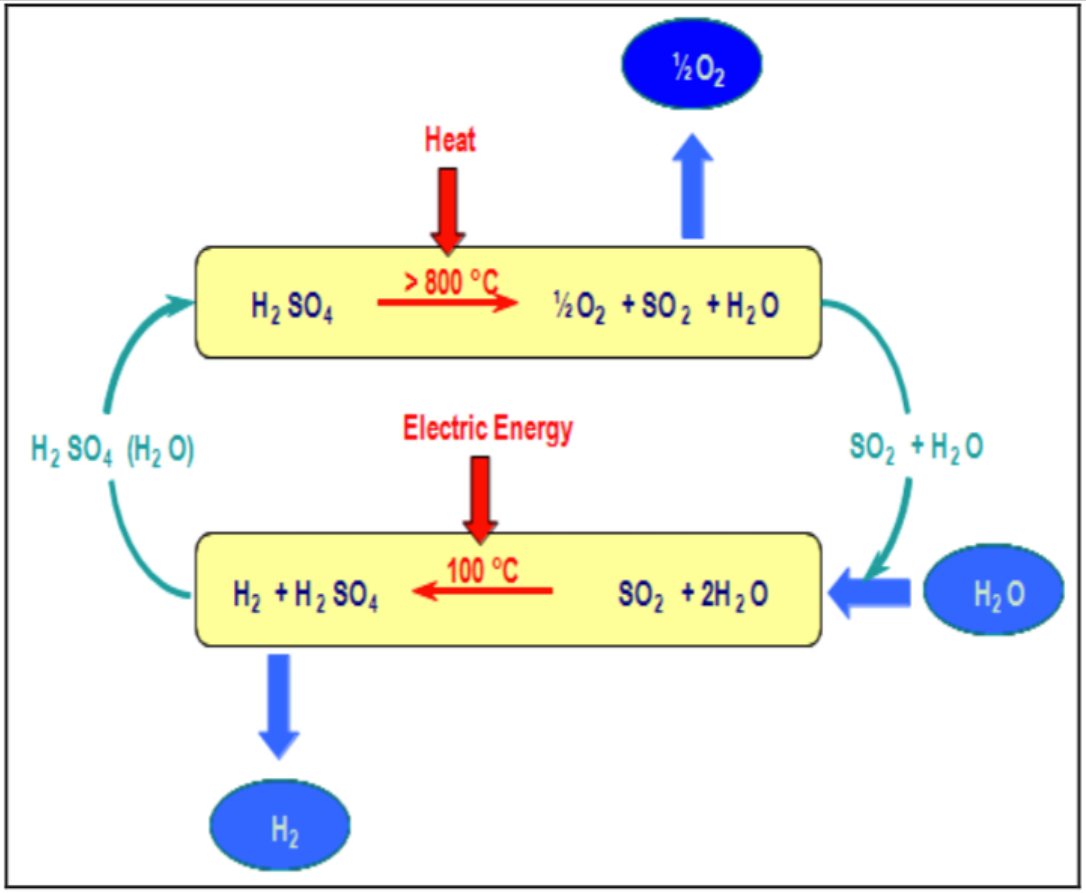

Figure 4.2.1. The Hybrid Sulfur cycle.

-Second process doesn't need electrolysis

-Doesn't need very high temperatures

-But involves additional steps

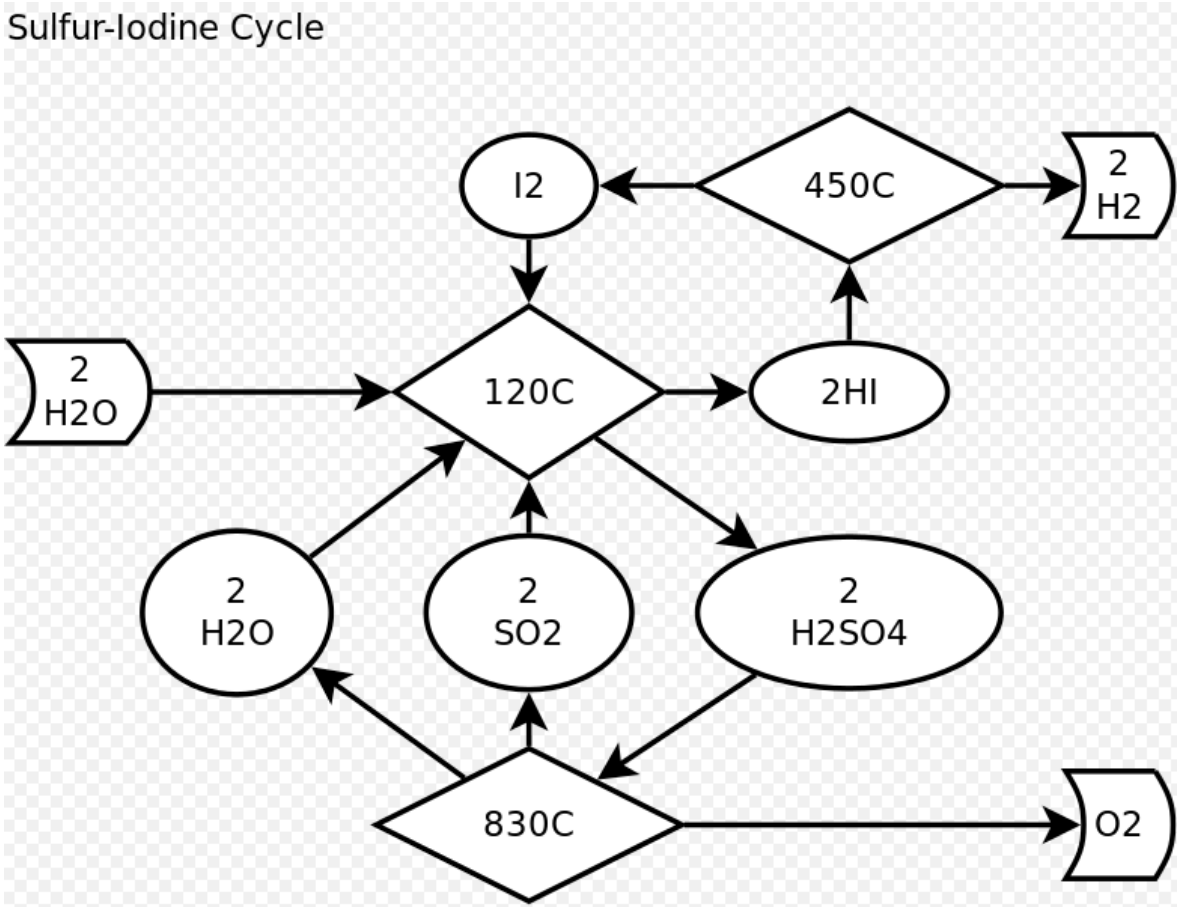

Sandia Study (no electricity needed)

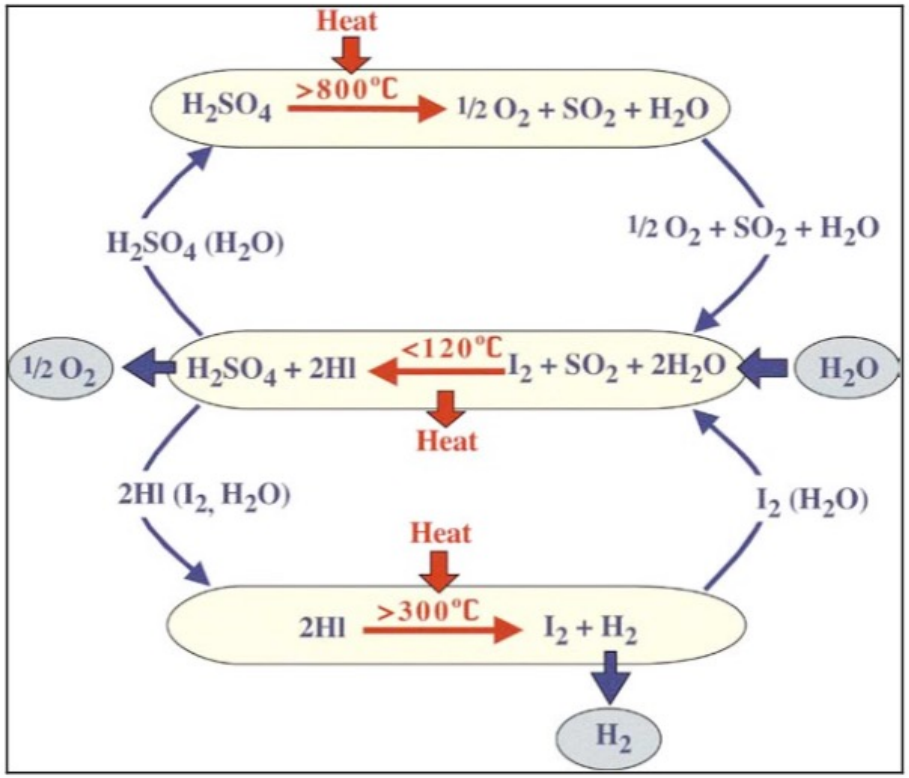

Figure 4.1.1. Sulfur Iodine three-step cycle.

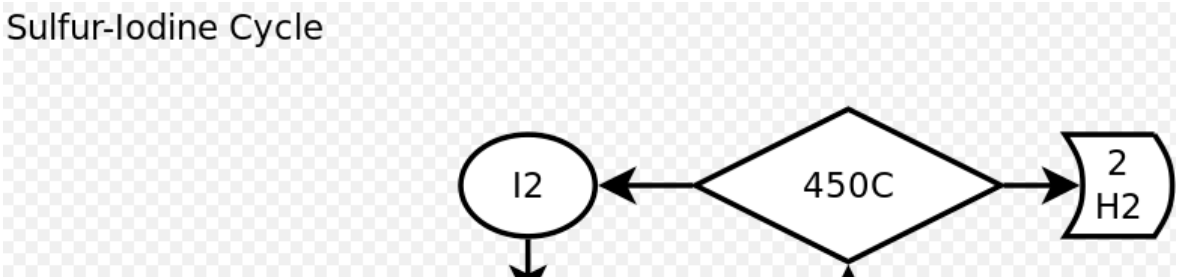

Advantages and disadvantages [edit]

The characteristics of the S–I process can be described as follows:

- All fluid (liquids, gases) process, therefore well suited for continuous operation;
- High utilization of heat predicted (about 50%), but very high temperatures required (at least 850 °C);
- Completely closed system without byproducts or effluents (besides hydrogen and oxygen);
- Corrosive reagents used as intermediaries (iodine, sulfur dioxide, hydriodic acid, sulfuric acid); therefore, advanced materials needed for construction of process apparatus;
- Suitable for application with solar, nuclear, and hybrid (e.g., solar-fossil) sources of heat;
- More developed than competitive thermochemical processes (but still requiring significant development to be feasible on large scale).

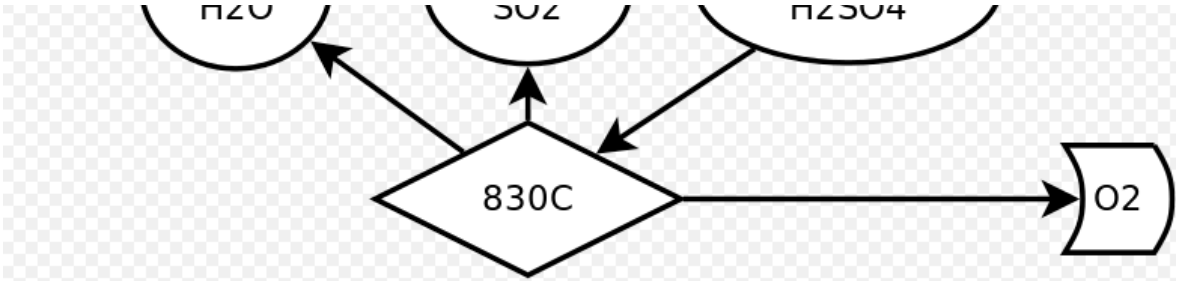

Hydrogen Production by the Solar-powered Hybrid Sulfur Process: Analysis of the Integration of the CSP and Chemical Plants in Selected Scenarios

Raffaele Liberatore[1], Michela Lanchi[1] and Luca Turchetti[1, a)]

[1]ENEA - Italian National Agency for New Technologies, Energy and Sustainable Economic Development, via Anguillarese 301 - 00123 Rome, Italy.

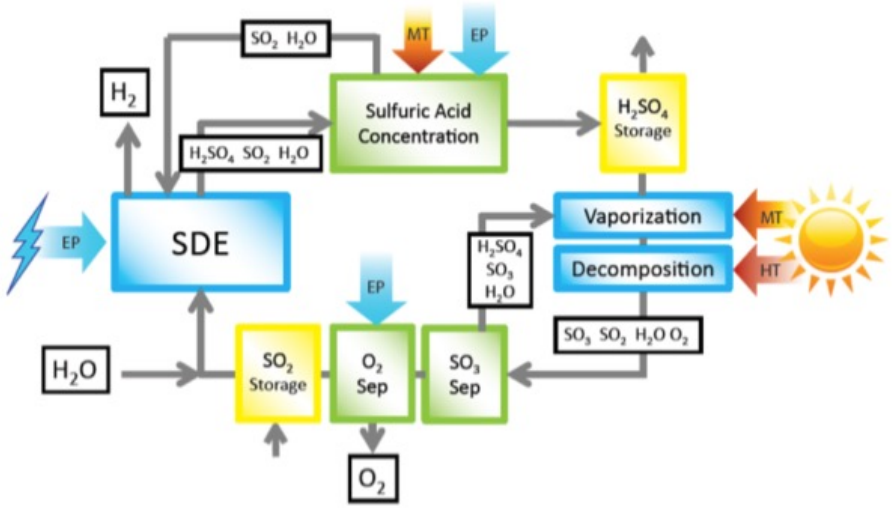

FIGURE 1. Simplified block diagram of the HyS process considered here. The main energy input type required by the different process blocks is highlighted (MT: medium temperature heat; HT: high temperature heat; EP: electric power; SDE: sulfur depolarized electrolyzer).

Hydrogen Production by the Solar-powered Hybrid Sulfur Process: Analysis of the Integration of the CSP and Chemical Plants in Selected Scenarios

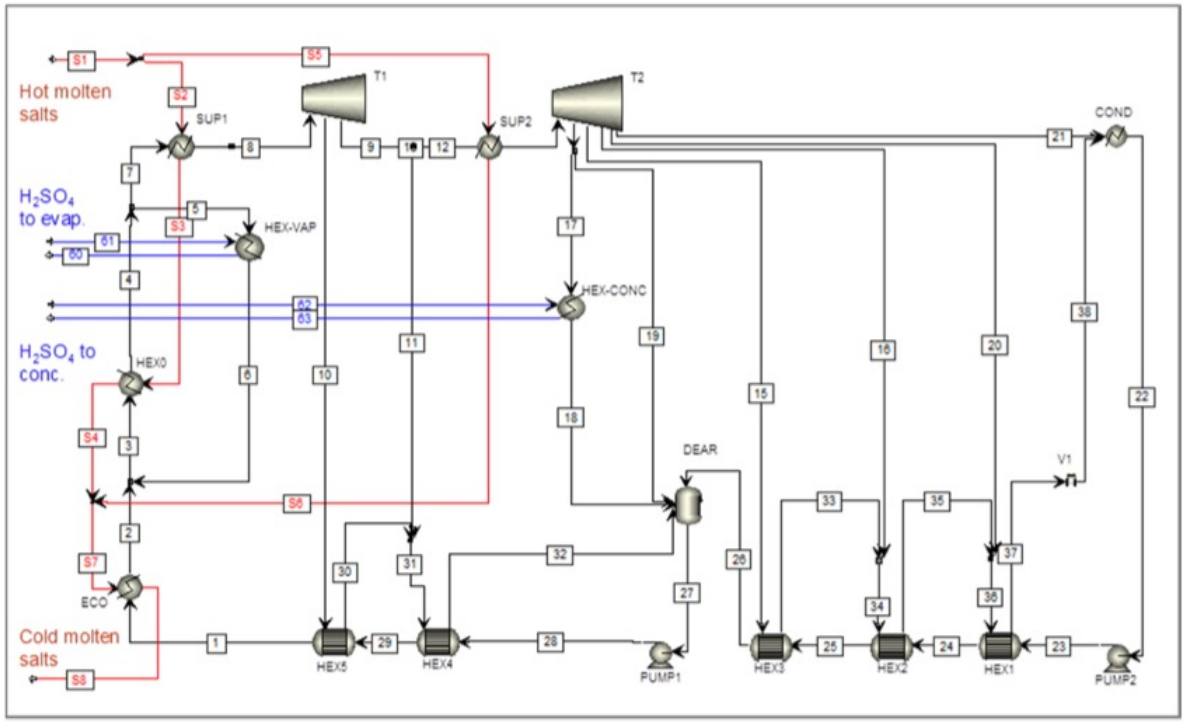

FIGURE 2. Process scheme of the Rankine cycle powered by molten salts sensible heat. In Case 1a (8 hours solar operation) both the heat exchangers HEX-VAP and HEX-CONC work, while in Case 1b (16 hours operation) only the HEX-CONC is in operation. In Case 2 the heat exchangers HEX-VAP and HEX-CONC are not present. HEX: exchangers; HEX-VAP: evaporator for the H2SO4 evaporation in the discontinuous step of the cycle; HEX-CONC: evaporator for the H2SO4 concentration in the continuous step; DEAR: degasifier; COND: condenser; T1, T2: steam turbines; ECO: economizer; SUP: super-heater; V: valve.

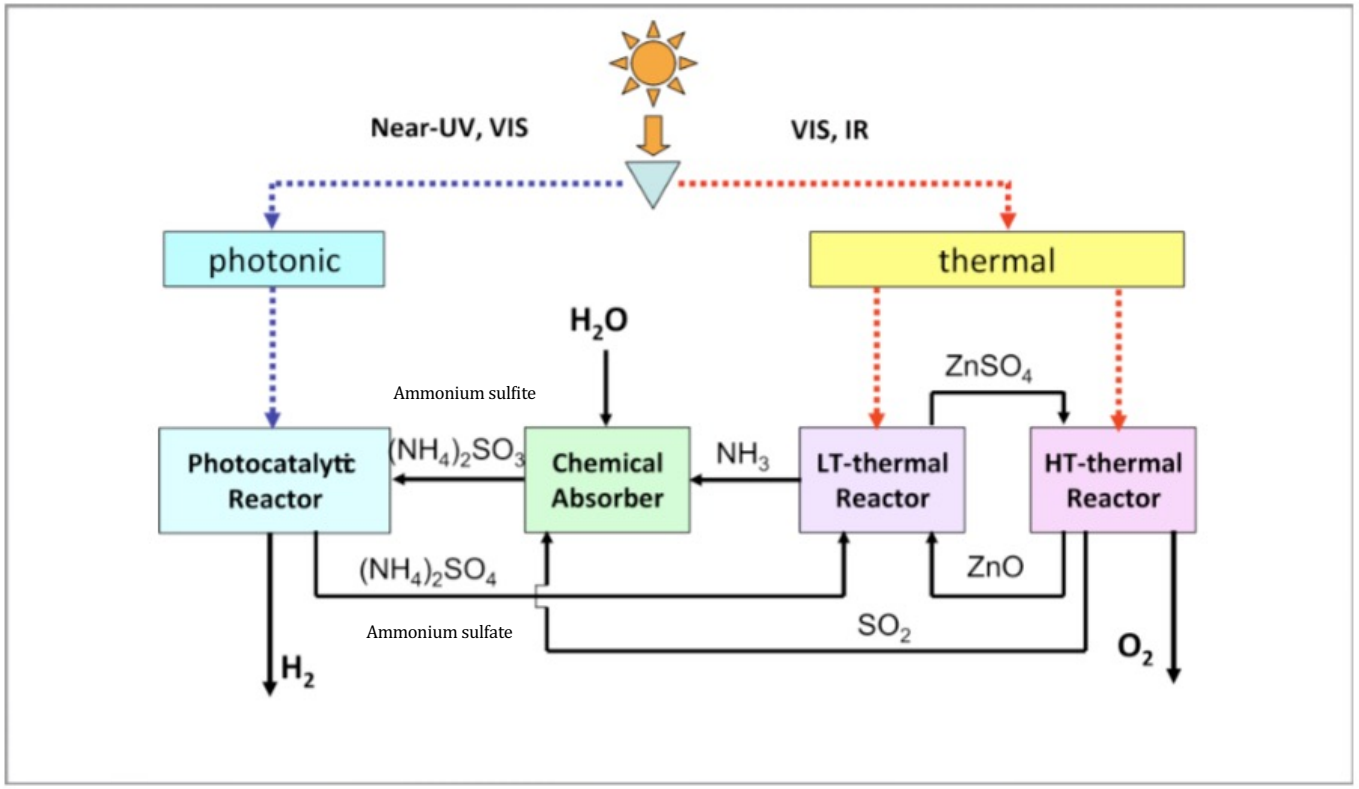

Figure 4.3.1. Photolytic Sulfur Ammonia schematic process.

More complex oxidation reduction processes for generation of hydrogen have been proposed

Low-temperature, manganese oxide-based, thermochemical water splitting cycle

Bingjun Xu, Yashodhan Bhawe, and Mark E. Davis[1]

Chemical Engineering, California Institute of Technology, Pasadena, CA 91125

Contributed by Mark E. Davis, April 17, 2012 (sent for review April 5, 2012)

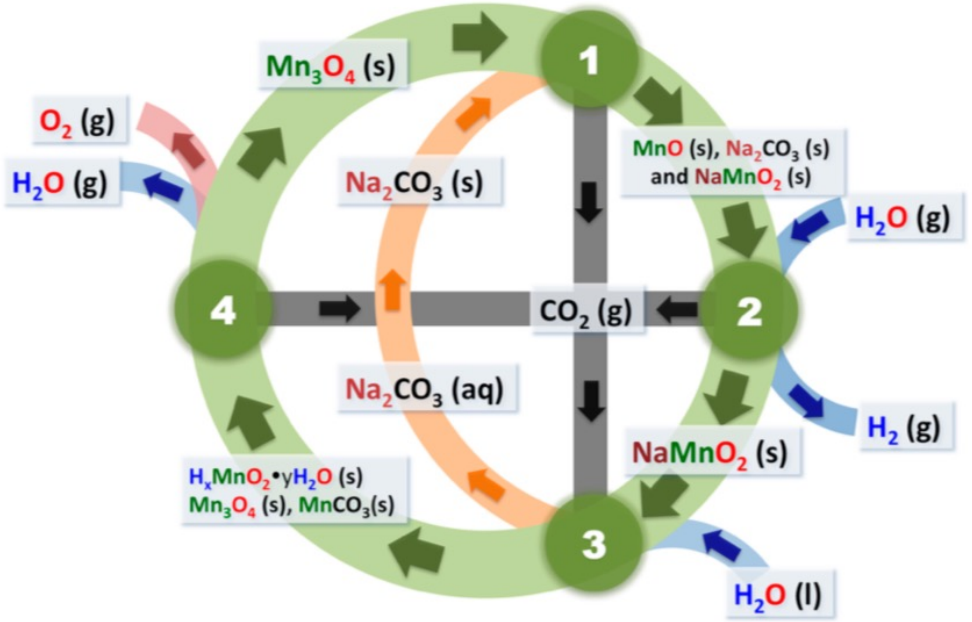

Step	Reaction	Temp (^{O}C)
1	$3Na_2CO_3(s) + 2Mn_3O_4(s) \rightarrow 4NaMnO_2(s) + 2CO_2(g) + 2MnO(s) + Na_2CO_3$	850
2	$2MnO(s) + Na_2CO_3(s) + H_2O(g) \rightarrow H_2(g) + CO_2(g) + 2NaMnO_2(s)$	850
3	$6NaMnO_2(s) + ayH_2O(l) + (3+b)CO_2(g) \rightarrow 3Na_2CO_3(aq) + aH_xMnO_2 \cdot yH_2O(s) + bMnCO_3(s) + cMn_3O_4(s)$	80
4	$aH_xMnO_2 \cdot yH_2O(s) + bMnCO_3 + \rightarrow (2-c)Mn_3O_4(s) + ayH_2O(g) + bCO_2(g) + 0.5O_2(g)$	850
Net	$H_2O(g) \rightarrow H_2(g) + 0.5O_2(g)$	

a, b and c satisfy following relations: $a + b + 3c = 6$ and $(4\text{-}x)a + 2b + 8c = 18$

Fig. 2. Schematic representation of the low-temperature, Mn-based thermochemical cycle.

Two Other Redox Systems (http://energy.gov/eere/fuelcells/hydrogen-production-thermochemical-water-splitting)

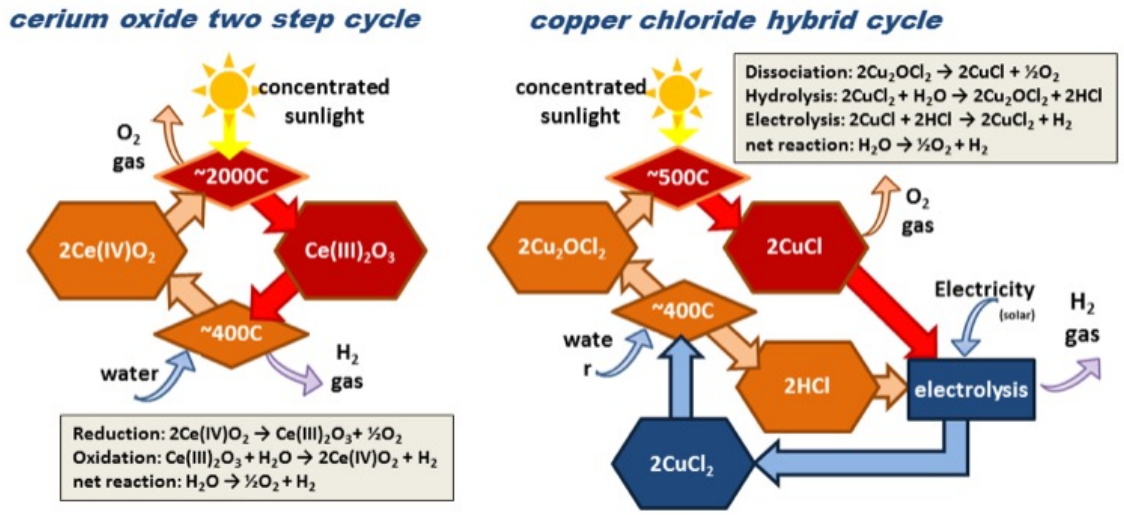

Figure 2. This illustration shows two example water-splitting cycles: (left) a two-step "direct" thermochemical cycle based on oxidation and reduction of cerium oxide particles; and (right) a multi-step "hybrid" thermochemical cycle based on copper chloride thermochemistry, which includes an electrolysis step that needs some electricity input.

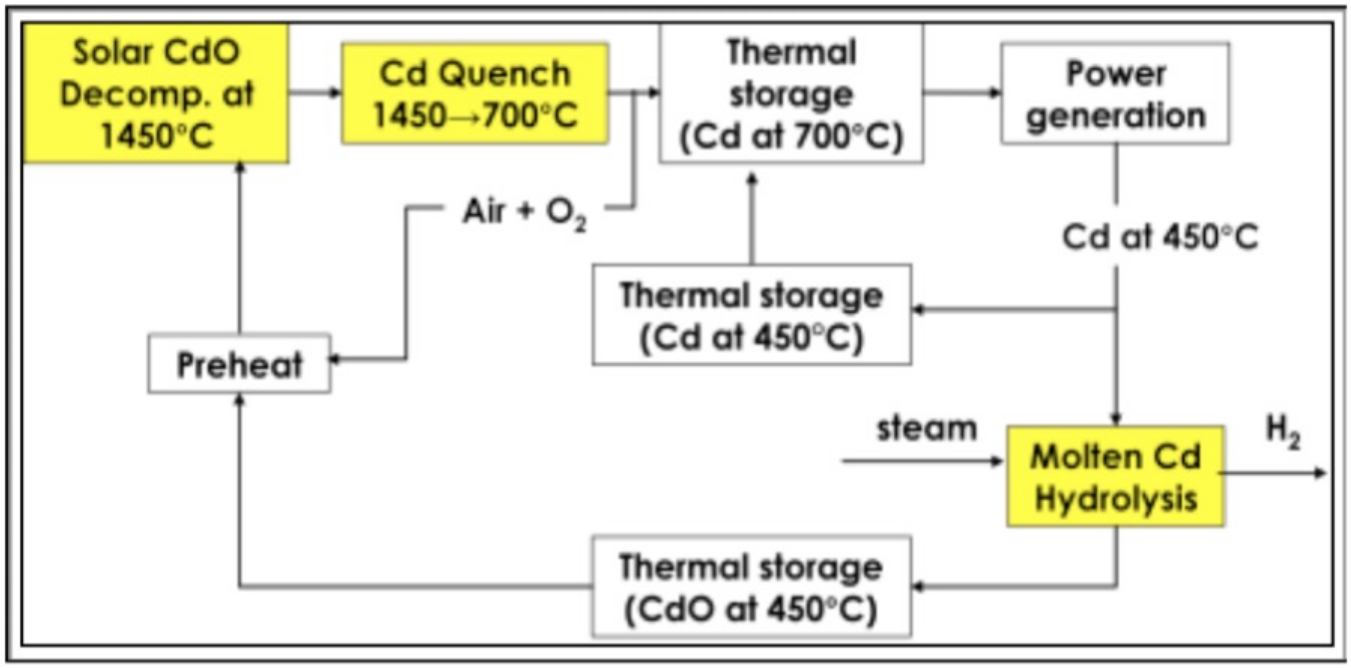

Figure 4.5.2. Process flow for a diurnal solar cadmium oxide hydrogen cycle.

$NiFe_2O_4$

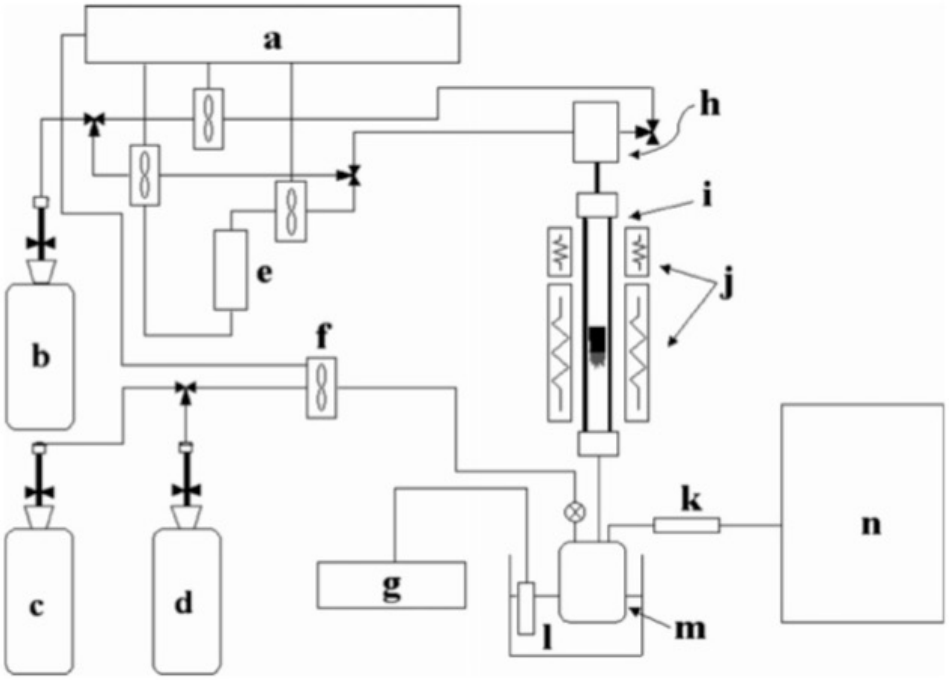

Fig. 1. Experimental apparatus for H_2O decomposition: (a) MFC & Temperature controller, (b) He, (c) H_2, (d) O_2, (e) water, (f) MFC, (g) Condenser, (h) Controlled evaporator mixer, (i) Reactor, (j) Furnace, (k) Silica-gel, (l) Ethanol, (m) Water trap, and (n) Mass.

S.B. Han et al. / Solar Energy 81 (2007) 623–628

Solar Thermochemical Hydrogen Production Research (STCH)
Thermochemical Cycle Selection and Investment Priority
Robert Perret

Volatile Metal Oxide:

$CdO(s) \rightarrow Cd(g) + ½\ O_2(g)$	(1450°C)
$Cd(l,s) + H_2O \rightarrow CdO(s) + H_2(g)$	(25-450°C)

Non-Volatile Metal Oxide:

Ferrite:

$NiMnFe_4O_8(s) \rightarrow NiMnFe_4O_6(s) + O_2(g)$	(~1800°C)
$NiMnFe_4O_6(s) + H_2O(g) \rightarrow NiMnFe_4O_8(s) + H_2(g)$	(~800°C)

Multi-step cycle:

$2a\text{-}NaMnO_2(s) + H_2O(l) \rightarrow Mn_2O_3(s) + 2NaOH(a)$	(~100°C)
$2Mn_2O_3(s) \rightarrow 4MnO(s) + O_2(g)$	(~1560°C)
$2MnO(s) + 2NaOH \rightarrow 2a\text{-}NaMnO_2(s) + H_2(g)$	(~630°C)

Sulfuric Acid:

$2H_2SO_4(g) \rightarrow 2SO_2(g) + 2H_2O(g) + O_2(g)$	(~850°C)
$I_2 + SO_2(a) + 2H_2O \rightarrow 2HI(a) + H_2SO_4(a)$	(~100°C)
$2HI \rightarrow I_2(g) + H_2(g)$	(~300°C)

Hybrid Copper Chloride:

$2CuCl_2 + H_2O \rightarrow Cu_2OCl_2 + 2HCl$	(~400°C)
$2Cu_2OCl_2 \rightarrow O_2 + 4CuCl$	(~500°C)
$2CuCl + 2HCl \xrightarrow{e^-} 2CuCl_2 + H_2$	(~100°C)

Figure 1.1. Thermochemical cycle class examples.

Solar Thermochemical Hydrogen Production Research (STCH)
Thermochemical Cycle Selection and Investment Priority
Robert Perret

2 Cycle Inventory Development and Initial Selection

Many hydrogen producing thermochemical cycles have been proposed over the last 40 years. A literature search was performed to identify all published cycles[1-58]. These were added to an

Table 2.4. Listing of non-zero efficiencies for top-scoring cycles.

PID	Cycle Name	Eff. (LHV)	PID	Cycle Name	Eff. (LHV)
110	Sodium-Mn-3	50.0	184	Hybrid Antimony-Br	30.6
106	High T Electrolysis	49.1	134	Cobalt Sulfate	29.9
147	Cadmium Sulfate	46.5	56	Cu Chloride	29.2
5	Hybrid Cd	45.1	114	Hybrid N-I	28.2
6	Zinc Oxide	45.0	62	Iron Bromide	27.7
182	Cadmium Carbonate	44.3	23	Mn-Chloride-1	26.6
2	Ni-Mn Ferrite	44.0	51	K-Peroxide	23.5
194	Zn-Mn Ferrite	44.0	61	Sodium-Iron	22.8
67	Hybrid Sulfur	43.1	185	Hybrid Cobalt Br-2	21.7
7	Iron Oxide	42.3	53	Hybrid Chlorine	21.6
191	Hybrid Copper Chloride	41.6	160	Arsenic-Iodine	21.2
149	Ba-Mo-Sulfate	39.5	152	Iron-Zinc	19.9
1	Sulfur-Iodine	38.1	103	Cerium Chloride	18.0
193	Multivalent Sulfur-3	35.5	26	Cu-Mg Chloride	17.4
131	Mn Sulfate	35.4	199	Iron Chloride-11	16.9
72	Ca-Fe-Br-2	33.8	200	Iron Chloride-12	16.9
70	Hybrid S-Br	33.4	104	Mg-Ce-Chloride	15.1
24	Hybrid Li-NO_3	32.8	132	Ferrous Sulfate-3	14.4
201	Carbon Oxides	31.4	68	As-Ammonium-I	6.7
22	Fe-Chloride-4	31.0	129	Mg Sulfate	5.1

Table 2.5. Cycles that could move to Phase 3 detailed theoretical and experimental study.

Cycle	PID	Efficiency %	Estimated Max T
Sulfuric Acid Cycles			
Hybrid Sulfur	67	43	900
Sulfur Iodine	1	45	900
~~Multivalent Sulfur~~	193	42	1570
Metal Sulfate Cycles			
~~Cadmium Sulfate~~	147	55	1200
~~Barium Sulfate~~	149	47	1200
~~Manganese Sulfate~~	131	42	1200
Volatile Metal Oxides			
Zinc Oxide	6	53	2200
~~Cadmium Carbonate~~: Cadmium Oxide	~~182~~: 213	~~52~~: 59	~~1600~~: 1450
~~Hybrid Cadmium~~	5	53	1600
Non-volatile Metal Oxides			
~~Iron Oxide~~	7	50	2200
Mised Metal Sodium Manganese; Sodium Mangante	110	59	1560
Nickel Manganese Ferrite	2	52	1800
Zinc Manganese Ferrite	194	52	1800
Hybrid Cycles			
Hybrid Copper Chloride	191	49	550

Table 3.1. Cycles considered in the formal evaluation process.

Class	Cycle	Lead Organization
Sulfuric Acid Cycles	Sulfur Iodine	General Atomics, Sandia National Labs, CEA
	Hybrid Sulfur	Savannah River National Laboratory
Volatile Metal Oxide Cycles	Zinc Oxide	University of Colorado
	Cadmium Oxide	General Atomics
Non-volatile Metal Oxide Cycles	Sodium Manganese and Sodium Manganate	University of Colorado
	Reactive Ferrite	Sandia National Laboratories
	ALD Ferrite	University of Colorado
Hybrid Cycles	Hybrid Copper Chloride	Argonne National Laboratory
	Photolytic Sulfur Ammonia	SAIC

Fig. 8: 1 MW_{th} solar plant in Broomfield, Colorado – The plant uses an array of 2700 mirrors to concentrate sunlight on a 20-meter-tall solar tower to produce heat needed to drive the chemical reactor. From [43].

California Mojave Desert

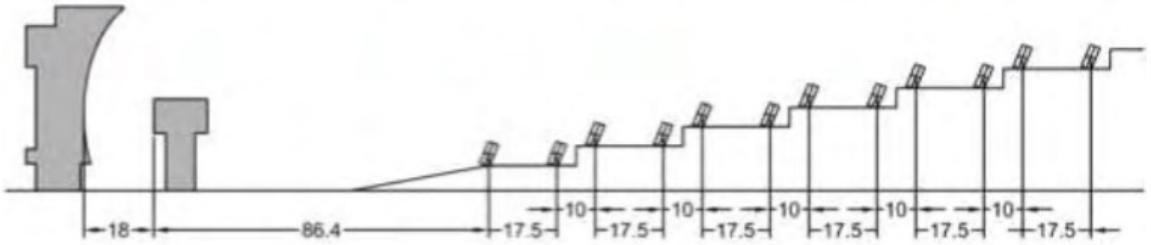

Elevation view of the Odeillo MWSF facility

Odeillo, France


A-349
Plataforma Solar
de Almería
Plataforma Solar
de Almería


Barcelona
Porto
Madrid
Portugal
Spain
Valencia
Palma
Lisbon
Murcia
Seville
Plataforma Solar
de Almería
Malaga
Gibraltar
Tangier

Hydrogen Production in Spain

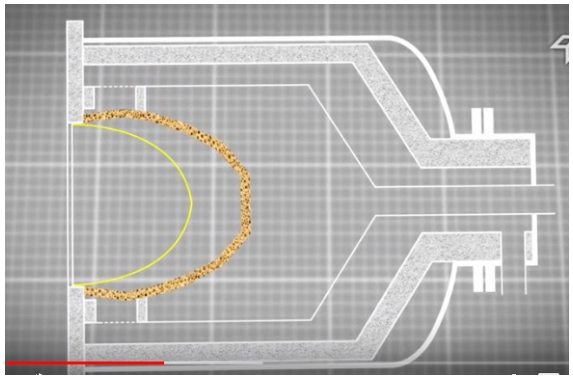

DLR Institute

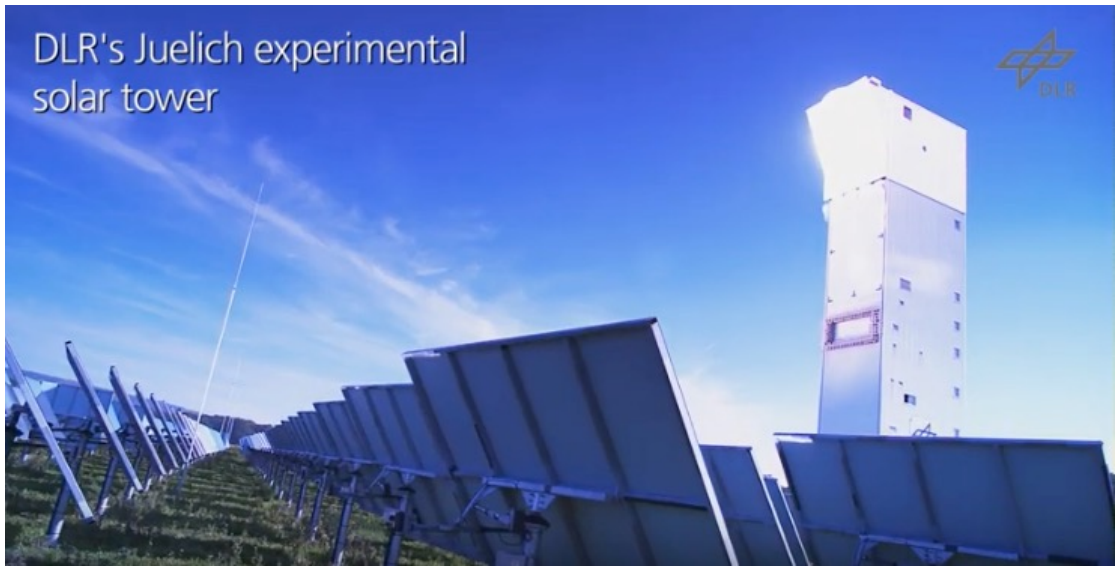


Portugal
Spain
Madrid
Seville
Gemasolar Thermosolar Plant
Malaga
Gibraltar
Tangier
Valencia
Murcia
Granada
Cadiz
Marbella
Oran

Crescent Dunes Nevada

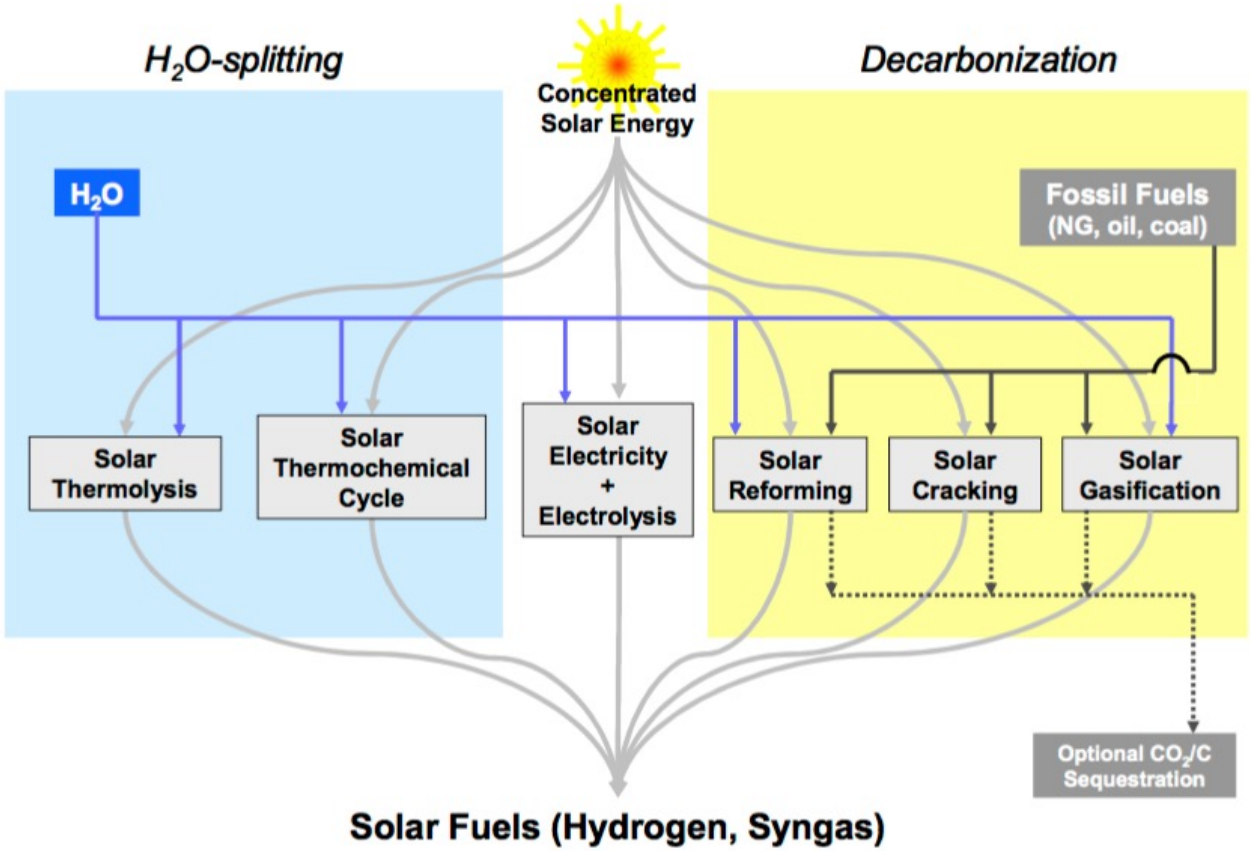

Fig. 2: Thermochemical routes for solar hydrogen production – Indicated is the chemical source of H_2: H_2O for the solar thermolysis and the solar thermochemical cycles; fossil fuels for the solar cracking, and a combination of fossil fuels and H_2O for the solar reforming and gasification. For the solar de-carbonization processes, optional CO_2/C sequestration is considered. All of those routes involve energy consuming (endothermic) reactions that make use of concentrated solar radiation as the energy source of high-temperature process heat. Adapted from [1,2].

Direct Use of Solar in the Petrochemical Industry

Energy &
Environmental Science

Dynamic Article Links

Cite this: *Energy Environ. Sci.*, 2011, **4**, 73

www.rsc.org/ees

REVIEW

Solar-driven gasification of carbonaceous feedstock—a review

Nicolas Piatkowski,[a] Christian Wieckert,[b] Alan W. Weimer[c] and Aldo Steinfeld*[ab]

Received 28th July 2010, Accepted 28th September 2010
DOI: 10.1039/c0ee00312c

Given the future importance of solid carbonaceous feedstocks such as coal, coke, biomass, bitumen, and carbon-containing wastes for the power and chemical industries, gasification technologies for their thermochemical conversion into fluid fuels are developing rapidly. Solar-driven gasification, in which concentrated solar radiation is supplied as the energy source of high-temperature process heat to the endothermic reactions, offers an attractive alternative to conventional autothermal processes. It has the potential to produce high-quality synthesis gas with higher output per unit of feedstock and lower specific CO_2 emissions, as the calorific value of the feedstock is upgraded through the solar energy input by an amount equal to the enthalpy change of the reaction. The elimination of an air separation unit further facilitates economic competitiveness. Ultimately, solar-driven gasification is an efficient means of storing intermittent solar energy in a transportable and dispatchable chemical form. This review article develops some of the underlying science, examines the thermodynamics and kinetics of the pertinent reactions, and describes the latest advances in solar thermochemical reactor technology.

Alan W. Weimer

Sears Professor • C2B2 Executive Director

alan.weimer@colorado.edu
(303) 492-3759

Curriculum Vitae
Google Scholar Profile
Weimer Research Group

JSCBB C224

Education

B.S., University of Cincinnati (1976)
M.S., Ph.D., University of Colorado (1978, 1980)
Dow Chemical Company(1980-1996)

Advances in Science and Technology Vol. 74 (2010) pp 303-312
© (2010) Trans Tech Publications, Switzerland
doi:10.4028/www.scientific.net/AST.74.303

Solar Thermochemical Production of Fuels

Anton Meier[1, a] and Aldo Steinfeld[1, 2, b]

[1]Solar Technology Laboratory, Paul Scherrer Institute, 5232 Villigen PSI, Switzerland

[2]Department of Mechanical and Process Engineering, ETH Zurich, 8092 Zurich, Switzerland

[a]anton.meier@psi.ch, [b]aldo.steinfeld@ethz.ch

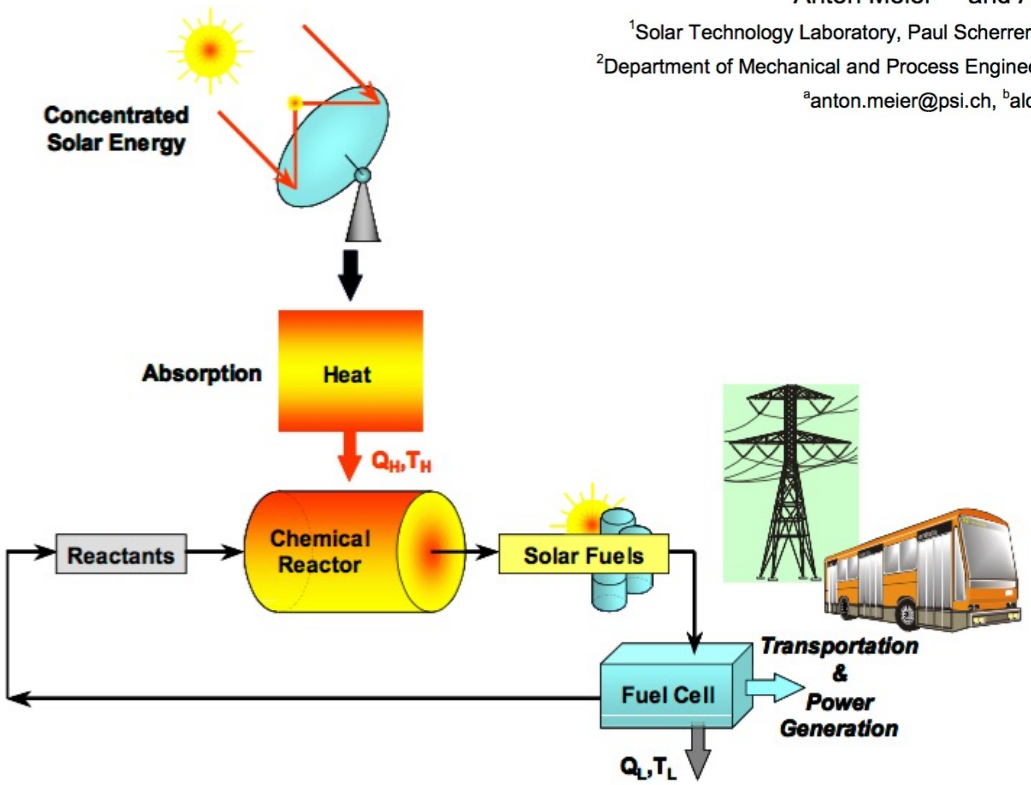

Fig. 1: Energy conversion into solar fuels for transportation and power generation – Concentrated solar radiation is used as the energy source of high-temperature process heat for driving thermochemical reactions towards the production of storable and transportable fuels. Adapted from [1].

Energy use in the petrochemical industry

Megaton oil equivalent
Mtoe

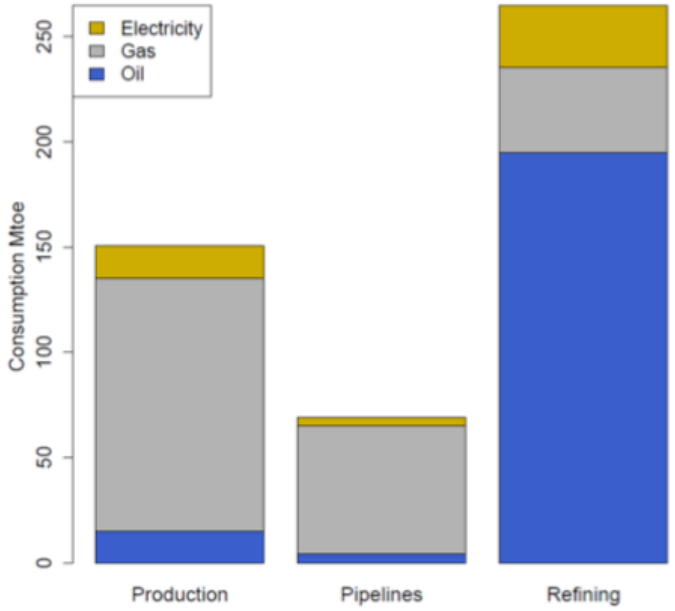

Blue is similar to the charcoal problem you burn a lot of oil to make gasoline

21 million barrels/day
7.33 barrel/ton
2.86 Mtoe/day
About 1000 Mtoe/year
About 1/3 to 1/2 is used to power refining, transport, and production

Figure 6. Energy consumption in oil and gas industry. *Adapted from* (Halabi, Al-Qattan and Al-Otaibi 2015)

How to cut US energy use in half: Power refining using solar

Heat Used in Oil Refining

-Oil is first heated to 200–300°F (90–150°C) and washed with water to remove salt and other suspended solids (Worrell, Corsten and Galisky 2015).
-Distillation then separates products based on their boiling point in the crude distillation unit (CDU), where crude oil is heated to temperatures around 750°F (390 ° C) (Worrell, Corsten and Galisky 2015).
-Heavy fuel oils are further treated in the vacuum distillation unit (VDU) at temperatures between 730 and 850°F (390 and 450 ° C) (Worrell, Corsten and Galisky 2015).
-Additional processing occurs in the fluid catalytic cracker (FCC), the hydrocracker, and coking unit. Each of these processes separate heavier oil products into lighter and more valuable products.

Other Petrochemical Processes

Hydrotreating mixes hydrogen with the feed stream at temperatures between 500 and 800°F (260 and 460 ° C) to remove sulfur (Worrell, Corsten and Galisky 2015).
A catalytic reformer uses a catalytic reactor to produce high octane gasoline and hydrogen.
Additional processes, such as alkylation, which uses steam, power, and various acids to produce alkylates, are also common.

Figure 7 displays yearly estimated energy use by refining process for U.S. refineries in 2012. Hydrotreatment and the crude distillation unit (CDU) account for nearly 50% of total energy requirements.

Trillion 10^{12}

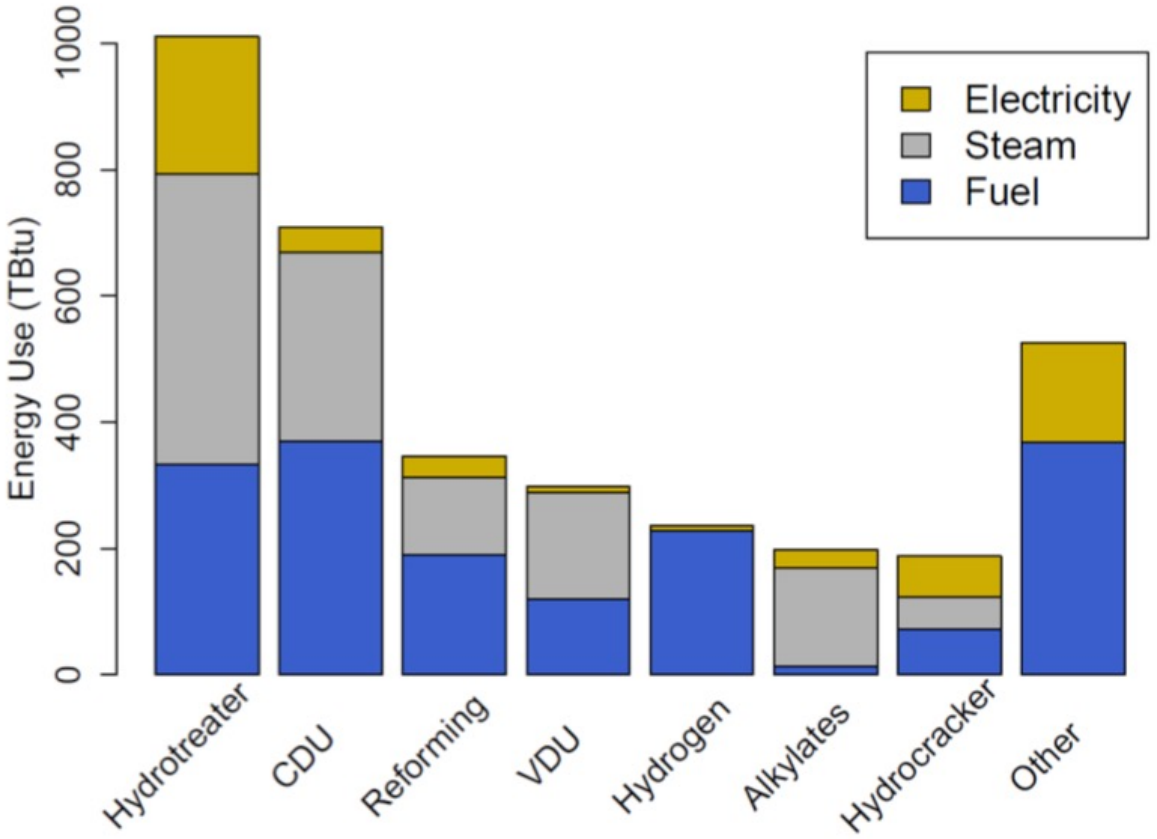

Figure 7. Energy use by refinery process. *Figure adapted from* (Worrell, Corsten and Galisky 2015)

Hydrogen Use/Production in Petrochemicals

-Hydrogen is used in the hydrotreatment process to lower the sulfur content of diesel fuel. Refinery demand for hydrogen has increased as demand for diesel fuel has risen and sulfur-content regulations have become more stringent (Hicks and Gross 2016).
-Hydrogen is produced as a co-product of the catalytic reformation of gasoline, demand for hydrogen exceeds supply produced from the refining process itself (Philibert, Cédric 2017).
-Hydrogen is produced primarily through steam-reforming natural gas (Likkasit, et al. 2016).
-Costs of hydrogen production from renewables is currently higher than conventional production methods (Likkasit, et al. 2016).

Electrification of Drilling
Drilling rig uses 1MW of power

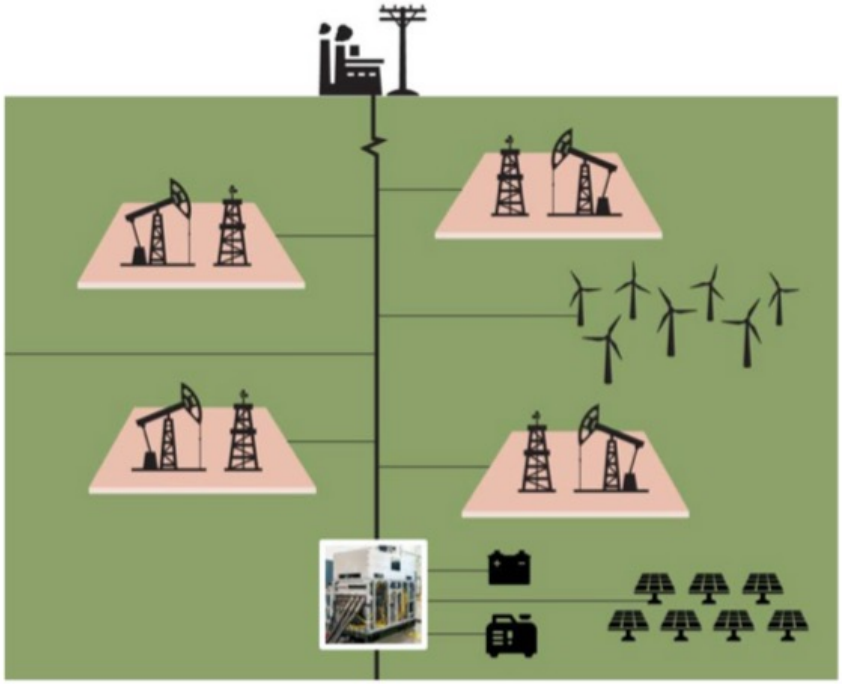

Figure 4. Schematic for a comprehensive approach to electrification of the wellpad and platform via microgrids

Rod Beam Artificial Lift Pump

-When there is not enough well pressure for oil to flow to the surface, a rod beam artificial lift pump—often referred to as a “sucker rod pump” or a “Jack pump”—is used to assist extraction.

-80% of oil production wells operating in the western United States are installed with a rod beam pump (Endurthy, Kialashaki and Gupta 2016).

-Solar power, combined with a capacitor to store regenerative power during the rod down-stroke, can be used to power a rod beam pump. Test cases have shown significant potential energy savings (Endurthy, Kialashaki and Gupta 2016), and solar powered oil pumps are now beginning to see commercial operation (Healing 2015).

-Combined with battery storage, solar power pumps could be applicable to off-grid locations with sufficient sunlight.

Secondary Oil Recovery

-Use offshore wind power to power water injection pumps.
-By one analysis, offshore wind was found in 2012 to be an economic and environmentally sound option for supplying electricity to offshore oil and gas platforms in some cases (Korpas, et al. 2012). -Substitute power from diesel and gas generators with power from wind platforms.
-Wind-powered water injection can provide water injection far from the platform, which reduces the need for lengthy water injection lines and can eliminate the need for costly modifications for oil platforms not initially designed for water injection.
-The Wind Powered Water Injection project recently completed an initial testing phase in which it was shown that wind power can provide water injection at competitive prices (Feller 2017).

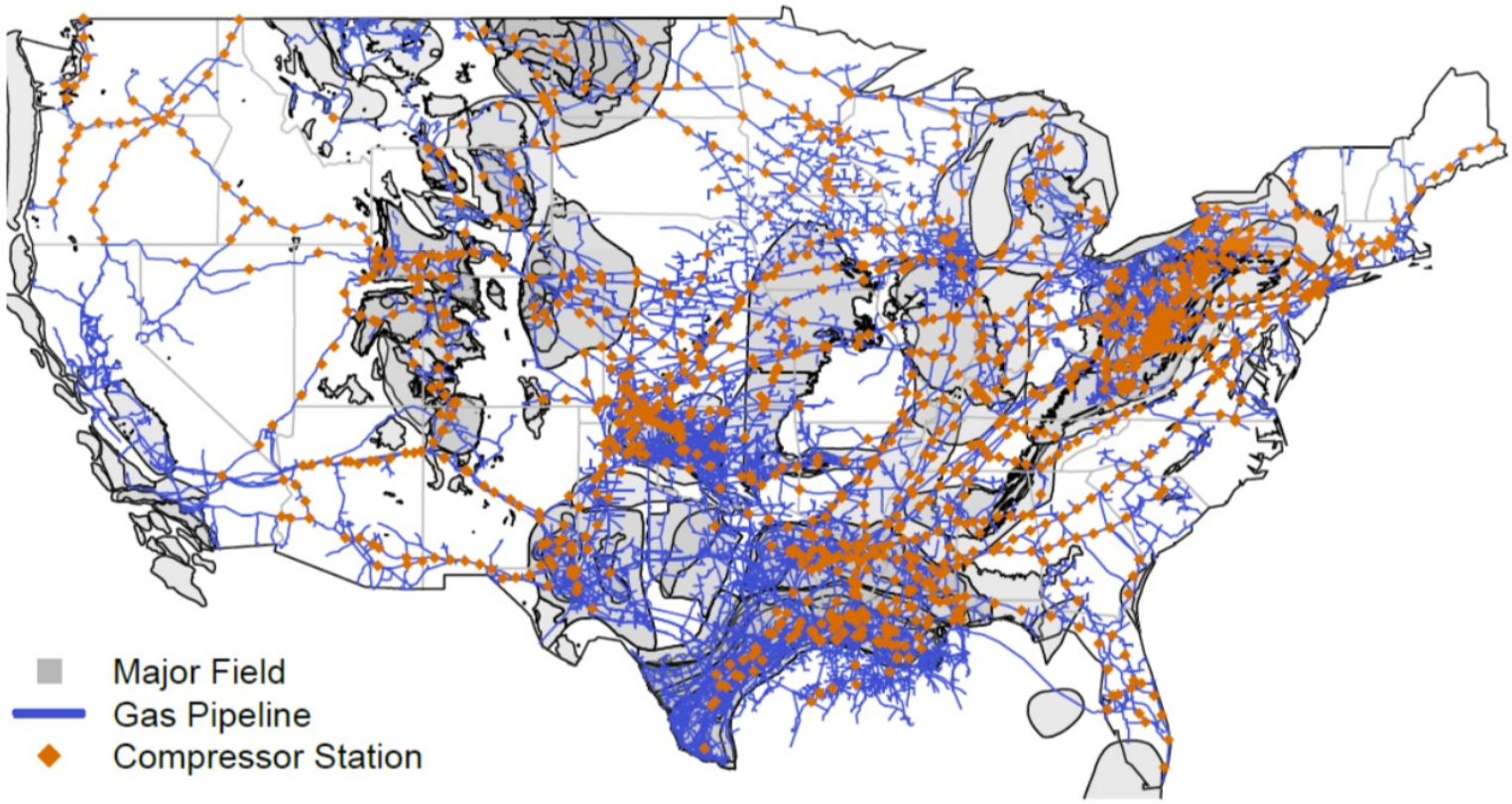

Figure 5. Natural gas transportation system. ***Figure produced using data from*** **(EIA 2018)**

Solar Thermal Carbon Black Production

New Link

Current method of Carbon Black production by industry

Carbon Black production via solar thermal cracking

Figure 1 Carbon black production by industry vs. via solar cracking

$$CH_4 \rightarrow C + 2H_2, \quad \Delta H = 75 \text{ kJ/mol}$$

The Boudouard reaction

$$C(s) + CO_2 = 2CO,\ \Delta H_{298K} = 172\ kJ\ mol^{-1} \quad (4)$$

$$C(s) + 2H_2 = CH_4,\ \Delta H_{298K} = -75\ kJ\ mol^{-1} \quad (5)$$

$$CH_4 + H_2O = CO + 3H_2,\ \Delta H_{298K} = 206\ kJ\ mol^{-1} \quad (6)$$

$$CO + H_2O = CO_2 + H_2,\ \Delta H_{298K} = -42\ kJ\ mol^{-1} \quad (7)$$

water–gas shift reaction

Solar Thermal Cracking for H_2

$$CH_{4(g)} + 2H_2O_{(l)} \rightarrow CO_{2(g)} + 4H_{2(g)} \qquad \Delta H^0_{25\,^\circ C} = 252.75\ \text{kJ/mol of } CH_4$$

Current method of Hydrogen production by industry

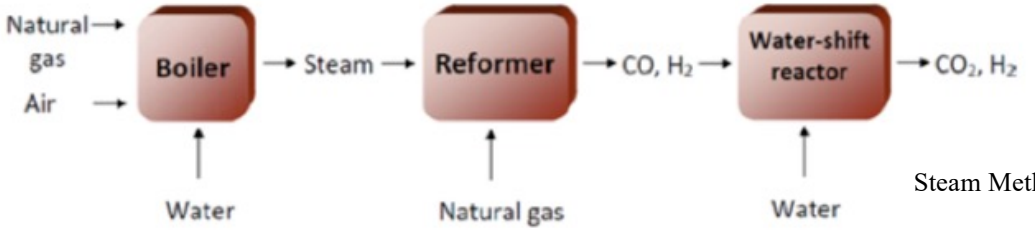

Steam Methane Reforming

Hydrogen production via solar thermal cracking

Figure 2 Hydrogen production by industry vs. via solar cracking

$$CH_4 \rightarrow C + 2H_2, \quad \Delta H = 75\ \text{kJ/mol}$$

energies

MDPI

Review

Methane Cracking for Hydrogen Production: A Review of Catalytic and Molten Media Pyrolysis

Malek Msheik, Sylvain Rodat and Stéphane Abanades *

Processes, Materials and Solar Energy Laboratory, PROMES-CNRS, 7 Rue du Four Solaire, 66120 Font Romeu, France; malek.msheik@promes.cnrs.fr (M.M.); sylvain.rodat@promes.cnrs.fr (S.R.)
* Correspondence: stephane.abanades@promes.cnrs.fr; Tel.: +33-(0)4-68-30-77-30

Citation: Msheik, M.; Rodat, S.; Abanades, S. Methane Cracking for Hydrogen Production: A Review of Catalytic and Molten Media Pyrolysis. *Energies* **2021**, *14*, 3107. https://doi.org/10.3390/en14113107

Academic Editor: Abdul-Ghani Olabi

Received: 16 April 2021
Accepted: 22 May 2021
Published: 26 May 2021

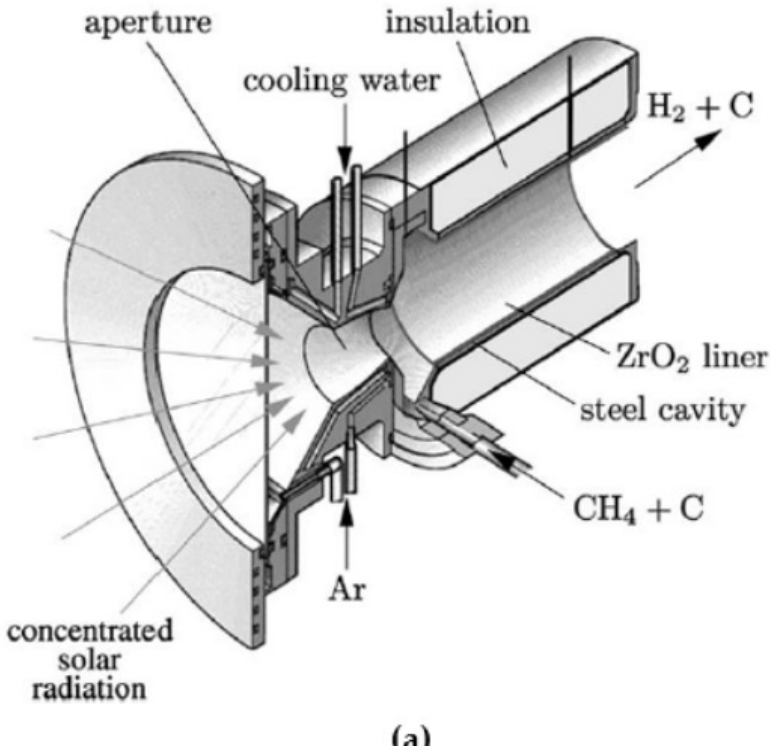

Figure 1. Directly- vs. indirectly-irradiated solar reactors used for methane pyrolysis: (**a**) 5 kW directly-irradiated reactor (Copied from Ref. [108] with Elsevier permission), (**b**) 50 kW indirectly-irradiated reactor (Copied from Ref. [102] with Elsevier permission).

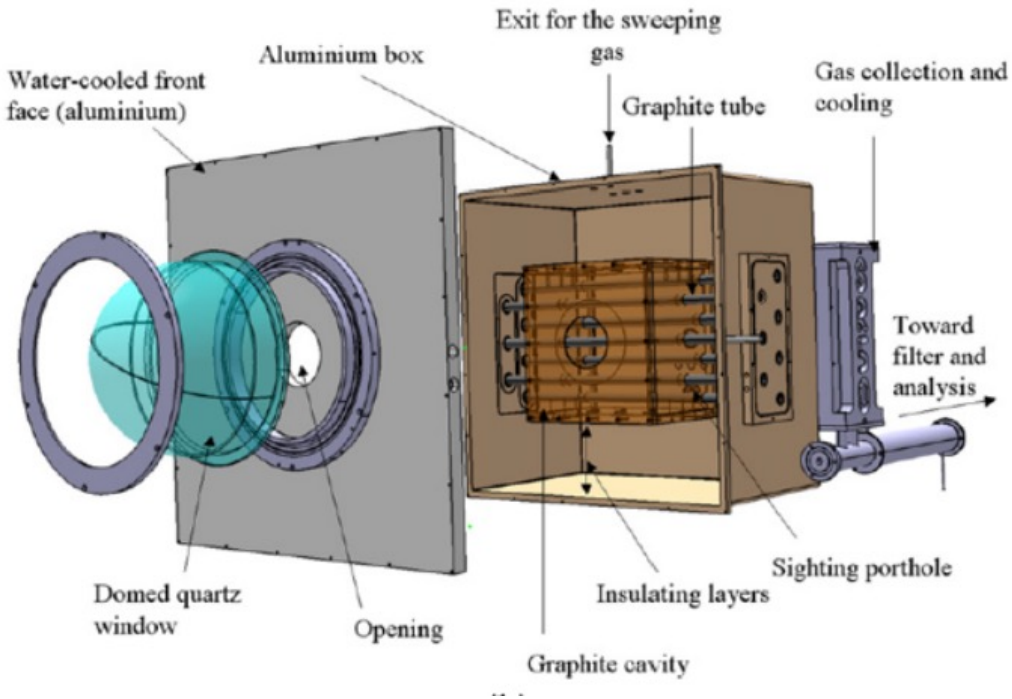

Figure 1. Directly- vs. indirectly-irradiated solar reactors used for methane pyrolysis: (**a**) 5 kW directly-irradiated reactor (Copied from Ref. [108] with Elsevier permission), (**b**) 50 kW indirectly-irradiated reactor (Copied from Ref. [102] with Elsevier permission).

Table 1. Main studies concerning solar methane cracking in gas phase (NA: not available).

Reference	Year	Heating Mode	Catalyst	Carbon Co-Feed	T (°C)	τ_r (s)	X_{CH4} (%)
Kogan and Kogan [107]	2003	Indirect irradiation	No catalyst	None	1047	NA	27.3
Dahl et al. [95]	2004	Indirect irradiation	No catalyst	CB	1860	0.01	90
Abanades and Flamant [14]	2007	Direct irradiation	No catalyst	None	1385	0.1	97
Abanades and Flamant [112]	2008	Direct irradiation	No catalyst	None	1400	0.25	99
Abanades et al. [98]	2008	Indirect irradiation	No catalyst	None	1580	0.018	99
Rodat et al. [103]	2009	Indirect irradiation	No catalyst	None	1550	0.011	78
						0.032	100
					1700	0.011	93
					1800	0.011	100
Rodat et al. [104]	2009	Indirect irradiation	No catalyst	None	1500	0.032	98
					1470	0.012	62
						0.035	98
Maag et al. [108]	2009	Direct irradiation	No catalyst	CB	1043	<2	98.8
Rodat et al. [102]	2010	Indirect heating	No catalyst	None	1520	0.061	99
Rodat et al. [96]	2011	Indirect irradiation	No catalyst	None	1700	0.011	93
					1800		100
Yeheskel and Epstein [106]	2011	Direct irradiation	No catalyst	None	1450	NA	100
			$Fe(CO)_5$		1200		50
			$Fe(C_5H_5)_2$		800		15–20
Abanades et al. [113]	2014	Indirect irradiation	CB	None	1200	0.12	≈100
Paxman et al. [109]	2014	Indirect irradiation	No catalyst	None	1100	NA	69
Abanades et al. [110]	2015	Indirect irradiation	CB (co-feed considered as catalyst)	CB	1250	0.113	50
						0.038	15

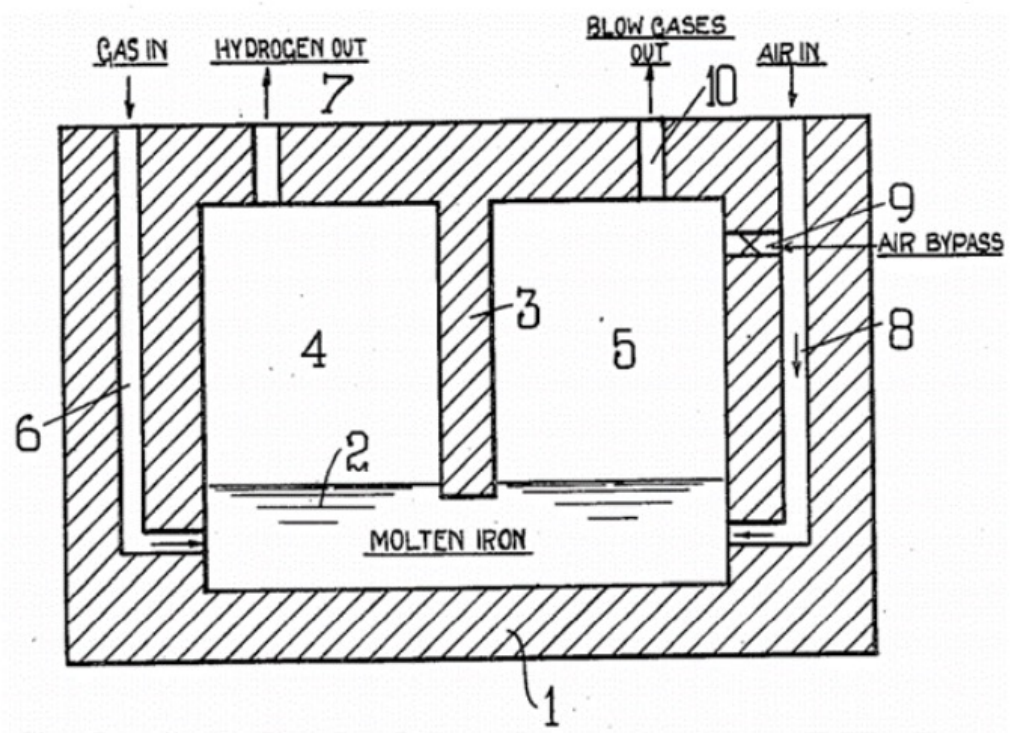

Figure 2. Two-chamber reactor design for pyrolysis in molten media from US patent of Tyrer (Copied from Ref. [29]).

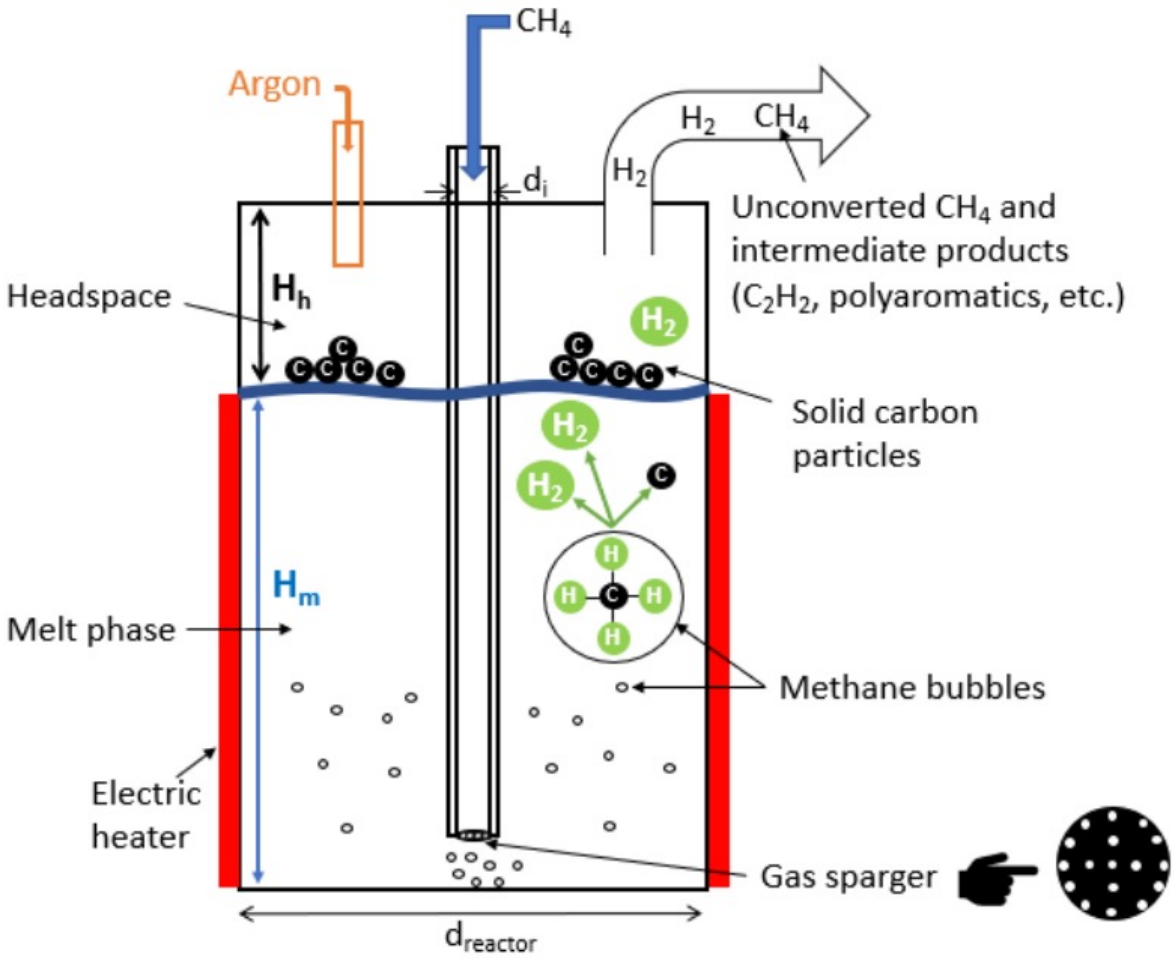

Figure 3. Representative scheme of a molten media reactor for methane pyrolysis.

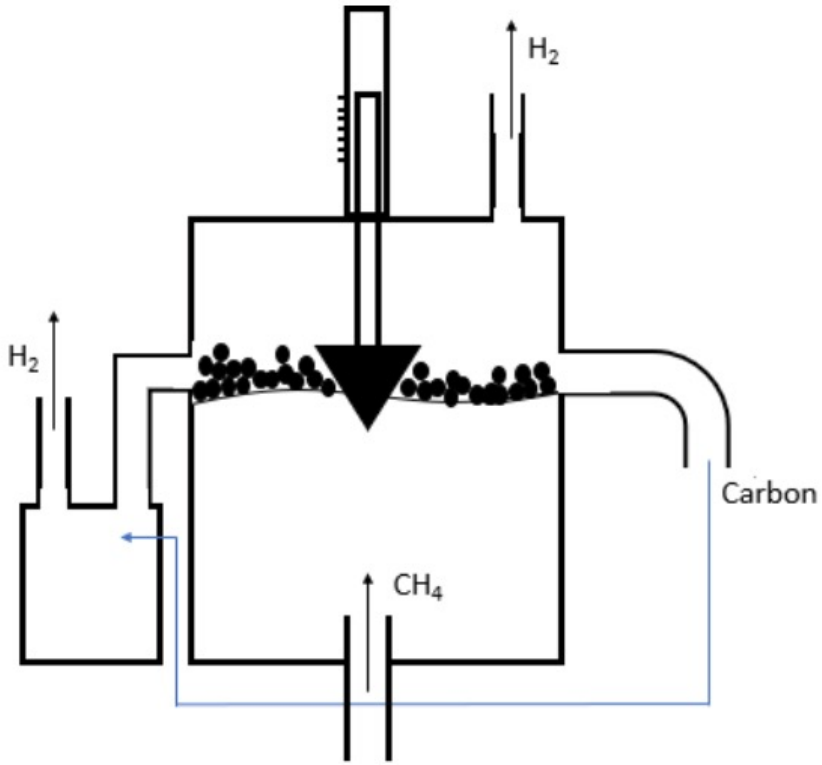

Figure 4. Reactor design for periodic carbon separation in a continuous molten media methane cracking process (adapted from Ref. [32] with Elsevier permission).

Table 2. Results of methane cracking main studies in molten media (gray: molten metals, white: molten salts, pink: two-phase molten media, green: metals suspended in molten salts).

Source	Year	Reactor Material	D (mm)	L(mm)	Filled Height (mm)	Methane Flow Rate (ml/min)	Bubble Generator Diameter	Molten Medium	Residence Time (s)	Temp (°C)	X_{CH4} (%)	X_{CH4} (%) Theoretical
Plevan et al. [3]	2015	SS	35.9	1190	600_1000	5	1 mm orifice	Tin	1.7–2.7	900	18	98
Geissler et al. [133]	2015	Quartz	40.6	1268	250 + (tin-packed bed combination (Quartz Glass, space porosity 76 vol.%, 850 mm long)	50	0.5 mm orifice	Tin	3.2–4.9	1000	32	99
Serban et al. [134]	2003	SS	25.4	355.6	101.6	15	Mott 0.5 µm porous distributor	Tin	0.3–0.5	750	51	93
Upham et al. [122]	2017	SS	30	1200	1200 (all)	10 (10% Ar)	3 mm orifice	NiBi (27:73)	≈7 s (calculated)	1065	95	99
Zeng et al. [130]	2020	Quartz	NA	70	NA	10 (43% Ar)	12 mm orifice	Te	0.5	977	22	98
Leal Pérez BJ et al. [129]	2020	NA	NA	NA	NA	450 (50% Ar)	Duran 0.2 mm porous distributor	Gallium	0.2–0.3	960–995	69–74	98–99
									0.5–0.8	936–1119	61–91	98–99
Wang et al. [123]	2008	SS	16	200	15 (calculated)	5	NA	Mg	NA	700	30	89
Parkinson et al. [135]	2021	Quartz	16	250	190	15	2 mm orifice	NaCl	0.69–0.76	1000	5.46	99
								KCl		1000	5.23	99
								NaBr		1000	4.36	99
								KBr		1000	6.22	99
								NaBr:KBr (48.7:51.3 mol%)		1000	5.85	99
Kang et al. [136]	2019	Quartz	25	250	125 (half)	20 (50% Ar)	2 mm orifice	$MnCl_2$/KCl (67:33)	0.6	1050	55 (starts at 45)	99
Kang et al. [131]	2020	Quartz	25	250	125 (half)	20 (50% Ar)	2 mm orifice	Fe (3 wt.%)/NaKCl	0.5	1000	9	99
Rahimi et al. [121]	2019	Quartz	22	300–430–1000	L-80	10 (43% Ar)	2 mm orifice	NiBi (27:73)/NaBr	4.2/1.1	1000	37.5	99
Patzschke et al. [137]	2021	Quartz	16	250	190	45 (67% Ar)	2 mm orifice	Co-Mn (molar ratio = 2) dispersed in NaBr:KBr (48.7:51.3 mol%)	NA	850–1000	10.52	98–99

Table 3. Main metal properties with calculated volumetric heat capacity (LME: London metal exchange) [138,139].

Metal	Symbol	Melting Point (°C)	Boiling Point (°C)	Density (g/cm³) Solid vs. Liquid		LME Price (EUR/ton)	Specific Heat (J/g.°C)	ρ.Cp (J/cm³.°C)
Tin (2 types: gray and white)	Sn	232	2602	5.77 (gray) / 7.27 (white)	6.99	25,891	0.21	1.46
Nickel	Ni	1455	2730	8.91	7.81	14,223	0.50	3.92
Cobalt	Co	1495	2900	8.90	7.75	36,957	0.42	3.24
Iron	Fe	1538	2861	7.87	6.98	422 (scrap)	0.46	3.21
Manganese	Mn	1246	2061	7.47	5.95	NA	0.48	2.84
Bismuth	Bi	271	1564	9.78	10.05	NA	0.13	1.26
Tellurium	Te	450	988	6.24	5.70	NA	0.20	1.15
Copper	Cu	1085	2562	8.96	8.02	8489	0.38	3.02
Aluminum	Al	660	2519	2.70	2.38	2006	0.92	2.19
Gallium	Ga	30	2204	5.90	6.10	NA	0.37	2.26

Table 4. Apparent activation energies for different catalysts used in methane pyrolysis reaction.

Medium	Catalyst	Apparent Activation Energy (kJ/mol)
Gas phase	Gas phase (uncatalyzed) [14–17]	356–452
	Carbon-based catalysts [14]	205–236
	Solid Ni [140]	65
	Solid Ni/SiO_2 [141]	96.1
Molten phase	Molten Fe(3 wt.%)-NaKCl: (Fe (III) introduced as $FeCl_3 \cdot 6H_2O$) [131]	171
	Molten $MnCl_2$(67%)-KCl(33%) [136]	161
	Molten Te [130]	166
	Molten Ni(67%)-Bi(33%) [122]	208
	Molten Cu(45%)-Bi(55%) [33]	222
	Molten Bi [122]	310
	Molten Tin	NA
	NaCl-KCl-NaBr-KBr [135]	231–236–278–224
	NaBr(48.7):KBr(51.3) [135]	246.7
	NaBr(48.7):KBr(51.3) [137]	236.3
	(Co-Mn)/NaBr:KBr (48.7:51.3) [137]	175.5

Table 5. Comparison of liquid catalyst activity for methane pyrolysis at 1000 °C when CH_4 is flowed over 38.5 mm^2 of molten metal in a differential reactor. (*) indicates that alloy is at the solubility limit of the dissolved active metal at 950 °C.

Liquid Catalyst	Rate of Hydrogen Production (mol H_2 Produced. cm^{-2} s^{-1})
In	8.2×10^{-11}
Bi	8.2×10^{-11}
Sn	8.5×10^{-10}
Ga	3.2×10^{-9}
Pb	3.3×10^{-9}
Ag	4.3×10^{-9}
Pb vapor	2.1×10^{-9}
17% Cu–Sn *	3.1×10^{-9}
17% Pt–Sn	1.6×10^{-9}
17% Pt–Bi	4.2×10^{-9}
62% Pt–Bi *	6.5×10^{-9}
17% Ni–In	4.7×10^{-9}
17% Ni–Sn	5.6×10^{-9}
73% Ni–In *	6.4×10^{-9}
17% Ni–Ga	7.9×10^{-9}
17% Ni–Pb	8.3×10^{-9}
17% Ni–Bi	9.0×10^{-8}
27% Ni–Au *	1.2×10^{-8}
27% Ni–Bi *	1.7×10^{-8}

Turn Over Frequency

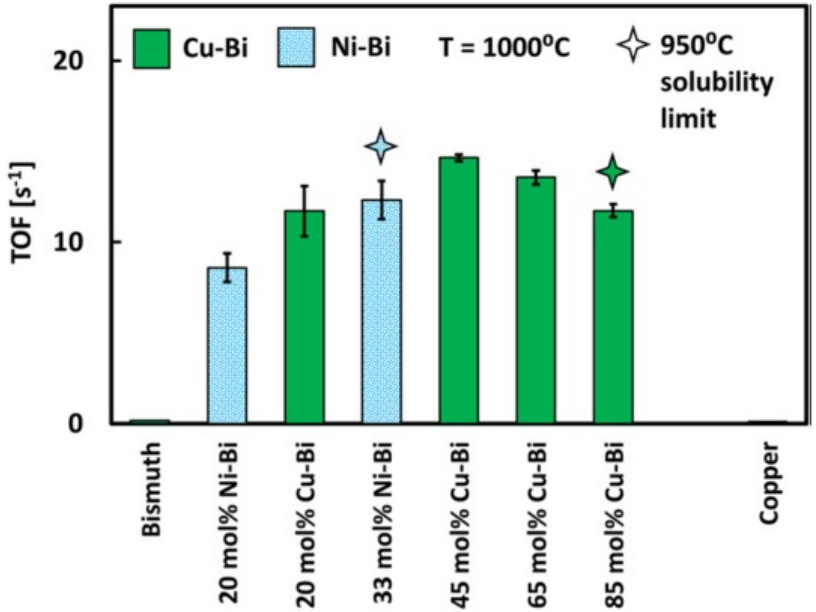

Figure 5. TOF for methane cracking over Cu–Bi, Ni–Bi alloys and pure Bi at 1000 °C. Pure copper is tested at 1100 °C (Copied from Ref. [33] with American Chemical Society permission).

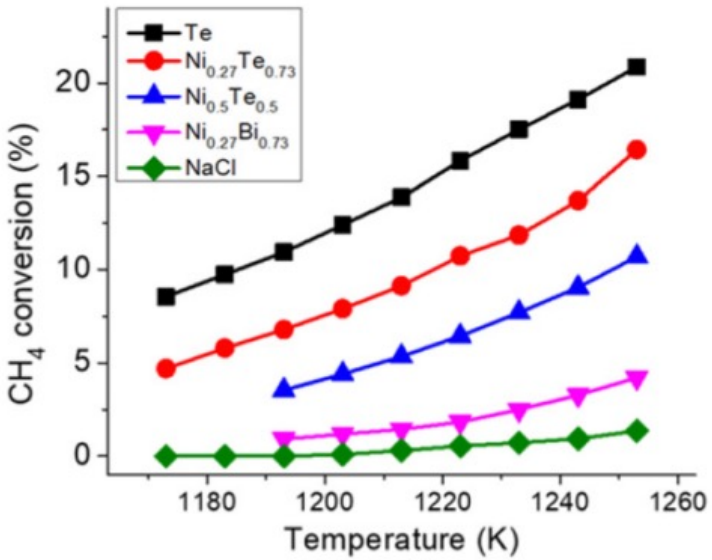

Figure 6. Methane conversion of pure Te compared with Ni–Bi and Ni–Te alloys, as well as with molten NaCl (Copied from Ref. [130] with American Chemical Society permission).

Table 7. Comparison between the features of molten metals and molten salts used in methane cracking.

	Cost	Catalytic Activity	Carbon Purification	Vapor Pressure	Melting Points
Metals	High	High	Complex	High	High
Salts	Low	Moderate or low	Easy	Low	Low

$$CH_aO_b + {}^{(1-b)}/_{\delta}\, MeO_x \rightarrow CO + {}^{a}/_{2}\, H_2 + {}^{(1-b)}/_{\delta}\, MeO_{x-\delta}$$

Reduce Metal Oxide
High Temp

$${}^{2}/_{\delta}\, MeO_{x-\delta} + O_2\ (air) \rightarrow {}^{2}/_{\delta}\, MeO_x + (O_2\ depleted\ air)$$

$${}^{1}/_{\delta}\, MeO_{x-\delta} + H_2O \rightarrow {}^{1}/_{\delta}\, MeO_x + H_2$$

Oxidize Metal Oxide
Low Temp

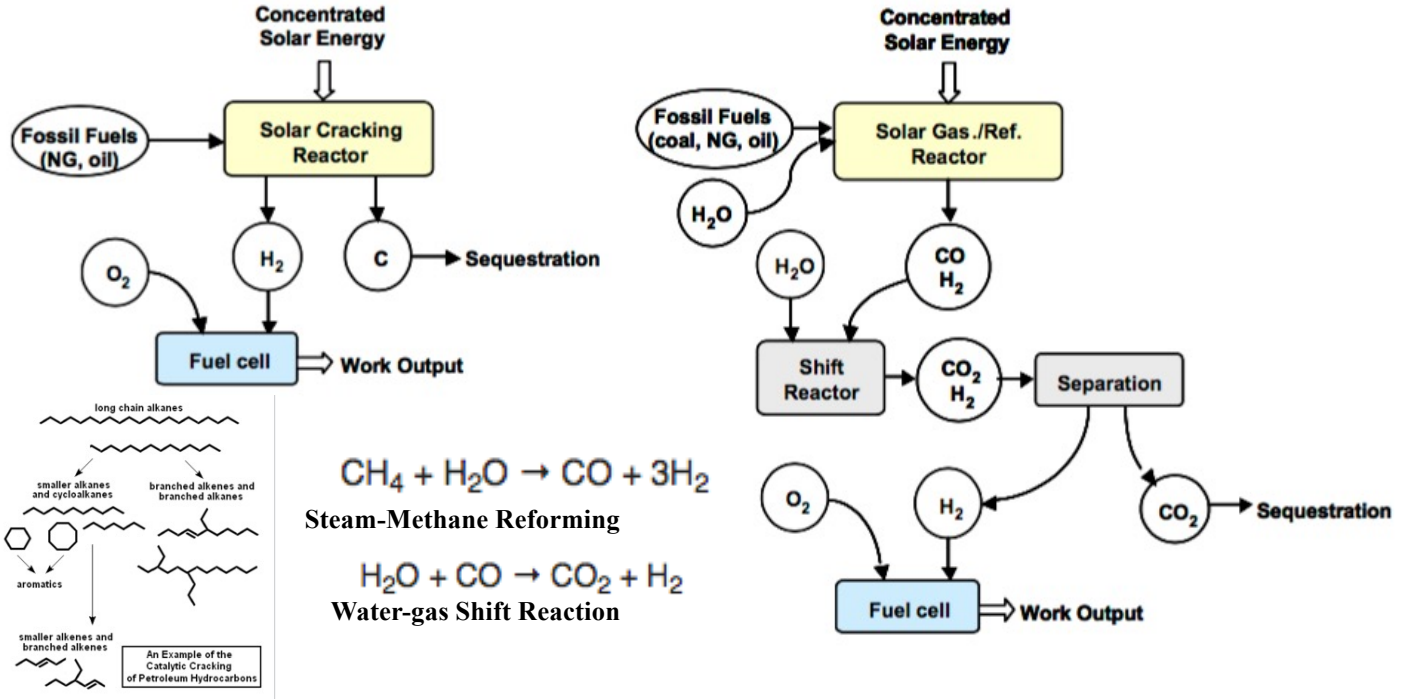

Fig. 7: Solar thermochemical routes for H_2 production using fossil fuels and H_2O as the chemical source – Solar cracking (left), and solar reforming and gasification (right). From [1].

Round-the-clock power supply and a sustainable economy via synergistic integration of solar thermal power and hydrogen processes

Emre Gençer[a], Dharik S. Mallapragada[a], François Maréchal[b], Mohit Tawarmalani[c], and Rakesh Agrawal[a,1]

[a]School of Chemical Engineering, Purdue University, West Lafayette, IN 47907; [b]Industrial Process and Energy Systems Engineering Group, École Polytechnique Fédérale de Lausanne, CH-1951 Sion, Switzerland; and [c]Krannert School of Management, Purdue University, West Lafayette, IN 47907

Edited by Hans Joachim Schellnhuber, Potsdam Institute for Climate Impact Research (PIK), Potsdam, Germany, and approved November 17, 2015 (received for review July 12, 2015)

We introduce a paradigm—"hydricity"—that involves the coproduction of hydrogen and electricity from solar thermal energy and their judicious use to enable a sustainable economy. We identify and implement synergistic integrations while improving each of the two individual processes. When the proposed integrated process is operated in a standalone, solely power production mode, the resulting solar water power cycle can generate electricity with unprecedented efficiencies of 40–46%. Similarly, in standalone hydrogen mode, pressurized hydrogen is produced at efficiencies approaching ∼50%. In the coproduction mode, the coproduced hydrogen is stored for uninterrupted solar power production. When sunlight is unavailable, we envision that the stored hydrogen is used in a "turbine"-based hydrogen water power (H_2WP) cycle with the calculated hydrogen-to-electricity efficiency of 65–70%, which is comparable to the fuel cell efficiencies. The H_2WP cycle uses much of the same equipment as the solar water power cycle, reducing capital outlays. The overall sun-to-electricity efficiency of the hydricity process, averaged over a 24-h cycle, is shown to approach ∼35%, which is nearly the efficiency attained by using the best multijunction photovoltaic cells along with batteries. In comparison, our proposed process has the following advantages: (*i*) It stores energy thermochemically with a two- to three-fold higher density, (*ii*) coproduced hydrogen has alternate uses in transportation/chemical/petrochemical industries, and (*iii*) unlike batteries, the stored energy does not discharge over time and the storage medium does not degrade with repeated uses.

solar | electricity | hydrogen | solar thermal power | process synthesis

metrics of interest. The STE efficiency refers to the fraction of incident solar energy that is recovered as the net electricity output and accounts for the losses in the solar concentrators and blackbody collection system. Heat-to-electricity efficiency refers to the fraction of process heat input that is recovered as the net electricity output and is a true measure of the efficiency of the power cycle. The third metric, OSTE efficiency (*SI Appendix*, Eq. **S4**), is the net STE efficiency for a constant power delivery round-the-clock—that is, over the average 24-h production accounting for energy storage and delivery of the stored energy. Hydrogen production cycles are evaluated based on sun-to-hydrogen efficiency, which refers to the fraction of incident solar energy that is recovered as the net hydrogen output based on its lower heating value (*SI Appendix*, Eq. **S10**).

Solar photovoltaic (PV) and solar thermal are the two main methods of solar power generation. Solar PV systems generate electricity using only a portion of the solar spectrum (7). However, PV systems are suitable for both diffuse and direct sunlight applications (8). To date, the maximum reported STE efficiencies for silicon–crystalline PV is 27.6%, single-junction gallium arsenide PV is 29.1%, and concentrator four-junction PV is 44.7% (9). Solar thermal systems use concentrators to absorb photons of all wavelengths in the incident spectrum as high-temperature heat (10, 11). Due to the use of optical concentrators, these systems can only be operated under direct sunlight, which imposes geographical limitations (12). Further, these systems are anticipated to be cost-effective only as large-scale power plants, owing to the capital costs of installing solar concentrators (12, 13). However, the highest STE

www.pnas.org/cgi/doi/10.1073/pnas.1513488112

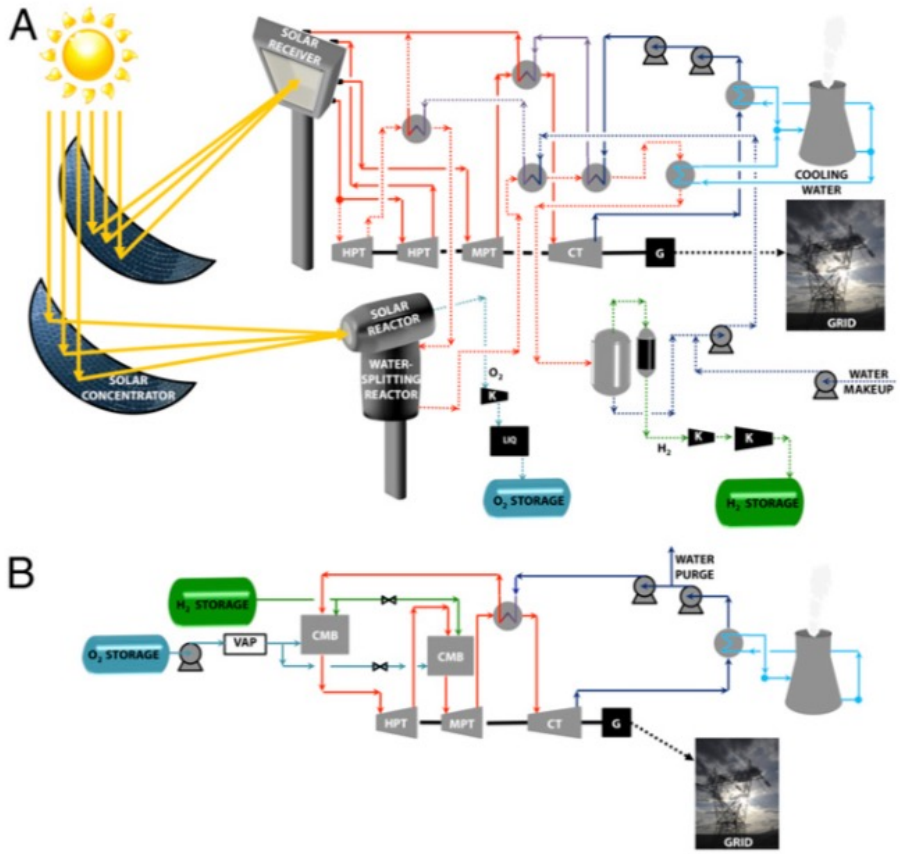

Fig. 1. (*A*) An example hydricity process: SWH_2P cycle with two-step hydrogen production using the FeO/Fe_3O_4 cycle. Solid lines represent streams that are solely involved in the electricity production (i.e., SWP-1). Dotted lines represent streams that are related to hydrogen production as well as electricity production. CT, condensing turbine; G, generator; HPT, high-pressure turbine; K, compressor; LIQ, liquefaction process; MPT, medium-pressure turbine. (*B*) H_2WP cycle, hydrogen oxy-combustion in water environment. CMB, hydrogen combustor.

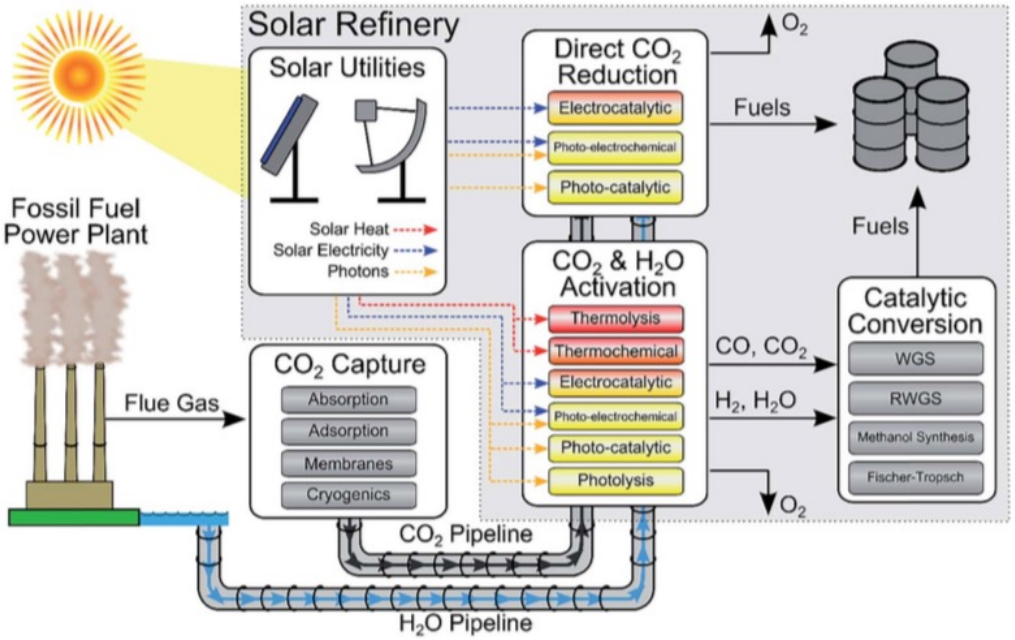

Fig. 1 Schematic for solar fuels production. Solar fuel feedstocks (CO_2, H_2O, and solar energy) are captured on-site and/or transported to the solar refinery. Solar energy provides solar utilities in the form of heating, electricity, and photons which are used in the solar refinery to convert CO_2 and H_2O into fuels. CO_2 and H_2O are converted to fuels through two principal routes: (1) direct solar-driven CO_2 reduction by H_2O to fuels or (2) solar activation of CO_2/H_2O to CO/H_2, respectively, and subsequent catalytic conversion to fuels *via* traditional processing (*i.e.* methanol synthesis or Fischer-Tropsch). The approximate temperature requirements for the solar-driven conversion processes are color-coded (red = high temperature, yellow = ambient temperature).

Energy & Environmental Science

ROYAL SOCIETY OF CHEMISTRY

ANALYSIS

View Article Online
View Journal | View Issue

Cite this: *Energy Environ. Sci.*, 2015, **8**, 126

A general framework for the assessment of solar fuel technologies†

Jeffrey A. Herron, Jiyong Kim,‡ Aniruddha A. Upadhye, George W. Huber and Christos T. Maravelias*

The conversion of carbon dioxide and water into fuels in a solar refinery presents a potential solution for reducing greenhouse gas emissions, while providing a sustainable source of fuels and chemicals. Towards realizing such a solar refinery, there are many technological advances that must be met in terms of capturing and sourcing the feedstocks (namely CO_2, H_2O, and solar energy) and in catalytically converting CO_2 and H_2O. In the first part of this paper, we review the state-of-the-art in solar energy collection and conversion to solar utilities (heat, electricity, and as a photon source for photo-chemical reactions), CO_2 capture and separation technology, and non-biological methods for converting CO_2 and H_2O to fuels. The two principal methods for CO_2 conversion include (1) catalytic conversion using solar-derived hydrogen and (2) direct reduction of CO_2 using H_2O and solar energy. Both hydrogen production and direct CO_2 reduction can be performed electro-catalytically, photo-electrochemically, photo-catalytically, and thermochemically. All four of these methods are discussed. In the second part of this paper, we utilize process modeling to assess the energy efficiency and economic feasibility of a generic solar refinery. The analysis demonstrates that the realization of a solar refinery is contingent upon significant technological improvements in all areas described above (solar energy capture and conversion, CO_2 capture, and catalytic conversion processes).

Received 25th June 2014
Accepted 1st October 2014

DOI: 10.1039/c4ee01958j

www.rsc.org/ees

$$C_1H_xO_yS_uN_v \xrightarrow{\text{heat}} C(s) + CO + CO_2 + H_2 + C_xH_y + \text{tars} \quad (2)$$

Pyrolysis has been extensively studied empirically for various coal ranks ranging from anthracite (~10 wt% volatile matter) to peat (>65 wt% volatile matter), as well as for scrap tires, plastics, biomass, and refuse derived fuels.[13–17] Solar-driven pyrolysis was investigated in early studies on biomass and coal.[18–21] Subsequent to pyrolysis, char serves as the reactant for the highly endothermic carbon-steam gasification reaction,

$$C(s) + H_2O = CO + H_2, \Delta H_{298K} = 131 \text{ kJ mol}^{-1} \quad (3)$$

Favorable conditions for this reaction are temperatures above 1100 K, where the reaction kinetics is fast and equilibrium is entirely on the side of the products. Eqn (3) summarizes the overall reaction, but a number of intermediate competing reactions need to be considered:

$$C(s) + CO_2 = 2CO, \Delta H_{298K} = 172 \text{ kJ mol}^{-1} \quad (4)$$ The Boudouard reaction.

$$C(s) + 2H_2 = CH_4, \Delta H_{298K} = -75 \text{ kJ mol}^{-1} \quad (5)$$

$$CH_4 + H_2O = CO + 3H_2, \Delta H_{298K} = 206 \text{ kJ mol}^{-1} \quad (6)$$

$$CO + H_2O = CO_2 + H_2, \Delta H_{298K} = -42 \text{ kJ mol}^{-1} \quad (7)$$ water–gas shift reaction

Haber Reaction to Produce NH_3 from H_2

$$\mathrm{N_2 + 3\,H_2 \longrightarrow 2\,NH_3 \quad \Delta H^\circ = -91.8\,kJ/mol}$$

100 bar 400-500 °C Iron Catalyst

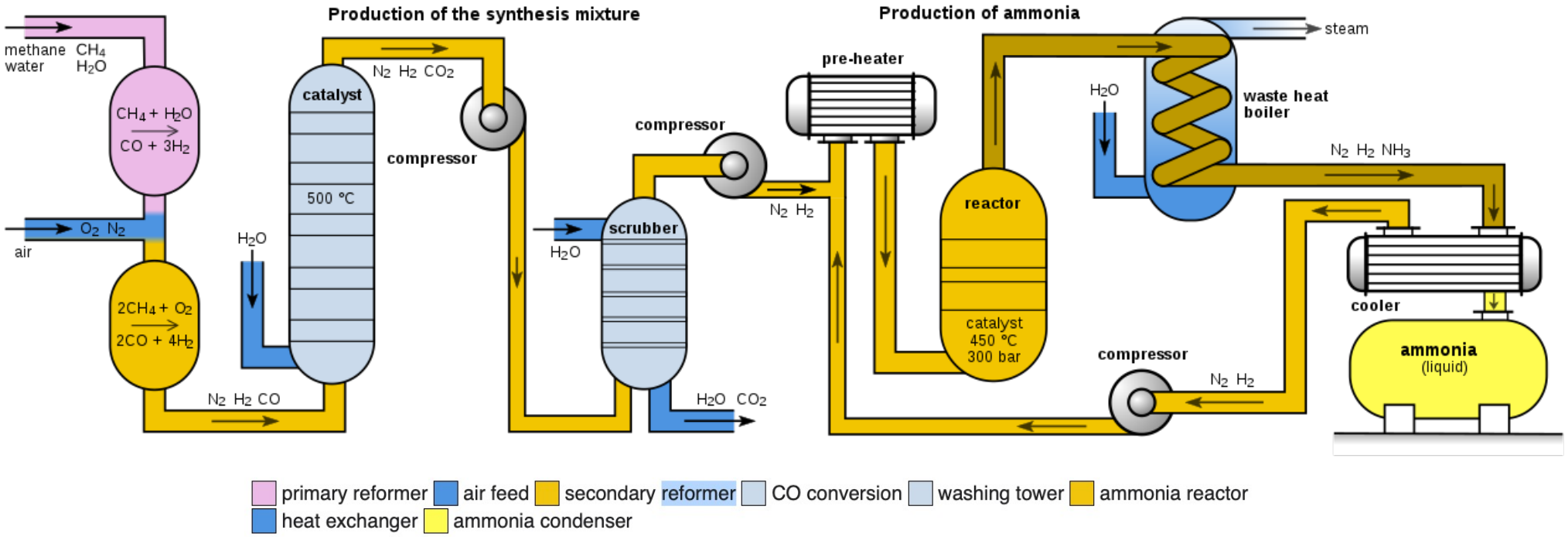

Fischer-Tropsch Reaction to Produce Hydrocarbons from H_2

$$(2n + 1)\,H_2 + n\,CO \rightarrow C_nH_{2n+2} + n\,H_2O$$

(ΔH) of −165 kJ/mol CO combined.

n = 10-20 330-250 °C 10-40 bar

Cobalt, Iron, Ruthenium Catalyst

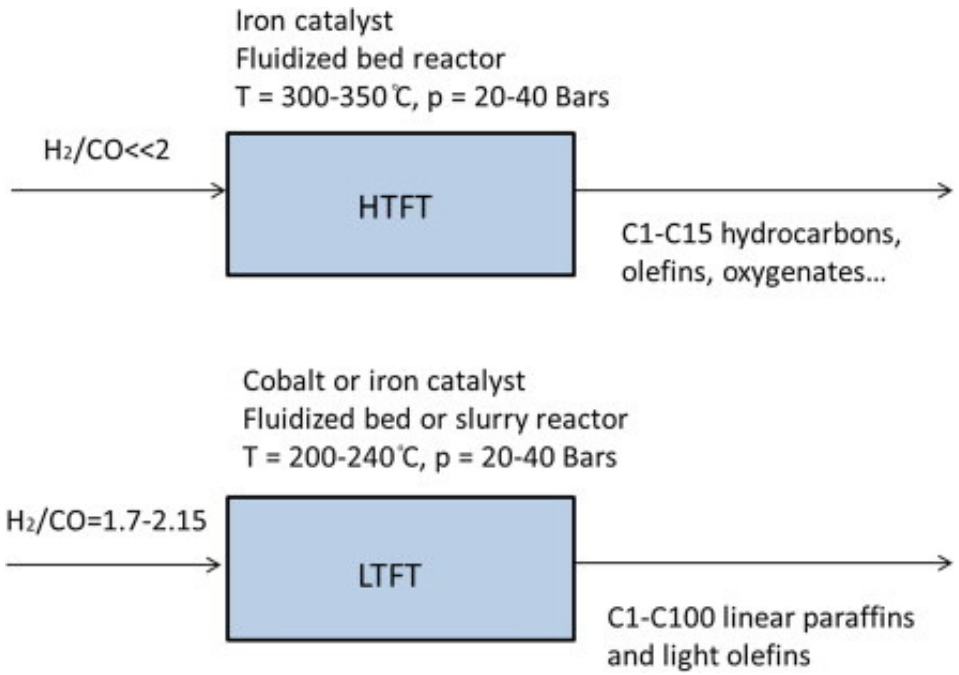

Catalytic Cracking of NH_3 to H_2

$$2NH_3 + 92.4kJ \rightarrow N_2 + 3H_2$$

10 MPa 425 °C Catalyst Fe, Ni, Pt, Ru, Ir, Pd, Rh etc.

Fuel / Storage System	P (bar)	Energy Density (GJ/m^3)	Specific Volumetric cost ($US\$/m^3$)	Specific Energy Cost ($US\$/GJ$)
Ammonia gas / pressurized tank	10	13.6	181	13.3
Hydrogen / metal hydride	14	3.6	125	35.2
Gasoline (C_8H_{18}) / liquid tank	1	34.4	1000	29.1
LPG (C_3H_8) / pressurized tank	14	19.0	542	28.5
CNG (CH_4) / integrated storage system	250	10.4	400	38.3
Methanol (CH_3OH) / liquid tank	1	11.4	693	60.9

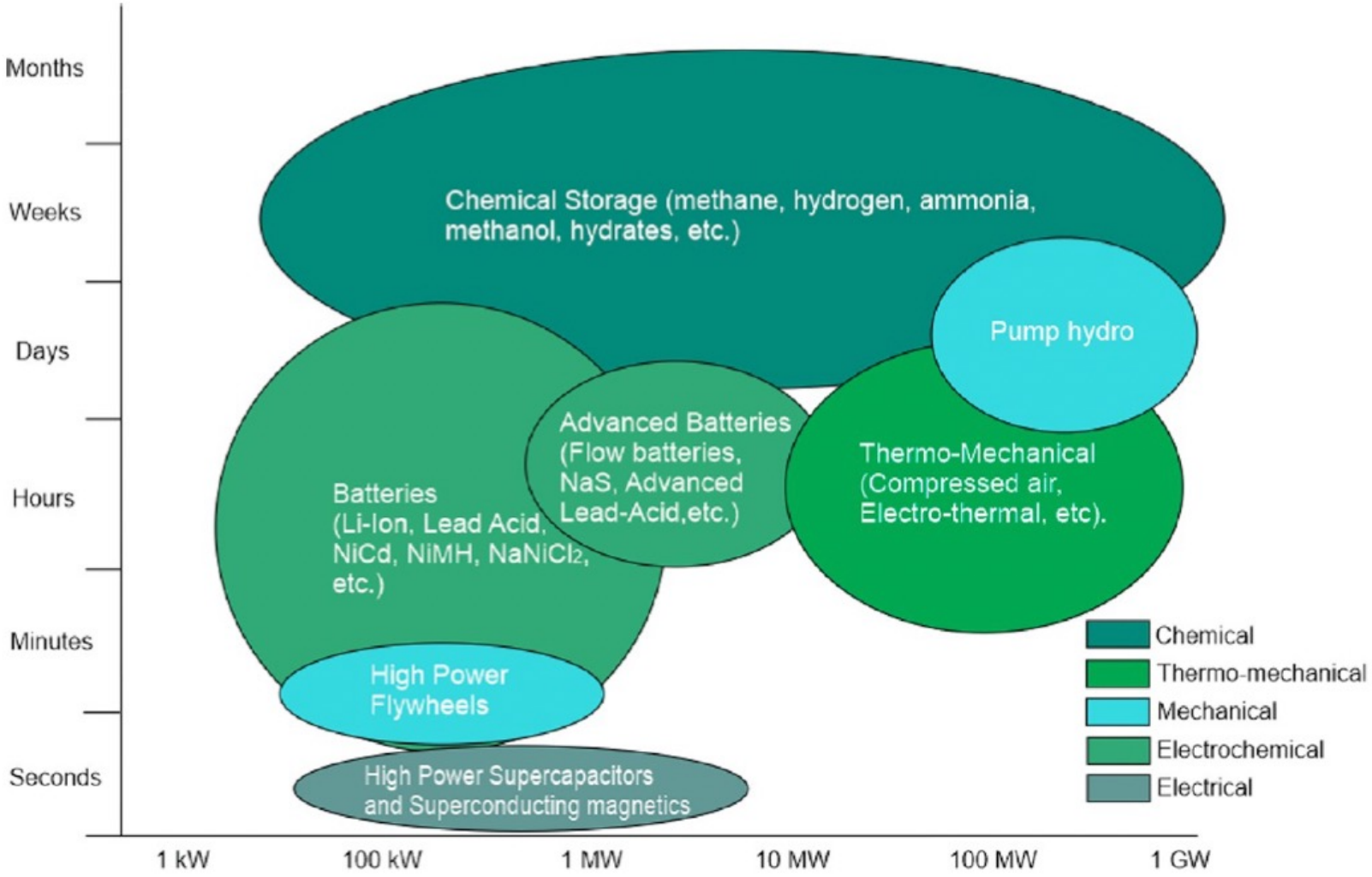

1. Comparison between different energy storage technologies. This figure was reproduced with permission from ref 11. Copyright 2

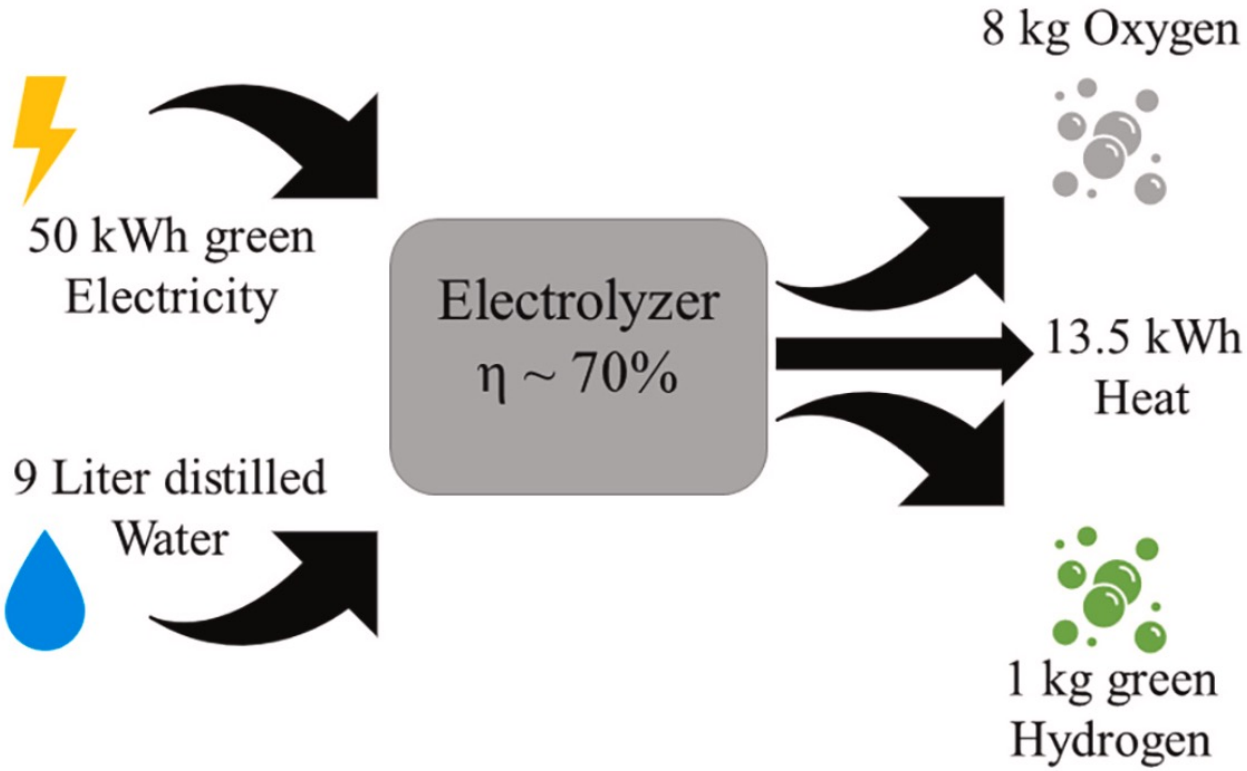

Fig. 1. Electrolysis of water requires 9 l of distilled water and approximately 50 kwh to generate 1 kg of hydrogen using an electrolyzer with 70 % electrical efficiency.

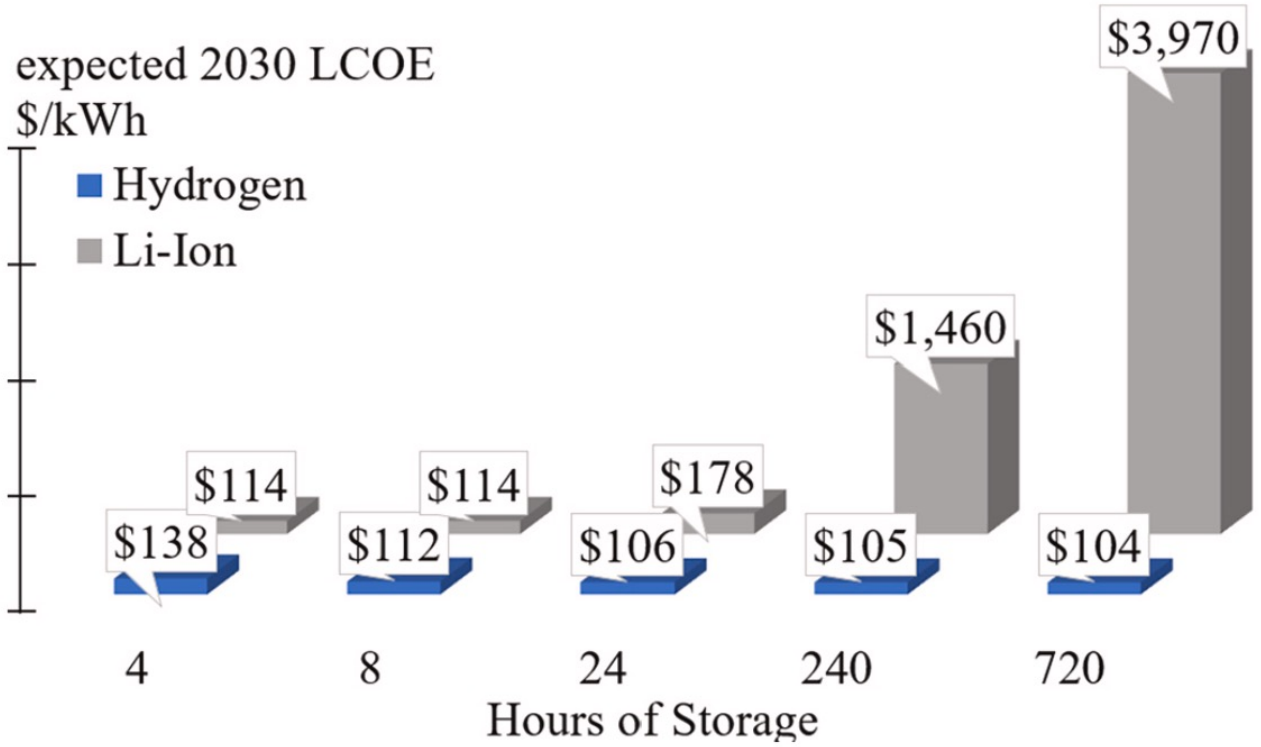

Fig. 3. Comparison of hydrogen and Li-ion electricity storage. Li-ion batteries are more cost-effective for shorter storage durations whereas hydrogen breaks even around 8 h of storage based on data presented in [70].

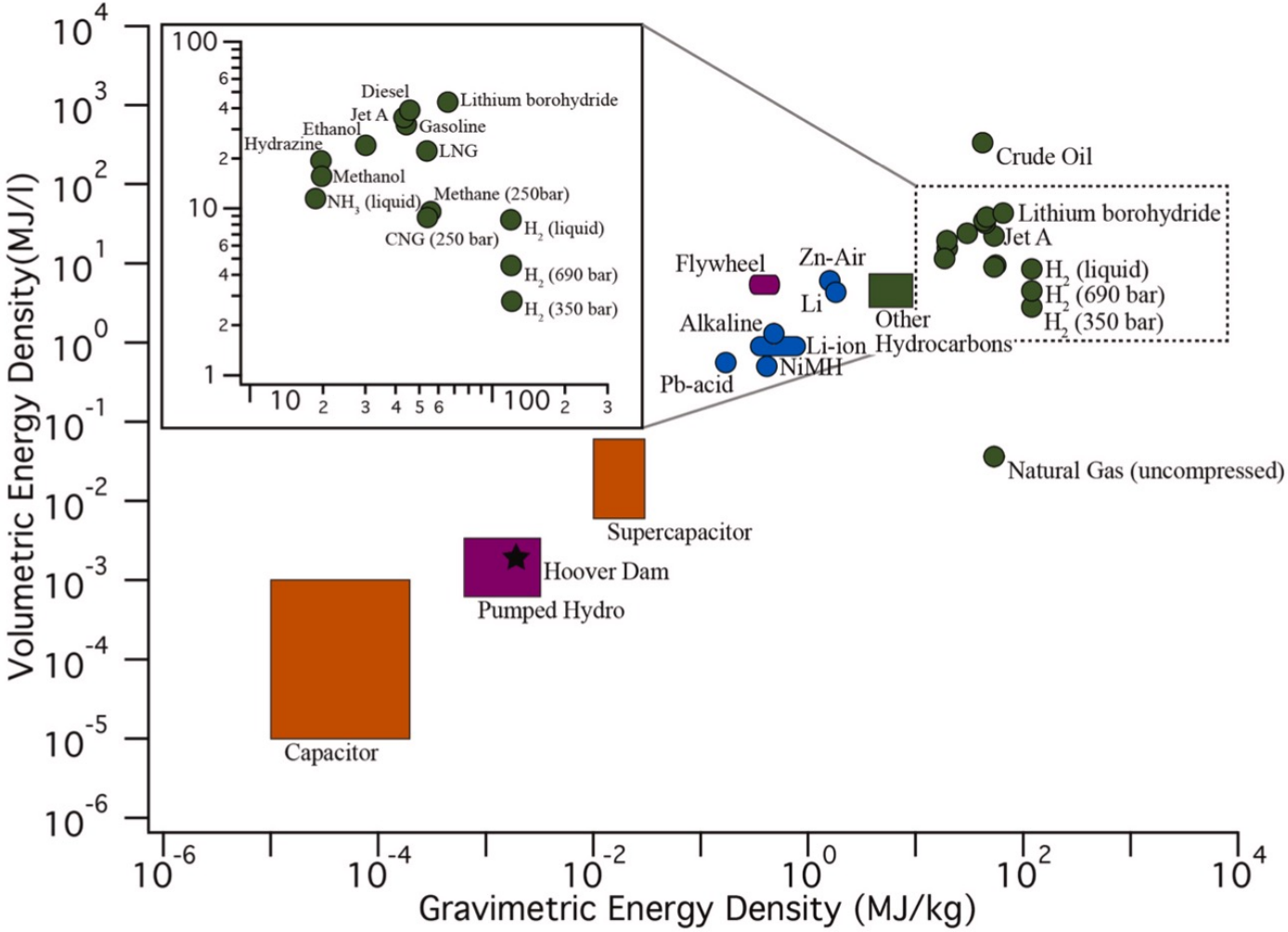

Fig. 4. Volumetric and gravimetric energy densities for the most common storage applications in direct comparison. Chemical compounds typically score high for both densities whereas battery-based storage technology requires more volume and mass to store energy. Pumped hydrogen and capacitors rank lowest in both categories. The color-coding of the categories is identical to the one found in Fig. 2.

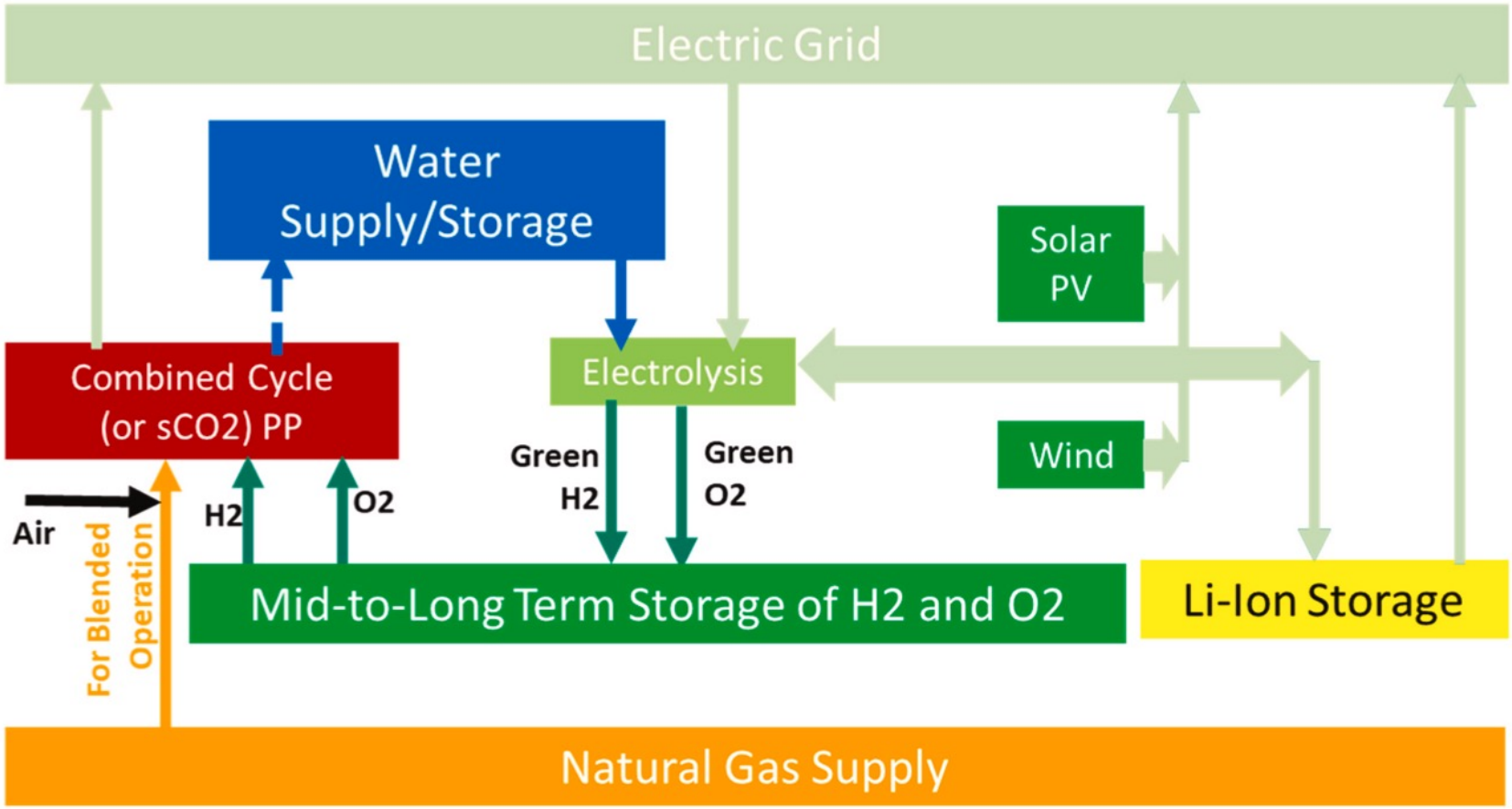

Fig. 5. The potential integration of hydrogen as a mid-to-longterm storage system into the power grids of the future.

Overview of power generation use cases and metrics.

Case	Name	Type	Fuel	Nameplate Power [MW]	Nominal Efficiency	Nominal Heat Rate [J/kWh]	Storage Duration [d]
#1	SGT-A05	Industrial GT for mechanical work	Natural gas	5	32.3 %	1.12E7	7
#2	SGT-A65	Aeroderivative for power generation	Natural gas	44	40.4 %	8.92E6	7
#3	SGT6-5000F	Heavy-duty for power generation	Natural gas	260	40 %	9E6	7

Table 2
Assumptions and values for Case #4 Boeing and Case #5 Airbus.

Case	Name	Engines	Fuel	TSFC cruise [lb/lbf.h]	TSFC cruise [kg/kN.s]	Thrust cruise [lbf]	Thrust cruise [kN]	Flight Duration [h]	Fuel Consumption [kg Jet A] [113]	Fuel Consumption [kg H_2]
#4	Boeing 737max	2x CFM Leap 1B	Jet A-1	0.53	15	5480	24.38	2.5	6587	2393
#5	Airbus A320neo	2x CFM Leap 1A	Jet A-1	0.51	14	5000	22.24	2.5	5783	2101

Case	Location	Assumed daily travel distance [127]	Fuel	Road type	Fuel Economy	Fuel Consumption
#6	Germany	540	Diesel	Highway	55.6 l/100 km	255 kg
			H2 + electric	Highway	10 km/kg	54 kg
			electric	Highway	190 kWh/100 km	1026 kWh
#7	USA	900	Diesel	Highway	55.6 l/100 km	403 kg
			H2 + electric	Highway	10 km/kg	85 kg
			electric	Highway	190 kWh/100 km	1620 kWh

Case	Type	Travel Distance [km]	Fuel	Travel Duration [d]	Fuel Economy [t/d]	Fuel Consumption [t]	Cargo Rating [TEU]
#8	Post-Panamax	22,224	Heavy Fuel Oil	30	100	3000	14,500

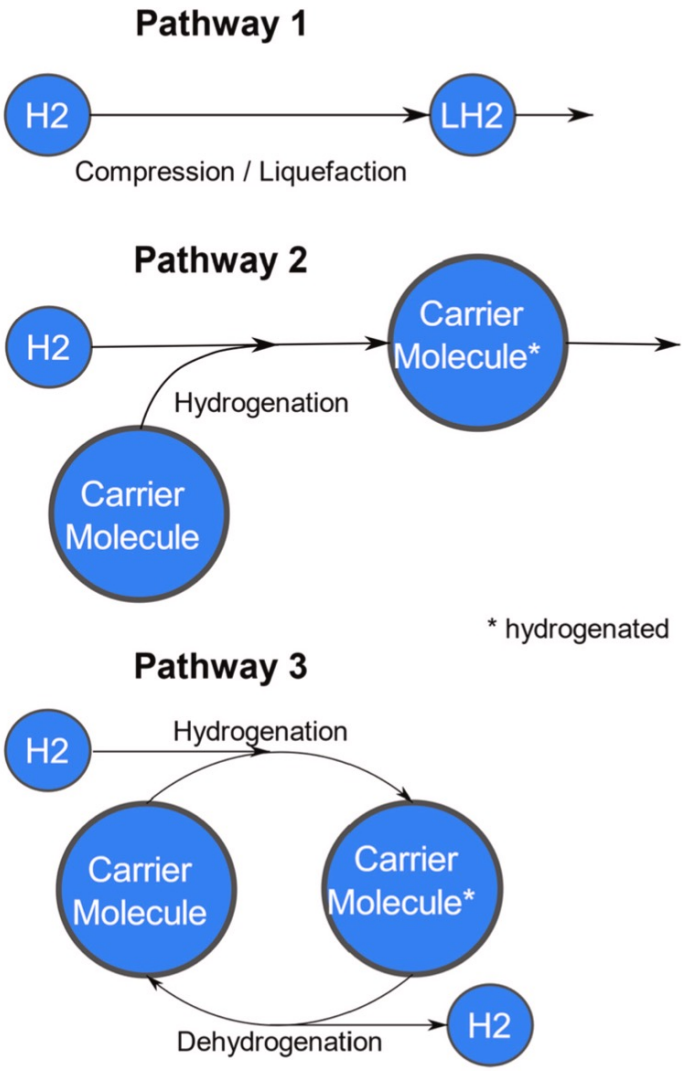

Fig. 6. Carrier reaction pathways.

Table 4
Overview of the hydrogen carrier and hydrogenated molecules discussed in this paper listed by chemical formula and CAS number.

Carrier			Hydrogenated carrier		
Name (*common name*)	Formula	CAS	Name (*common name*)	Formula	CAS
Carbon dioxide	CO_2	124-38-9	Formic acid	H_2CO_2	64-18-6
			Methane	CH_4	74-82-8
Nitrogen	N_2	7727-37-9	Ammonia	NH_3	7664-41-7
Benzene	C_6H_6	71-43-2	Cyclohexane	C_6H_{12}	110-82-7
Toluene	$C_6H_5CH_3$	108-88-3	Methylcyclohexane	$C_6H_{11}CH_3$	108-87-2
1,3-Dimethylbenzene (*m-Xylene*)	$C_6H_4(CH_3)_2$	108-38-3	1,3-dimethylcyclohexane	$C_6H_{10}(CH_3)_2$	638-04-0
1,2,4-Trimethylbenzene (*Pseudocumene*)	$C_6H_3(CH_3)_3$	95-63-6	1,2,4-trimethylcyclohexane	$C_6H_9(CH_3)_3$	2234-75-5
1,2,3,4-Tetramethylbenzene	$C_6H_2(CH_3)_4$	488-23-3	1,2,3,4-tetramethylcyclohexane	$C_6H_8(CH_3)_4$	3726-45-2

$$CO_2\ (g) + H_2\ (g) \underset{catalyst}{\rightarrow} H_2CO_2\ (l) \quad (3)$$

$$CO_2\ (g) + 4H_2\ (g) \underset{catalyst}{\rightarrow} CH_4\ (g) + 2H_2O\ (l) \quad (4)$$

$$N_2\ (g) + 3H_2\ (g) \underset{catalyst}{\rightarrow} 2NH_3\ (g) \quad (5)$$

Table 5
Overview of the hydrogen carrier molecules and their key chemical properties. The roundtrip energy requirement is calculated and a corrected H_2 LHV is given for each carrier molecule.

Hydrogen Carrier (*Common name*)	Molecular Formula	Mol. Weight (g/mol)	Hydrogenated Molecule	Molecular Formula	Mol. Weight (g/mol)	Density (g/ml)	H available (# atoms)	Mass fraction available H_2	Volumetric hydrogen in 1 l(l)	Carrier H_f (kJ/mol)	ΔH Hydrogenation (kJ/mol)	S carrier molecule (J/mol.K) @ STP	ΔSrxn (J/K)	Gibbs Free Energy (kJ/mol)	Total Roundtrip Energy Cost (kJ/mol Carrier)	LHV_eff (kJ/mol H2)	Transportation loss
Carbon dioxide	CO_2	44.0	Formic Acid	H_2CO_2	46.0	1.22	2	4.4 %	1187.4	−393.5	−31.6	213.8	−81.9	−15.2	31.6	210.4	13 %
Benzene	C_6H_6	78.1	Cyclohexane	C_6H_{12}	84.2	0.78	6	7.2 %	1244.0	49.0	−206.7	173.3	31.1	−218.4	206.7	173.1	28 %
Toluene	$C_6H_5CH_3$	92.1	Methylcyclohexane	$C_6H_{11}CH_3$	98.2	0.77	6	6.2 %	1054.0	12.0	−202.2	221.0	26.9	−212.3	202.2	174.6	28 %
1,3-dimethylbenzene (*m-Xylene*)	$C_6H_4(CH_3)_2$	106.2	1,3-dimethylcyclohexane	$C_6H_{10}(CH_3)_2$	112.2	0.80	6	5.4 %	953.4	−24.4	−193.8	253.8	15.7	−199.7	193.8	177.4	27 %
1,2,4-trimethylbenzene	$C_6H_3(CH_3)_3$	120.2	1,2,4-trimethylcyclohexane	$C_6H_9(CH_3)_3$	126.2	0.78	6	4.8 %	828.3	−58.6	−196.2	283.4	8.5	−199.4	196.2	176.6	27 %
1,2,3,4-tetramethylbenzene	$C_6H_2(CH_3)_4$	134.2	1,2,3,4-tetramethylcyclohexane	$C_6H_8(CH_3)_4$	140.3	0.80	6	4.3 %	766.6	−90.2	−212.7	290.8	−8.3	−209.6	212.7	171.1	29 %
Nitrogen	N_2	28.0	Ammonia	NH_3	17.0	0.86	3	17.8 %	3393.5	0.0	−91.9	191.6	193.9	−193.7	45.9	211.4	13 %
Carbon dioxide	CO_2	44.0	Methane	CH_4	16.0	0.66	4	25.2 %	3670.0	−393.5	−252.7	213.8	112.4	−292.1	252.7	274.6	32 %

$$C_6H_6\ (l) + 3H_2\ (g) \underset{catalyst}{\rightarrow} C_6H_{12}\ (l) \quad (6)$$

$$C_6H_5CH_3\ (l) + 3H_2\ (g) \underset{catalyst}{\rightarrow} C_6H_{11}CH_3\ (l) \quad (7)$$

$$C_6H_4(CH_3)_2\ (l) + 3H_2\ (g) \underset{catalyst}{\rightarrow} C_6H_{10}(CH_3)_2\ (l) \quad (8)$$

$$C_6H_3(CH_3)_3\ (l) + 3H_2\ (g) \underset{catalyst}{\rightarrow} C_6H_9(CH_3)_3\ (l) \quad (9)$$

$$C_6H_2(CH_3)_4\ (l) + 3H_2\ (g) \underset{catalyst}{\rightarrow} C_6H_8(CH_3)_4\ (l) \quad (10)$$

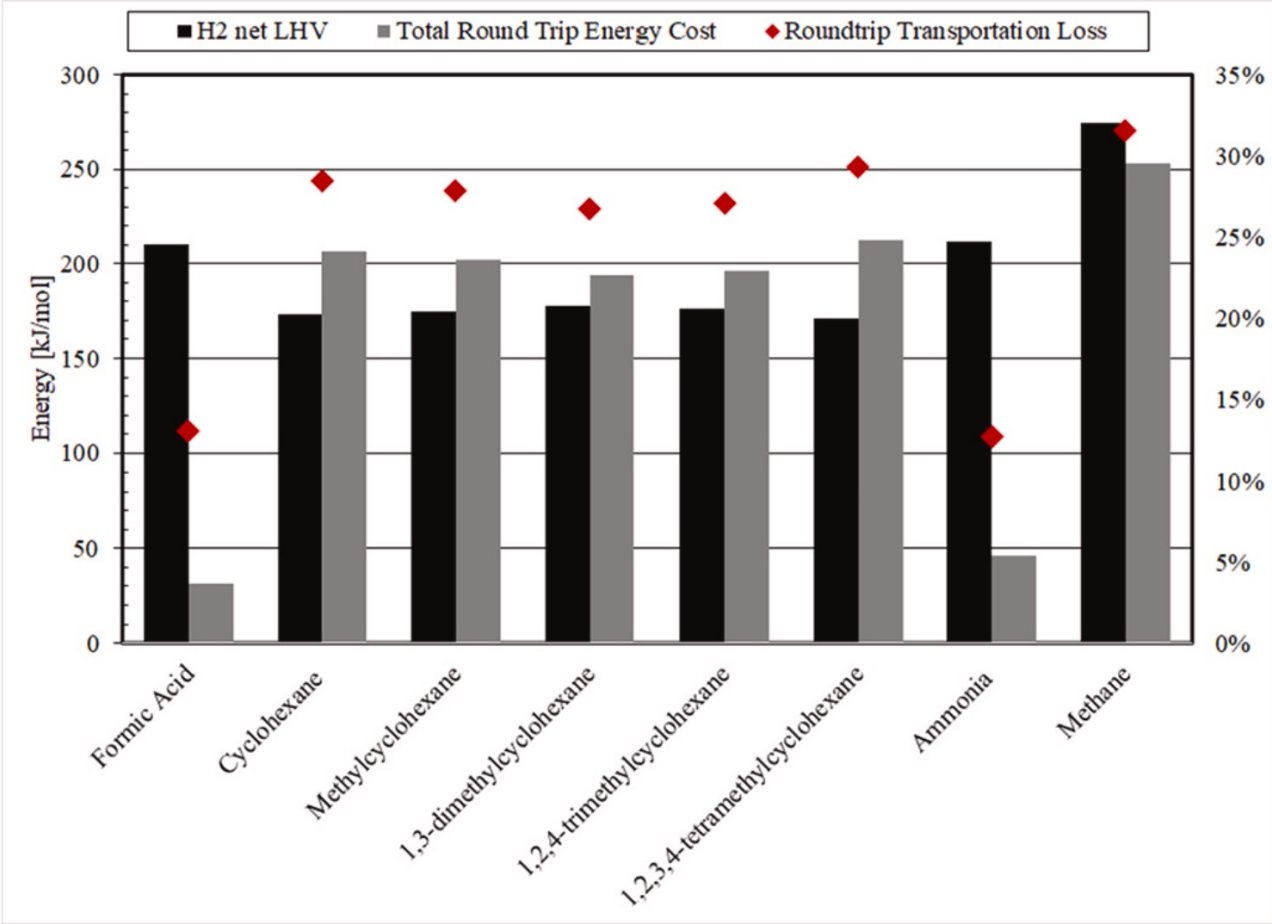

Fig. 7. Bar chart comparing the roundtrip energy cost per mole of carrier molecule, the loss-corrected LHV per mole of transported hydrogen, and the roundtrip efficiency.

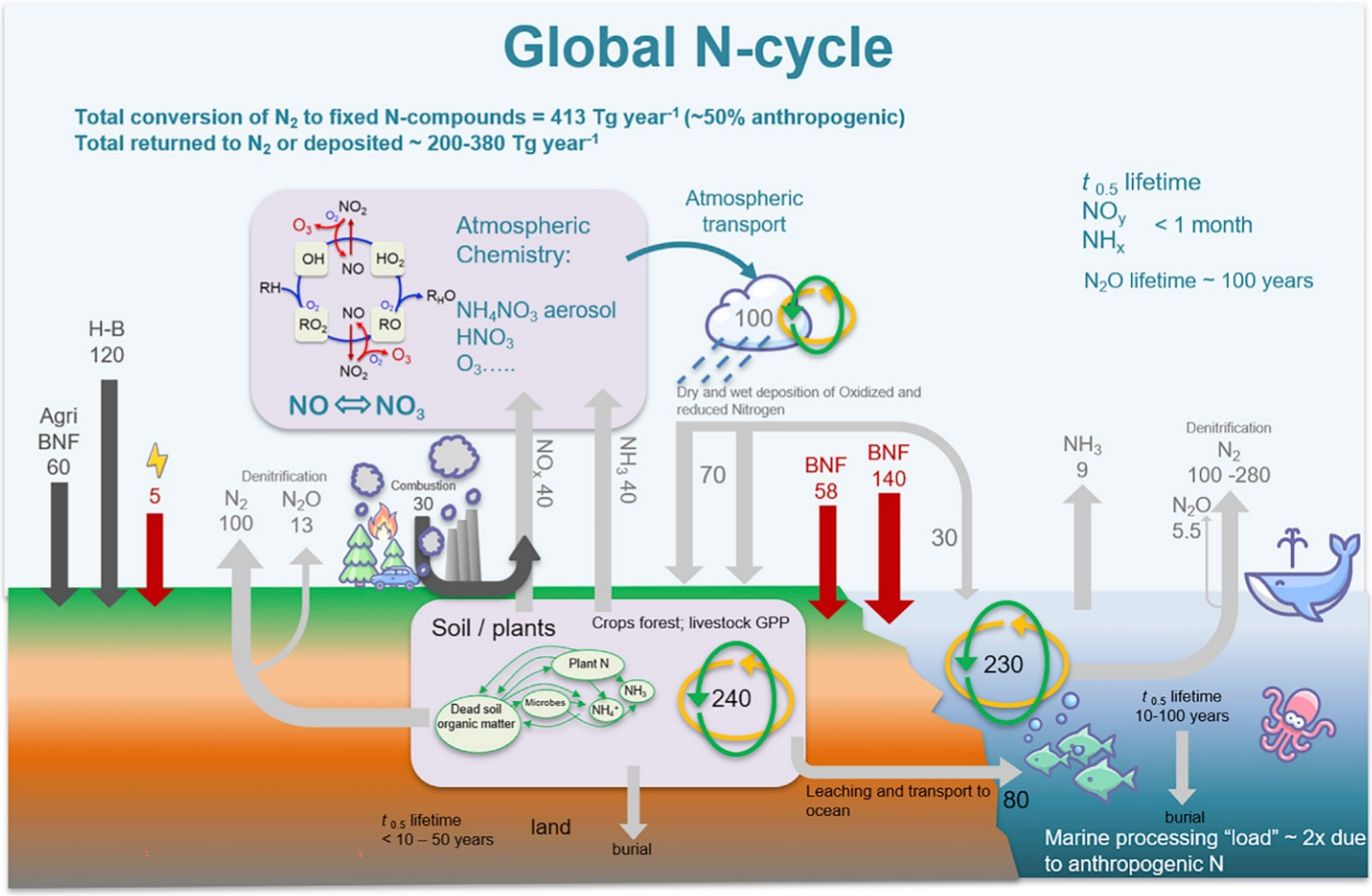

Figure 4. The Planetary Nitrogen Cycle

Planetary nitrogen cycles and fluxes in Tg per year (BNF, biological nitrogen fixation; H-B, Haber-Bosch nitrogen fixation; GPP, gross primary productivity). Curved "combustion" arrow shows nitrogen fixation from fossil fuel and other combustion process and resultant emissions of NO_x compounds to the atmosphere. 1 Tg = 1 teragram = 1 × 10^6 tonne. Redrawn and appended from Fowler et al.[86]

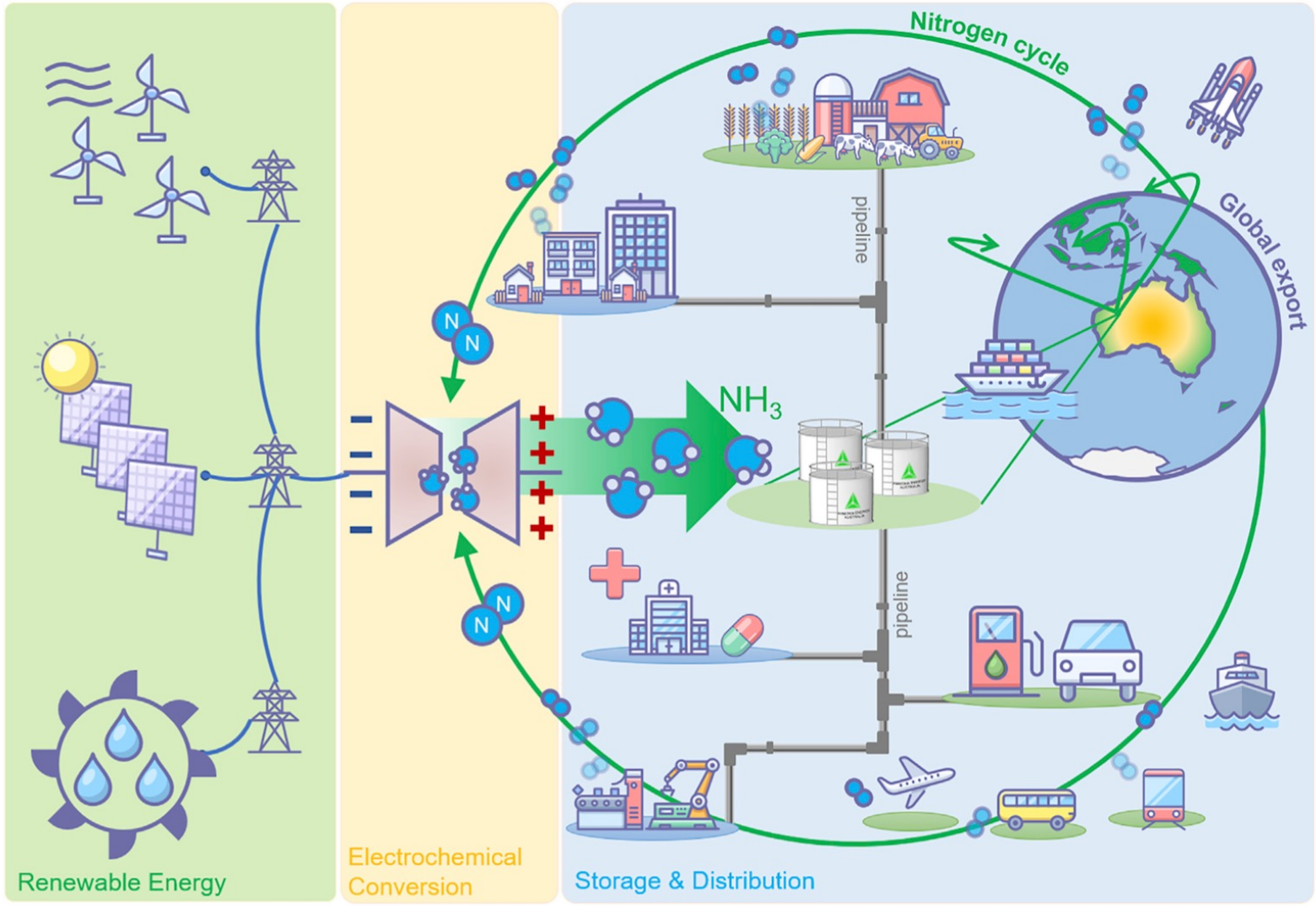

Figure 1. Vision of the "Ammonia Economy" in which the Energy Sources and Uses Are All Based on Ammonia

Table 1. Relative Properties and Costs of Ammonia Compared with Liquid Fossil Fuels

Fuel	P (Bar)	Density (kg m^{-3}) (15°C)	LHV (kWh kg^{-1}) (25°C)	LHV (MWh m^{-3}) (25°C)	Cost (USD kg^{-1})	Cost (USD kWh^{-1})
Ammonia	10	603	5.18	3.12	0.30	0.058
Diesel	1	846	12.1	10.2	1.00 (USA)	0.083
LPG	14	388	12.6	4.89	1.00 (Germany)	0.079
Gasoline	1	736	12.1	8.87	1.81 (Japan)	0.15
Bunker Fuel	1	980	10.8	10.6	0.59 (Global average)	0.055

Adapted and Updated from Zamfirescu and Dincer.[71] LPG, diesel, and gasoline costs from Global Petrol Prices,[64] which include local taxes and delivery costs. Other data from the engineering ToolBox.[65] Bunker fuel prices from Ship & Bunker.[66] Ammonia price from Apodaca and Ewing. [4,63]

Ammonia as a Fuel

The problem with hydrogen as a fuel:

1) Storage 70 MPa ($50,000 pump)
2) Low enthalpy of combustion 5.6 MJ/L at 70MPa
   (@1 MPa 15.6 MJ/L for ammonia; 25 MJ/L for propane)
1) Embrittlement of steel
2) Flammability from 4% to 75%
3) Permeability through metals and plastics
4) Platinum catalyst needed for fuel cells

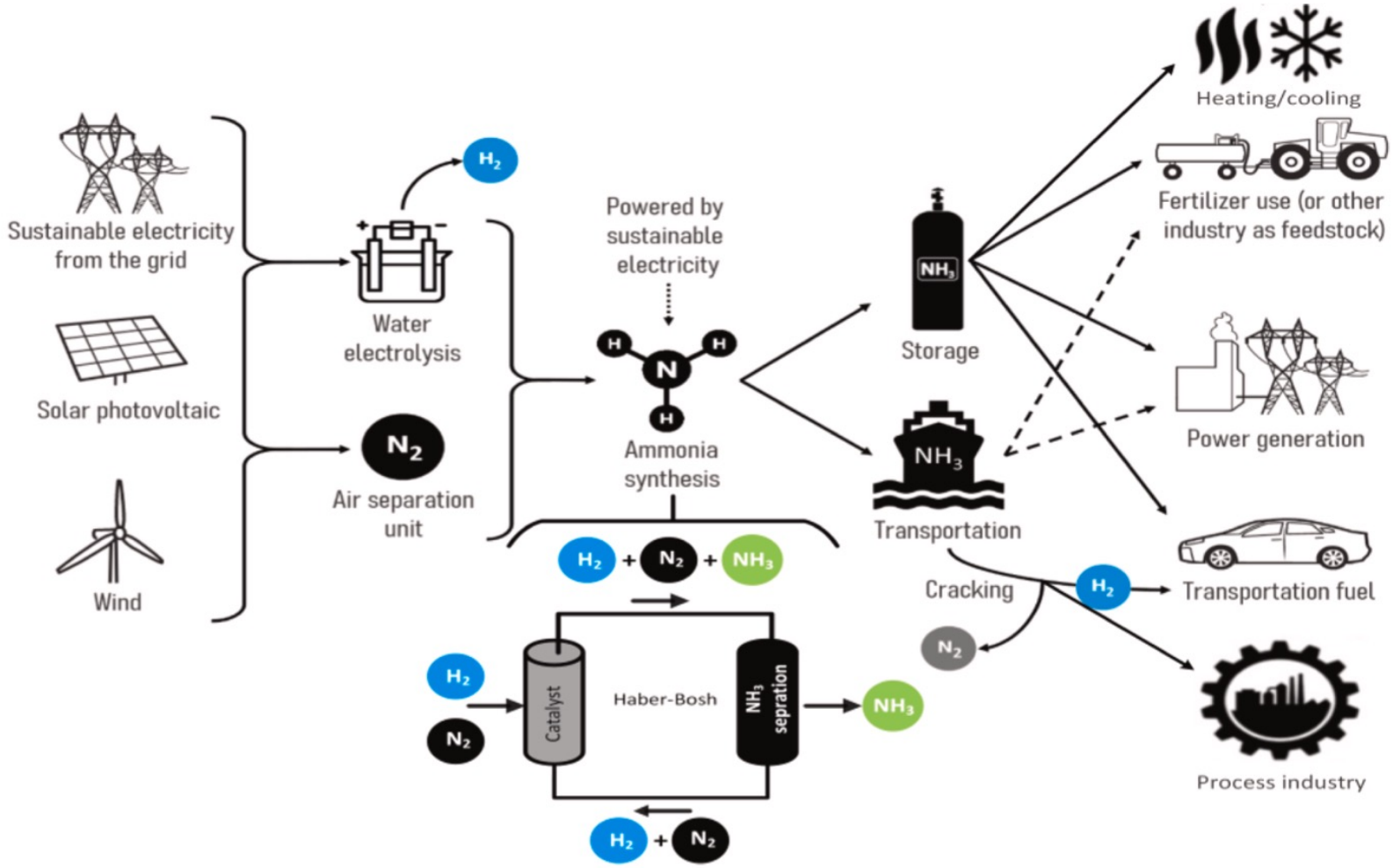

Fig. 2. Carbon-free ammonia production roadmap and its various end-use, modified from [9] and [14].

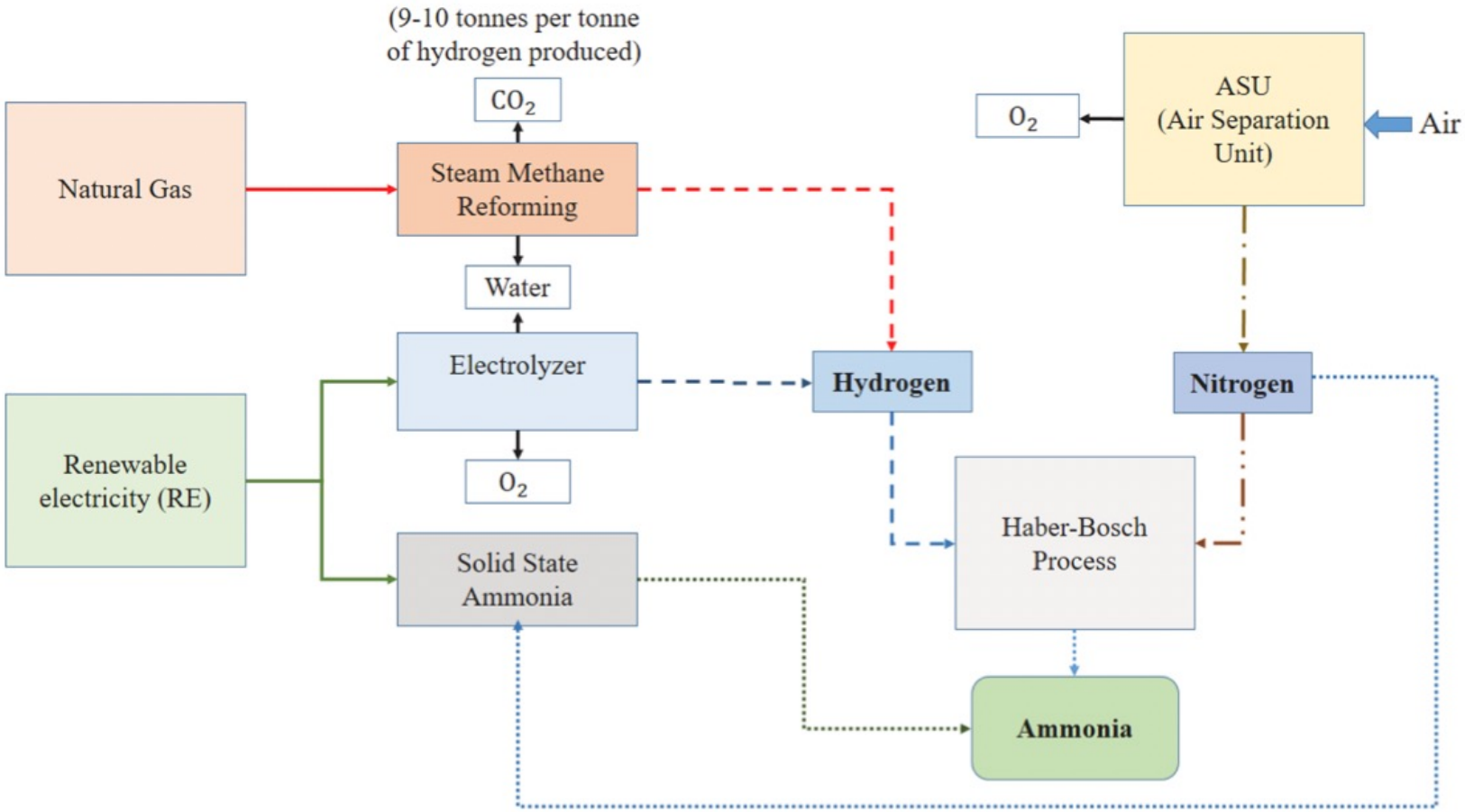

Fig. 1. Schematic representation of processes involved for ammonia production [49,50].

Table 1
Thermodynamic properties of ammonia and other fuels [84859899100].

Property	Ammonia	Gasoline	Diesel	Methane	Hydrogen
Lower Heating Value (MJ/kg)	18.8	44.5	45	50	120
Density at 1 bar and 25 deg. C (kg/cub. m)	0.718	736	849	0.667	0.0837
Specific heat C_p (kJ/kg K)	2.190	2.22	1.75	2.483	14.30
Latent heat of vaporization (kJ/kg)	1370	348.7	232.4	511	455
Auto-ignition temperature (K)	930	503	527–558	859	773–850
Laminar Burning Velocity at $\phi = 1$ (m. s^{-1})	0.07	0.58	0.86	0.38	3.51
Flammability limit (vol. %)	15–28	0.6–8	1–6	5–15	4.7 – 75
Stoichiometric air fuel ratio by mass	6.05	15	14.5	17.3	34.6
Boiling point (°C)	–33.34	35–200	282–338	−161.5	−252.7
Melting point (°C)	−77.73	−90 - −95	−30 - −18	−182	−259
Octane rating (RON)	130	90–98	–	120	>100
Volumetric Energy Density (GJ/m^3) at 300 K and 0.1 MPa	11.3	33	36.4	9.35	4.7
Adiabatic flame temperature (° C)	1800	2138	2300	1950	2110

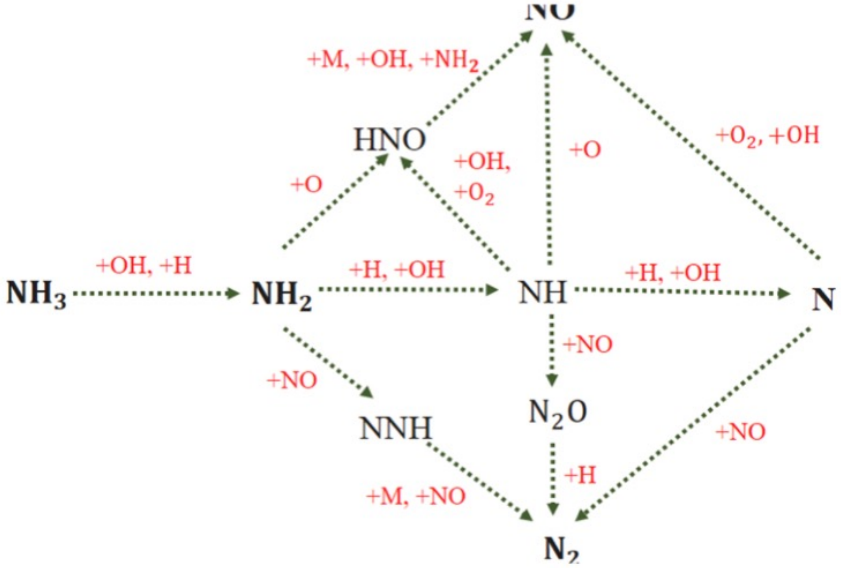

Fig. 4. Reaction pathways for ammonia combustion [90].

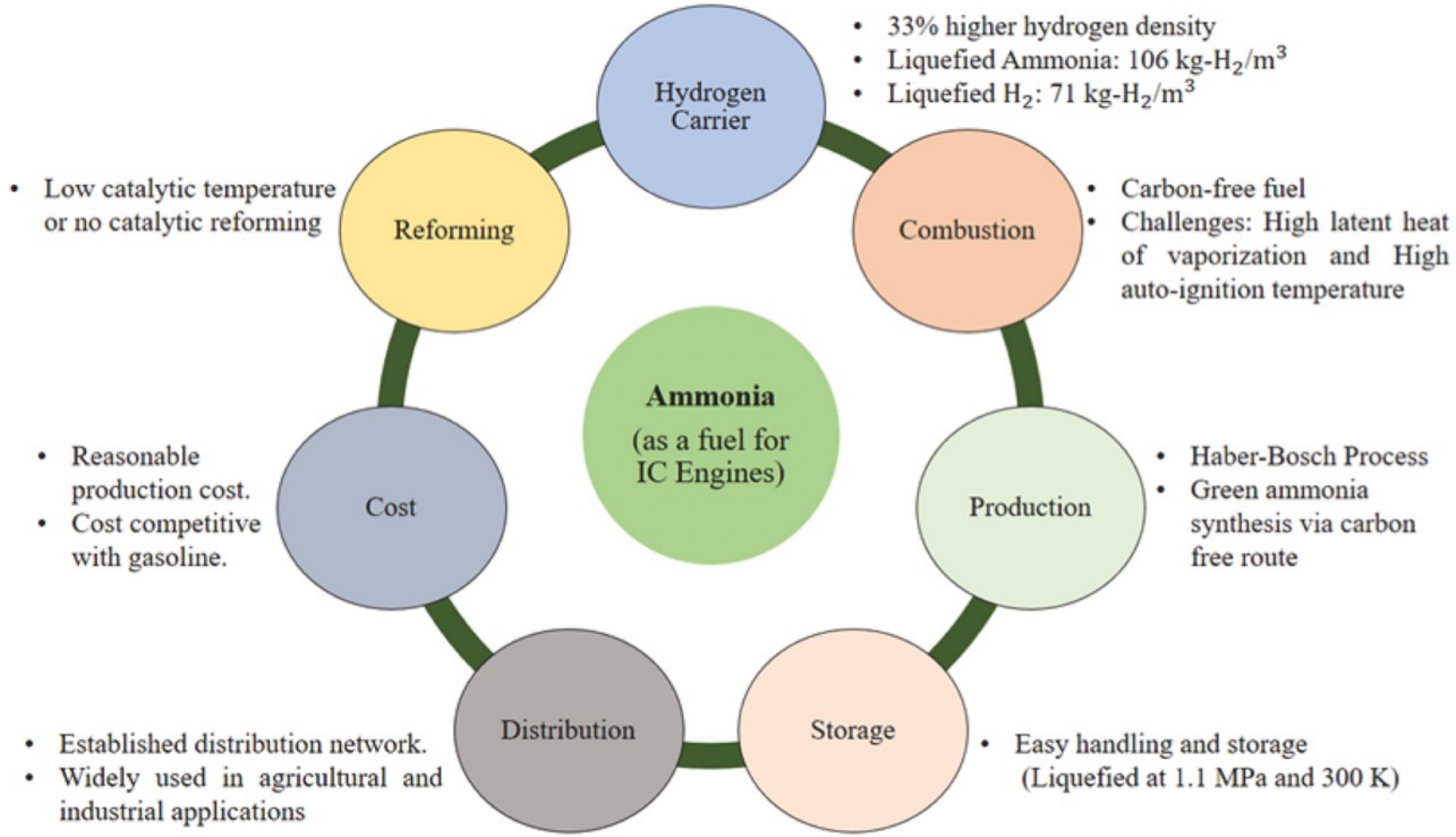

Fig. 5. Properties of ammonia as a fuel for IC engines.

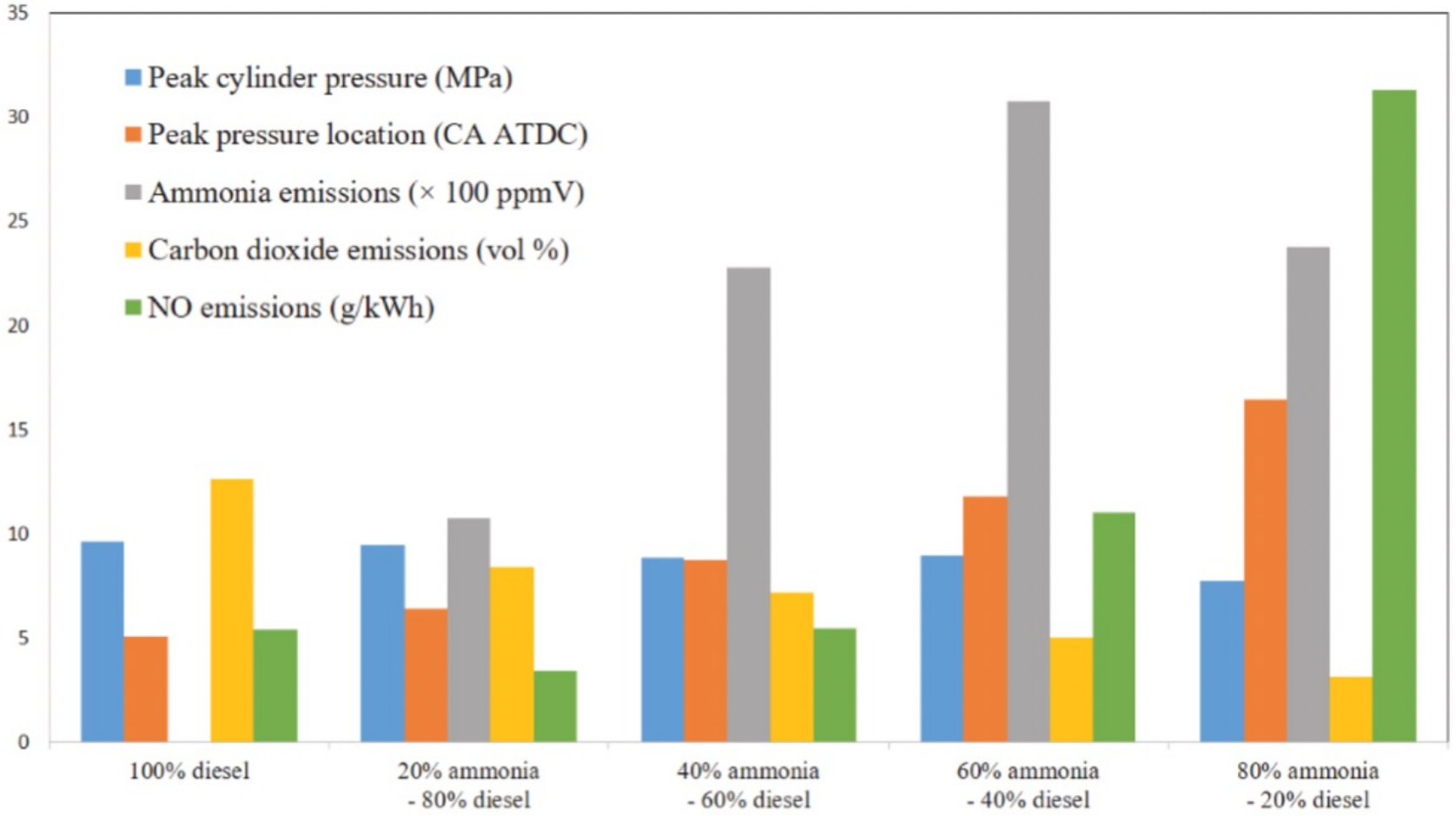

ects of ammonia share on combustion and emission characteristics of dual fuel engine at constant power output condition (40 kW at 1000 130,131].

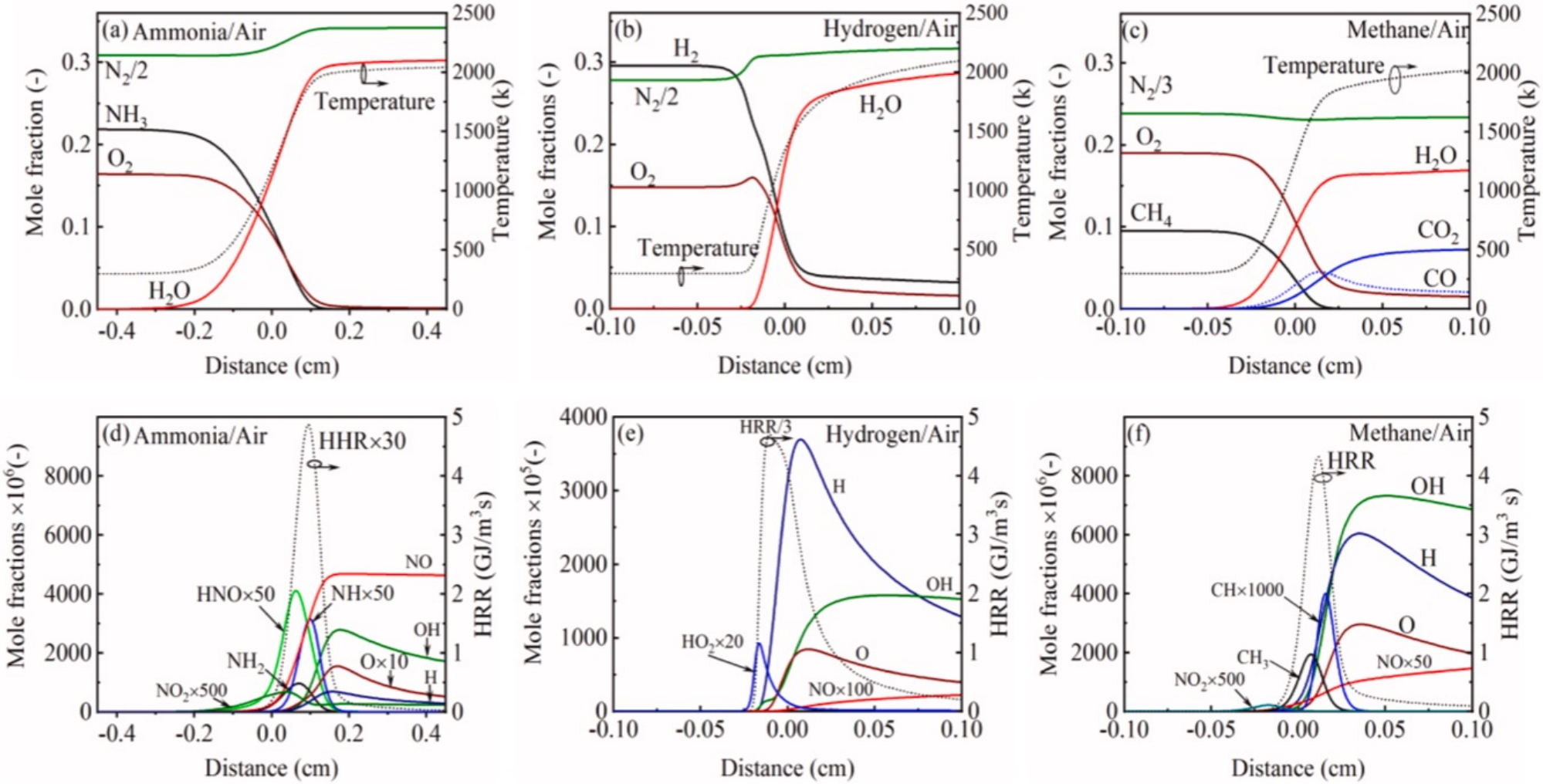

Fig. 3. Flame structure of premixed flames: NH_3-air (a)-(d), H_2-air(b)-(e), and CH_4-air (c)-(f) at $\Phi = 1$ and P = 0.1 MPa

Table 1

Combustion properties of NH_3, H_2, and other hydrocarbon fuels [2]. The auto-ignition data of (NH_3, H_2) and of (CH_4 and C_3H_8) are from [20] and [21], respectively.

Fuel	NH_3	H_2	CH_4	C_3H_8
Maximum burning velocity (cm/s)	7	291	37	43
Lower calorific value (MJ/kg)	18.6	120	50	46.4
Flammability limit (in terms of Φ)	0.63-1.4	0.1-7.1	0.5-1.7	0.51-2.5
Auto-ignition temperature (K)	924	844	813	739
Adiabatic flame temperature (K)	2073	2383	2223	2273

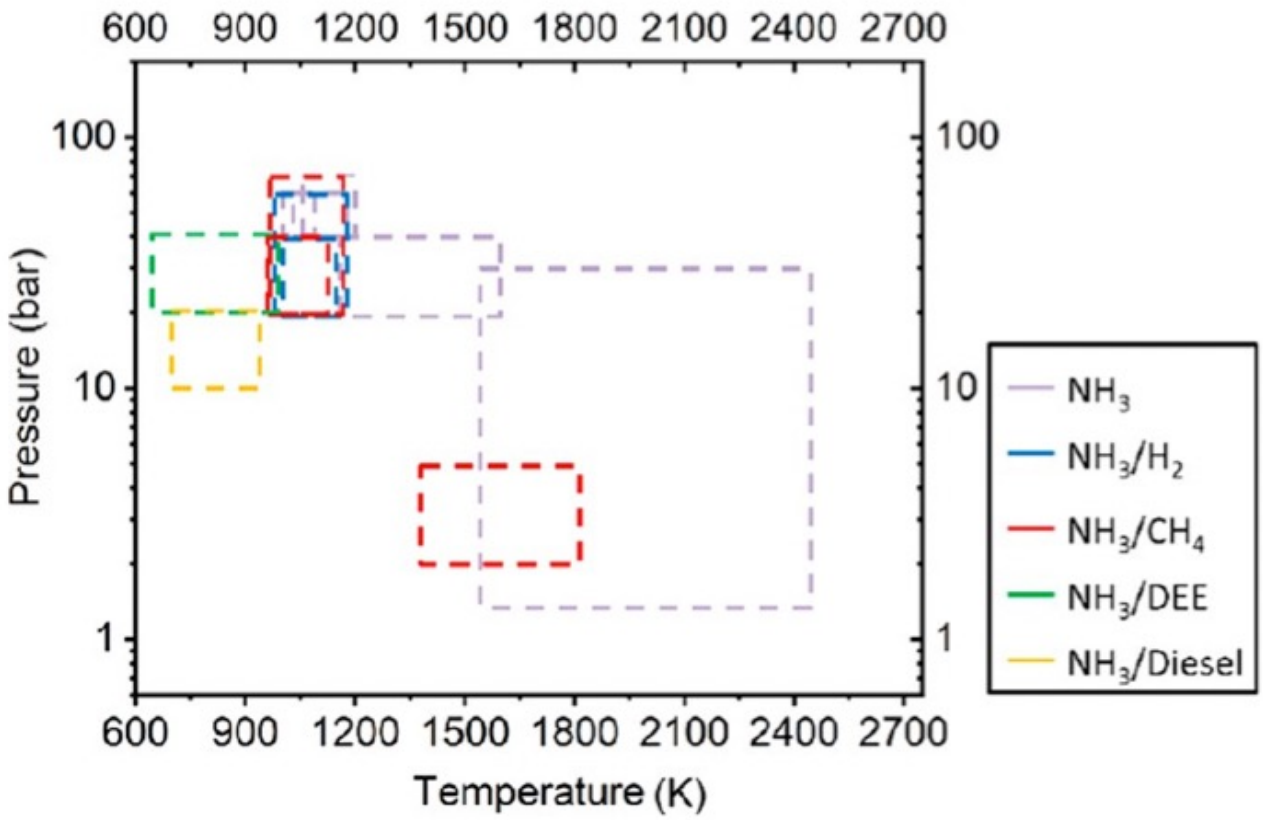

Figure 7. Summary of the conditions of IDT measurements of mixtures containing ammonia from the literature.[59,67−71,73,74,76]

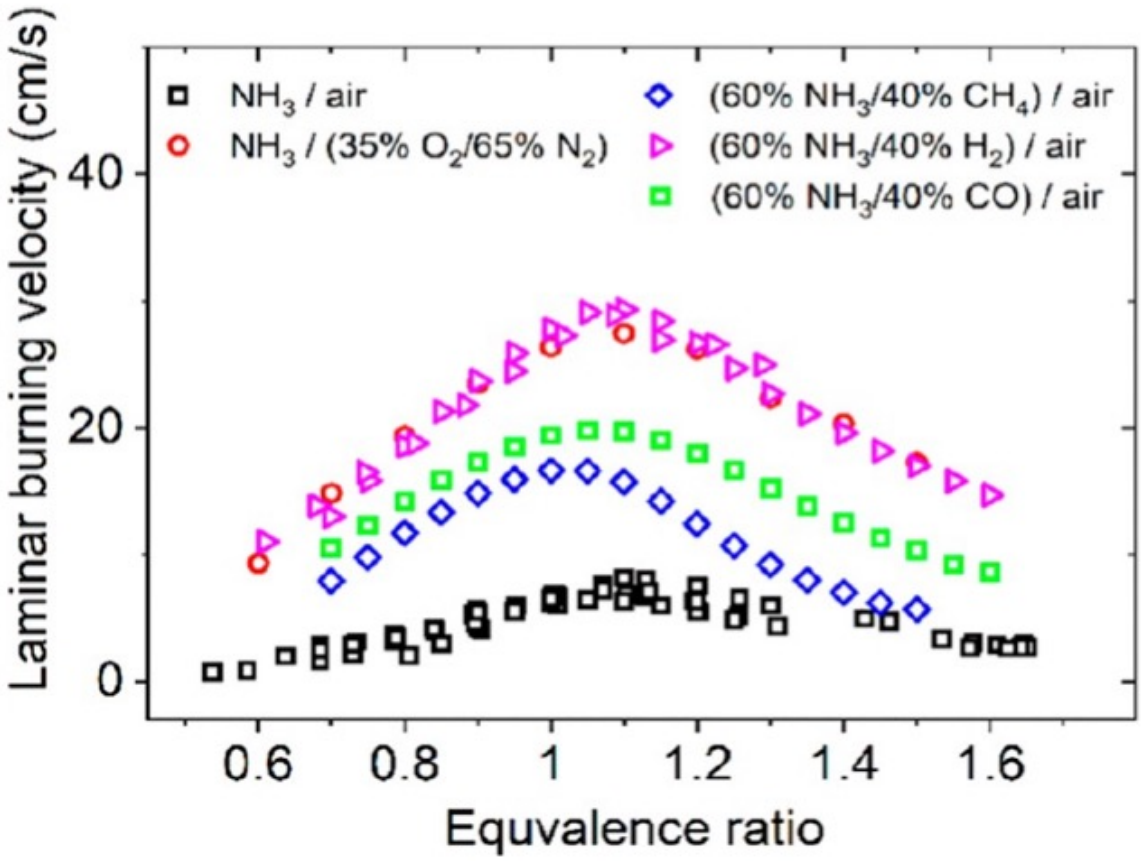

Figure 8. Summary of the LBV of mixtures containing ammonia from the literature.[81,90−92,114]

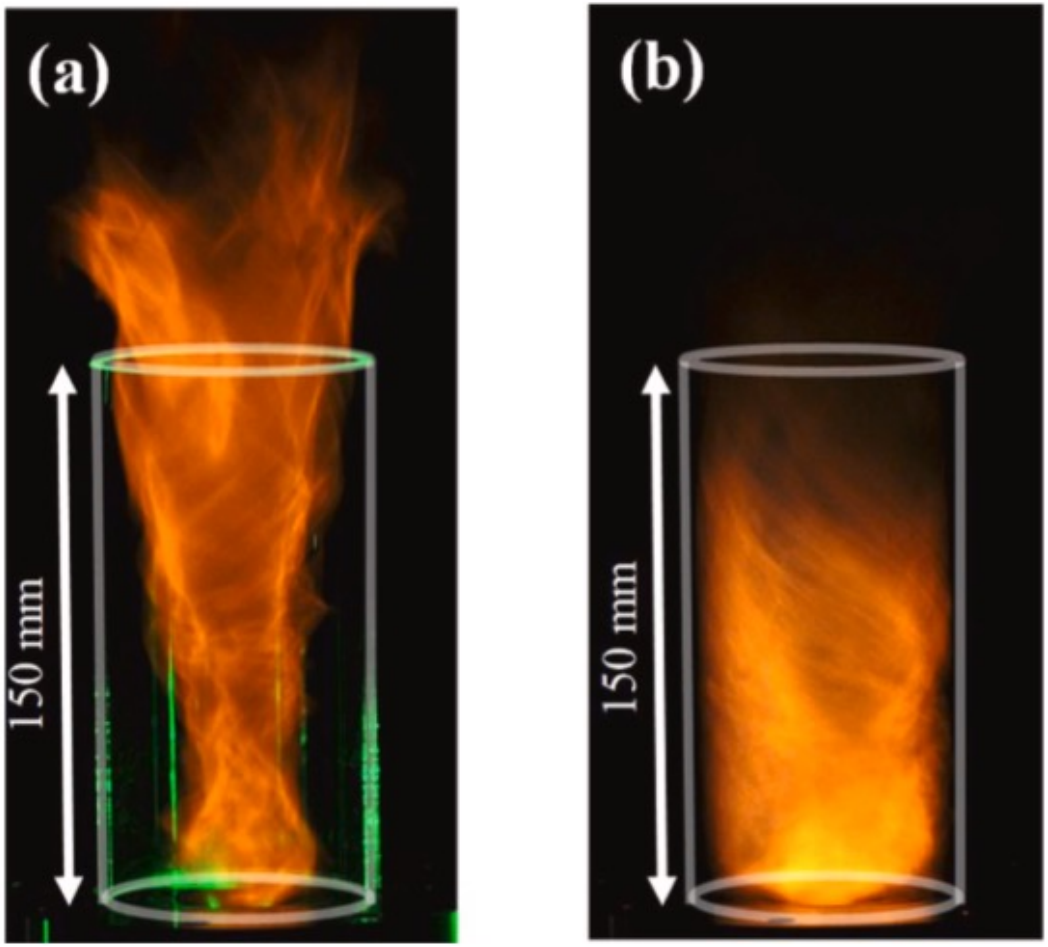

Fig. 32. Photographs of (a) a pure liquid ammonia spray flame and (b) a liquid ammonia spray flame co-fired with methane. Reproduced from [158].

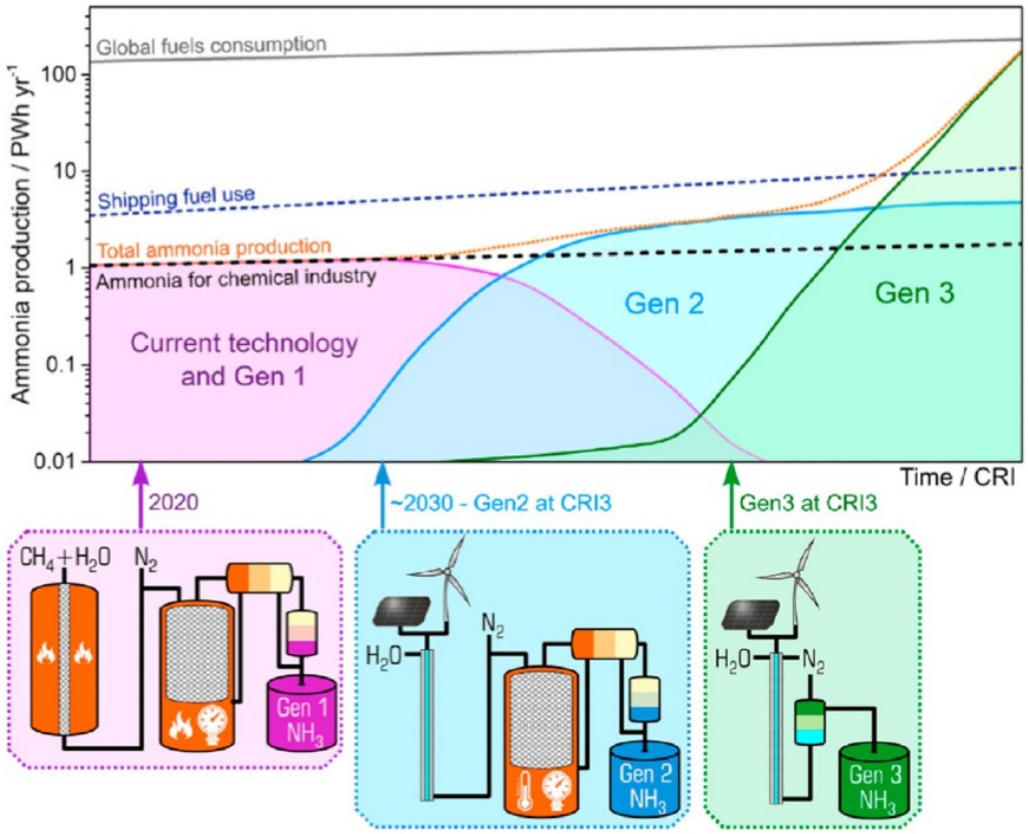

Figure 2. Ammonia economy roadmap showing current and projected contributions of the current and generation 1 (purple), generation 2 (light blue), and generation 3 (green) ammonia production technologies. This figure was reproduced with permission from ref 14. Copyright 2020 Elsevier.

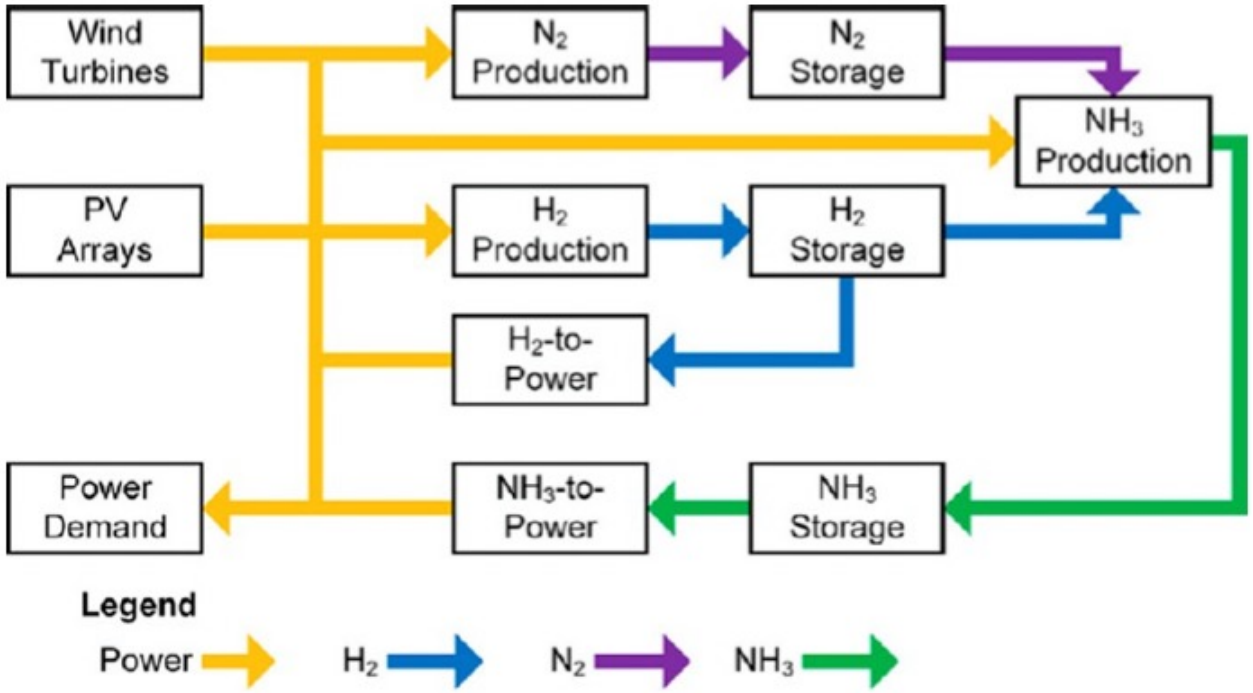

Figure 3. Conceptual superstructure of the renewable energy supply, which uses hydrogen and ammonia for energy storage. This figure was reproduced with permission from ref 20. Copyright 2020 Elsevier.

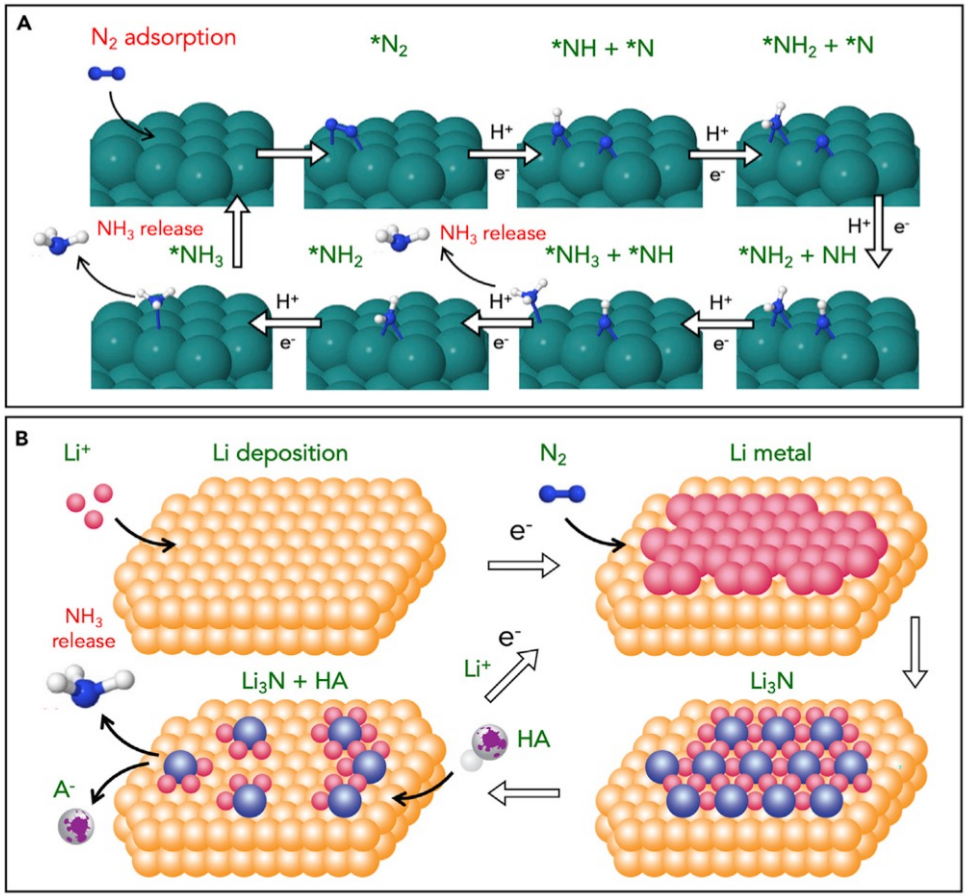

Figure 2. Mechanisms of Direct Nitrogen Reduction to Ammonia

(A and B) Possible mechanisms of (A) direct eNRR via absorption of N_2 onto the catalyst surface, followed by progressive proton and electron additions to produce a first, followed by a second molecule of ammonia (adapted from Wang et al.[19]); (B) indirect electrochemical N_2 reduction to ammonia based on lithium as a mediator, forming Li_3N as an intermediate on a copper substrate (atom and ion sizes approximately to scale; differences in Li and N sizes reflect their differing states during the process; A, anion).

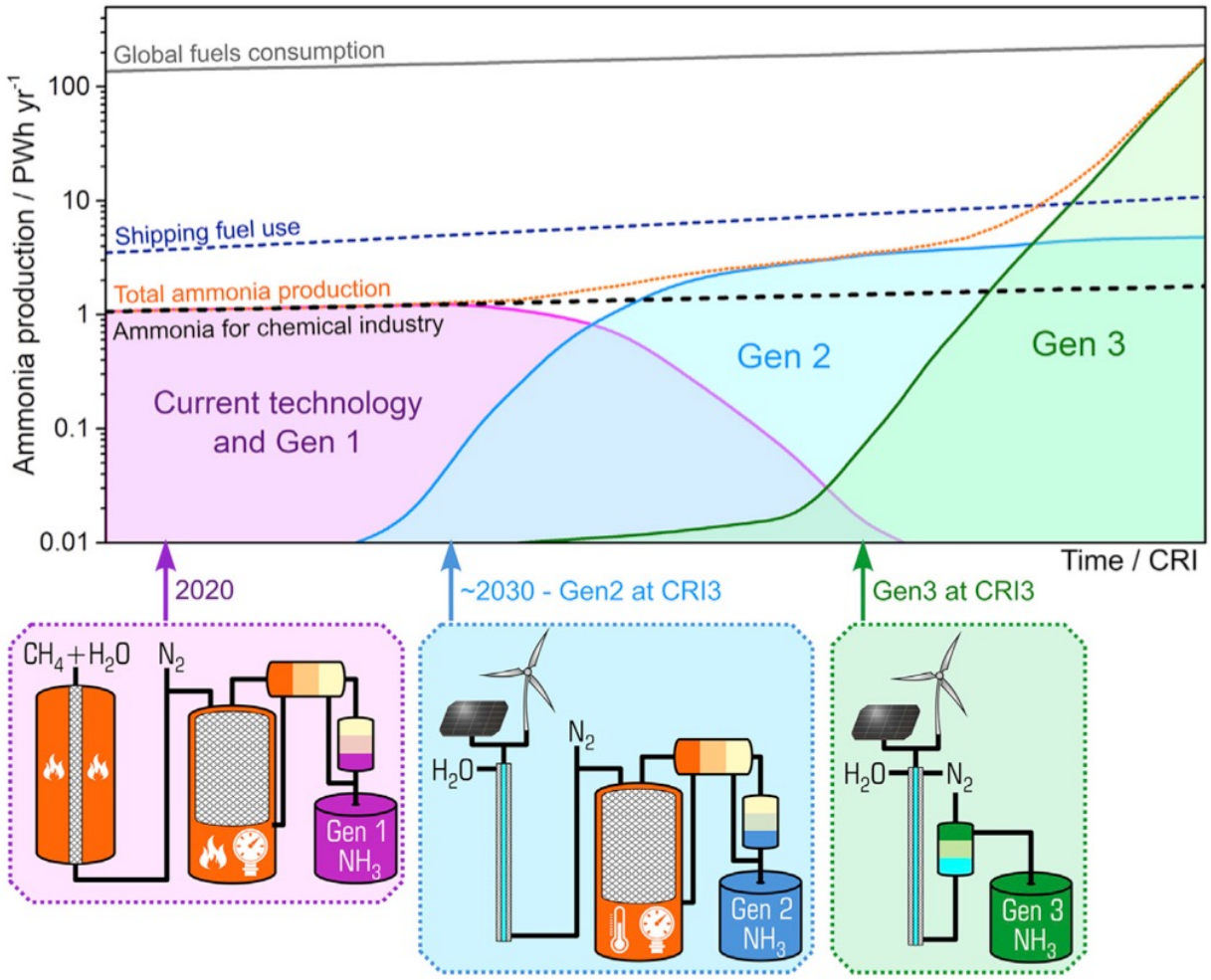

Figure 5. Ammonia Economy Roadmap Showing Current and Projected Contributions of the Current and Gen 1 (purple), Gen 2 (light blue), and Gen 3 (green) Ammonia Production Technologies

Table 8
Comparative cost analysis of gasoline, hydrogen, ammonia, and electricity adapted from ARPA-E REFUEL [175].

	Gasoline	Hydrogen	Ammonia	Electricity
Fuel cost [$/kg]	0.54	1.95	0.325	
Fuel cost, [$/kWh]	0.047	0.058	0.063	0.065
Transmission Cost [$/kWh]	0.001	0.06	0.004	0.038
Storage Cost [$/kWh]	0.001	0.03	0.007	0.160
Conversion Efficiency [%]	30	55	55	92
Source-to-use energy cost [$/kWh]	0.159	0.292	0.135	0.285

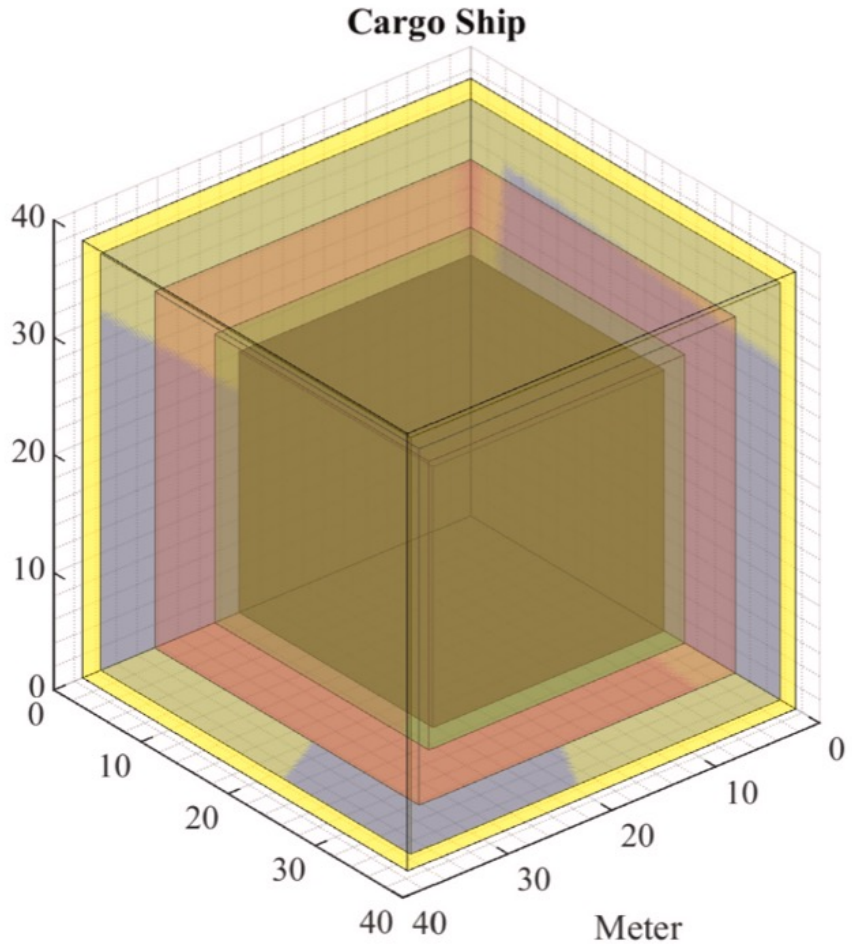

Fig. 11. Volume requirements for various storage methods for cargo ships traveling between Shanghai and Rotterdam (black = NH_3, Green = LH_2, red = H_2@690 bars, blue = H_2@350 bars, yellow = Li-ion Battery). (For interpretation of the references to color in this figure legend, the reader is referred to the web version of this article.)

- Power generations can draw the largest benefits from the use of hydrogen directly.
- Aviation is challenging to decarbonize with many roadblocks. *E*-fuels, hydrogen, and ammonia as a carrying vector come with their advantages and disadvantages. At this point, no ideal hydrogen carrier can be named.
- Trucking requires only relatively small amounts of hydrogen compared to all other use cases. Here, the direct storage of hydrogen, either cryogenic or compressed, appears to be the most suitable and economical solution in conjunction with the high purity requirements of fuel cells.
- In the case of marine shipping, ammonia's volumetric and combustion properties besides economic considerations make it the ideal energy carrier. This is not only true for the consumed fuel itself but also as a carrier to transport green energy and hydrogen.

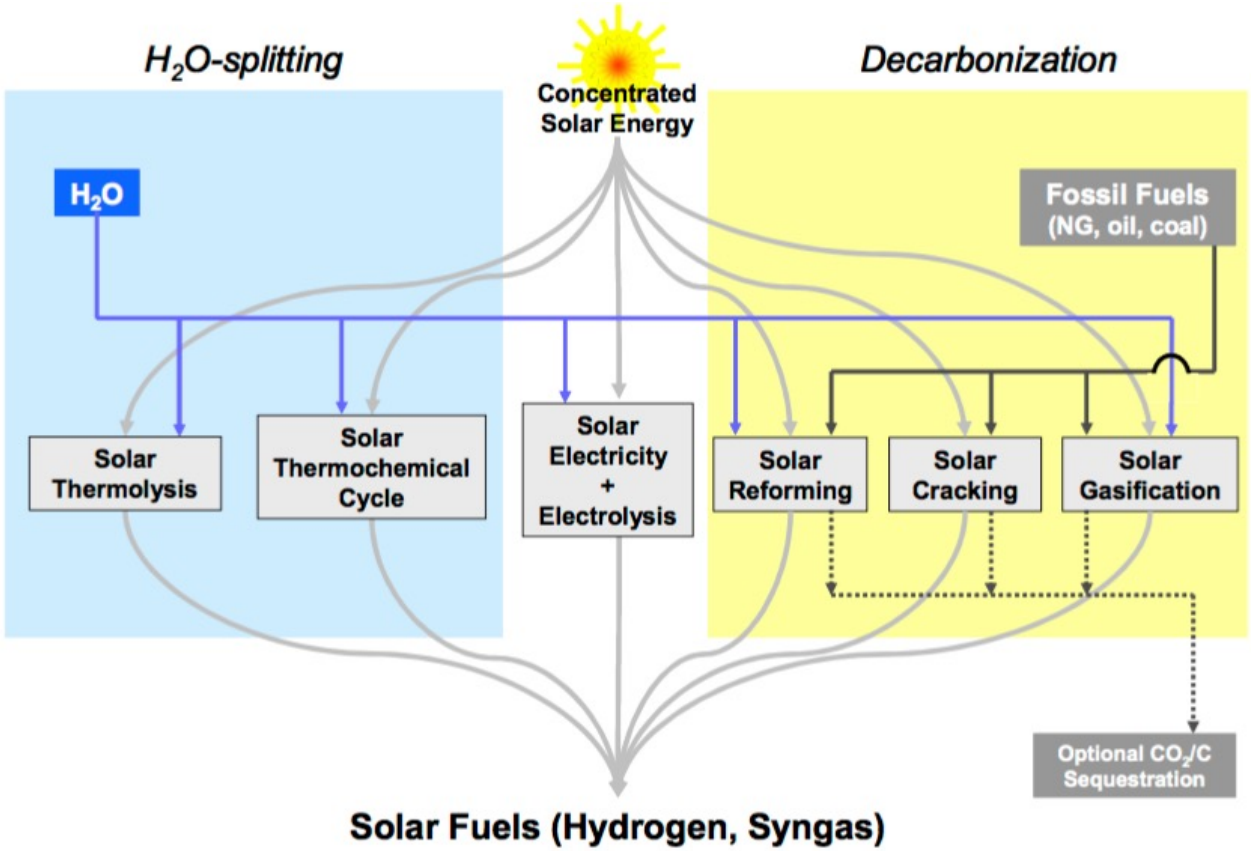

Fig. 2: Thermochemical routes for solar hydrogen production – Indicated is the chemical source of H_2: H_2O for the solar thermolysis and the solar thermochemical cycles; fossil fuels for the solar cracking, and a combination of fossil fuels and H_2O for the solar reforming and gasification. For the solar de-carbonization processes, optional CO_2/C sequestration is considered. All of those routes involve energy consuming (endothermic) reactions that make use of concentrated solar radiation as the energy source of high-temperature process heat. Adapted from [1,2].

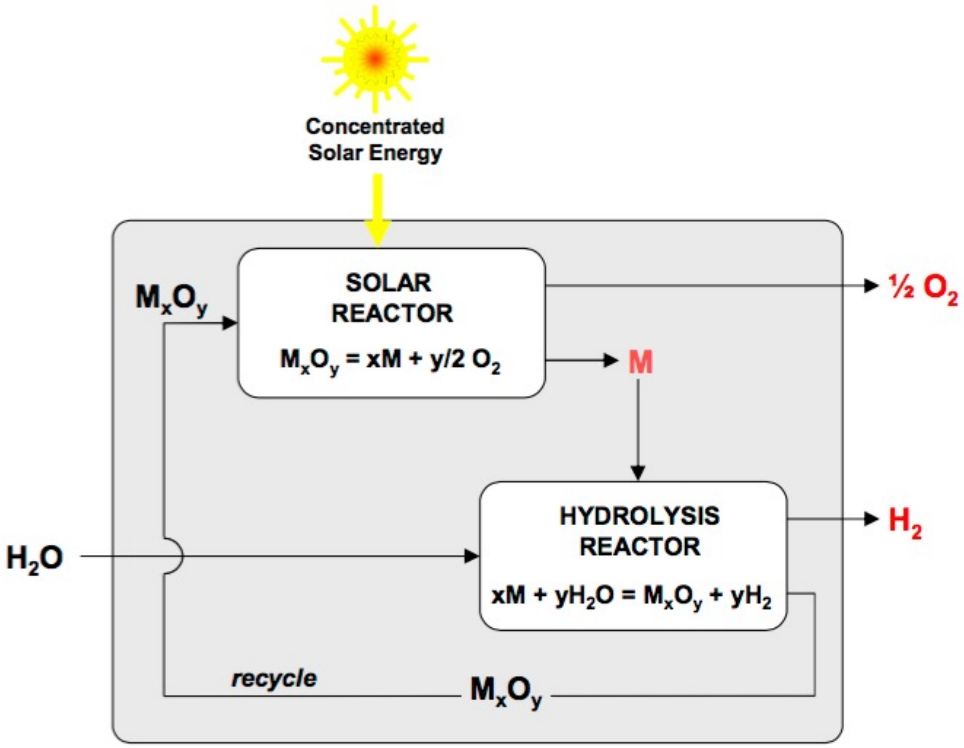

Fig. 3: Thermochemical route based on metal oxide redox reactions – The first step of the cycle is the solar thermal release of O_2 from the metal oxide (M_xO_y). This step requires very high temperatures. The second step is the reaction of the metal (M) with H_2O to form H_2 and the corresponding M_xO_y. This step proceeds at lower temperatures and does not require additional heating in some cases. Since H_2 and O_2 are formed in different steps, the need for high-temperature gas separation is thereby eliminated. This cycle was originally proposed for an iron oxide FeO/Fe_3O_4 redox system. Adapted from [1].

Need to rapidly quench and dilute Zn + O_2 mixture

Zn => ZnO Cycle
(Solar Driven Redox Reactions)

fossil-based fuels in sustainable future transportation systems. Economic analyses have been carried out to determine the long-term potential of the Zn/ZnO-cycle realized in a solar tower system. The cost of H_2 ranged between 0.10 and 0.15 $/kWh (based on its LHV and a heliostat field cost at 100 to 150 $/m^2), and thus might become competitive *vis-à-vis* other paths for producing solar H_2 from H_2O [15,72,73,74]. Credit for pollution abatement and CO_2 mitigation can accelerate the deployment of the solar thermochemical technology. A comparison of H_2 produced via steam methane reforming and the Zn/ZnO cycle concluded that a significantly higher carbon tax is required to make the Zn/ZnO competitive than is likely to be implemented [75]. Therefore, the economic viability of the Zn/ZnO cycle must also include competitive, incentive policies that lead to early implementation of solar H_2 plants. On the other hand, the Zn/ZnO cycle can be applied to split both H_2O and CO_2 and produce both H_2 and CO, thereby laying the path to the solar production of synthetic liquid hydrocarbons for fueling the transportation sector and the existing massive global infrastructure.